Dissertation
submitted to the
Combined Faculties for the Natural Sciences and for Mathematics
of the Ruperto-Carola University of Heidelberg, Germany,
for the degree of
Doctor of Natural Sciences

Put forward by

Dipl. phys. Anton Kurz
born in Bad Reichenhall, Germany

Oral examination: January 31, 2013

Characterization and Application of Photon-Statistics in Single-Molecule Measurements for Quantitative Studies of Fluorescently Labeled Samples

Referees: PD Dr. Dirk-Peter Herten
Prof. Dr. Wolfgang Petrich

Characterization and Application of Photon-Statistics in Single-Molecule Measurements for Quantitative Studies of Fluorescently Labeled Samples

The lack of reliable quantitative methods in fluorescence microscopy prevents the detailed investigation of basic molecular processes. Single-molecule fluorescence spectroscopy offers several techniques to determine the stoichiometry of fluorescent probes. Among them, an approach using the single-photon emission of an individual quantum system, also known as photon antibunching, yields access to both the emitter number and their molecular brightness. Previous work demonstrated the feasibility of the method to estimate up to five dyes without further physical characterization. In this work, I investigated and improved the reliability and robustness of this method. I developed different fluorescent probes with a defined label stoichiometry to explore the performance of our approach in experiments. I could demonstrate, in combination with simulations, that it can provide reliable estimates of up to 18 fluorescent emitters at a time resolution of approximately 200 ms. Furthermore, I inspected the dependency of the estimation bias and precision on the laser intensity, the analysis time and the number of expected molecules in detail. My results designate the scope for future stoichiometry determinations. In initial experiments, I analyzed the labeling distributions of different fluorescent probes. In addition, I could combine our counting approach with super-resolution STED-microscopy and identify critical parameters for possible applications

Charakterisierung und Anwendung der Photonenstatistik in Einzelmolekülmessungen zur quantitativen Untersuchung fluoreszenzmarkierter Proben

Das Fehlen quantitativer Methoden in der Fluoreszenzmikroskopie verhindert eine präzise Untersuchung molekularer Prozesse. Die Einzelmolekülfluoreszenzspektroskopie bietet verschiedene Möglichkeiten die Stöchiometrie fluoreszenzmarkierter Proben nicht-invasiv zu bestimmen. Eine Möglichkeit nutzt das Antibunching, ein Phänomen von Einzelphotonenemittern, zur Schätzung von Anzahl und Helligkeit der Emitter. In vorhergegangenen Arbeiten wurde die erfolgreiche Anwendung dieser Methode für maximal fünf Farbstoffmoleküle demonstriert, jedoch nicht weitergehend charakterisiert. Daher habe ich in dieser Arbeit die Robustheit der Schätzmethode untersucht und weiter verbessert. Ich habe verschiedene Fluoreszenzsonden mit definierter Stöchiometrie entwickelt, mit denen ich die Methode experimentell untersuchen und mit simulierten Daten vergleichen konnte. In verschiedenen Experimenten konnte ich zeigen, dass die Methode zuverlässig bis zu 18 Moleküle mit einer Zeitauflösung von 200 ms zählen kann. In weiteren Untersuchungen habe ich die Abhängigkeiten des systematischen Fehlers und der Präzision des Schätzers von der Laserintensität, der Zeitauflösung und der Anzahl der Moleküle untersucht. Damit konnte ich den Bereich zukünftiger Anwendungen eingrenzen. In ersten Arbeiten konnte ich damit den Markierungsgrad verschiedener Fluoreszenzsonden untersuchen. Zusätzlich konnte ich die Methode in Verbindung mit der STED-Mikroskopie charakterisieren und kritische Parameter für eine mögliche Anwendung identifizieren.

Contents

1. Introduction

The understanding of complex processes in living organisms is of emerging interest for today's science. The rapid development of current microbiological techniques allows nowadays the observation of single proteins at work.[1, 2] The interactions and kinetics are tangible on the most basic level of single molecules. We begin to grasp the working principles and to imagine how proteins can effect a response of the complete system. Recurrent enhancing or mitigating effects of single proteins influence the cellular environment, and sometimes the proteins might even team up to amplify their stimulus.[3] A good example, which has recently drawn enormous interest because of the Nobel Prize in 2012,[4] are the G-protein coupled receptors (GPCRs).[5, 6]
To shed light on the number of involved molecules, quantitative methods are necessary. However, some requirements need to be met. The native role of proteins can only be monitored in the living cell, therefore the method needs to be non-invasive. As we are interested in the dynamics and basic mechanisms, away from the thermal equilibrium, we require information on the single molecule level. These requirements complicate the development of quantitative methods in single-molecule experiments.
A prominent method to obtain information from living systems is fluorescence microscopy.[7] As a non-invasive, fast and sensitive method, it seems perfectly suited to acquire quantitative information. However, due to the wave nature of light and inherent diffraction, the resolution is limited to a few hundred nanometers [8] and therefore orders of magnitude above the size of single proteins.[9] Single entities cannot be discerned and their actual number is not accessible. Different approaches to obtain dynamics and changes in stoichiometry have to be applied.
A common requirement for all methods to be developed is the possibility to observe single molecules. Fluorescence spectroscopy is perfectly suitable because of the high signal to noise ratio.[10] The fluorescence emission can be separated spectrally from excitation and the signal to noise ratio is large. Another important feature is the possibility to detect single photons in the visible spectrum with high efficiency, e.g. by avalanche photo diodes (APDs). A drawback, however, is the relatively large observation volume, limited by diffraction. It has to be ensured that only single molecules are measured at a time. This can be achieved by diluting or by immobilizing the fluorophores. The acquired data differs by method, as in solution experiments the observation time is limited to the short time, the molecule diffuses through the observation volume and many molecules can be observed for a short time. By immobilization, the same single molecule can be observed until photobleaching occurs.
Single-molecule spectroscopy is a standard tool in molecular biology and many techniques have been developed to obtain quantitative data from samples. In the next section I will introduce the most prominent quantitative methods and reveal advantages and drawbacks.

1.1. Quantitative Methods in Fluorescence Spectroscopy

1.1.1. Ensemble Spectroscopy

Quantitative information by spectroscopic methods can be obtained using of absorption spectroscopy.[10] To determine the concentration of chemicals in a solution the absorbance $A(\lambda)$ can be measured.[11] By referring to a known molar absorption coefficient $\epsilon_{\text{abs}}(\lambda)$ the relative decrease in excitation intensity (I/I_0) at selective wavelengths λ can be linked via Lambert-Beer's Law [12] to the average concentration c inside the beam path with length d.

$$\mathrm{A}(\lambda) = \log \frac{I}{I_0} = \epsilon_{\text{abs}}(\lambda) c d \tag{1.1}$$

The acquired information is the weighted sum of all solute concentrations and the detection limit is determined by the inherent shot noise of the light source and the sensitivity of the detector.[13, 11]
In recent years many endeavors have been made to measure the absorbance of single molecules at cryogenic [14] as well as at room temperature.[15, 16, 17] As the absorption cross-section of a single molecule ($2.5 \cdot 10^{-16}\,\mathrm{cm}^2$ for ATTO 647N) is small compared to the diffraction limited excitation volume ($2.8 \cdot 10^{-9}\,\mathrm{cm}^2$), a sophisticated setup is required to detect the low signal in the noise of the excitation source.

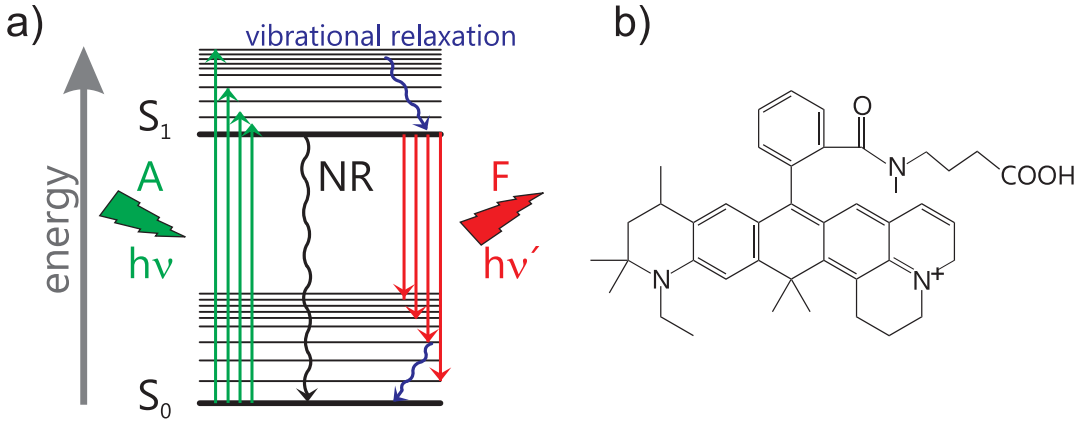

Figure 1.1.: a) Image of a Jablonski diagram, showing the Stokes shift. By absorption A of an incident photon (green) a vibrational excited electronic state S_1 is occupied, but relaxes very fast via vibrational relaxation (blue) to the electronic excited state S_1. The average lifetime of S_1 ground state is about nanoseconds. The relaxation to the ground state S_0 can be non-radiative (NR, black) or upon emission of a fluorescence photon with longer wavelength (red, F). b) Structure of the commercially available dye ATTO 647N.

The detection of fluorescence is a more sensitive approach because the emission from the excited electronic state S_1 to the electronic ground state S_0 can be spectrally separated from excitation. During the absorption and emission process some energy is lost

in vibrational relaxations and emitted photons show longer wavelengths than incident photons (Stokes shift,[18] see Figure 1.1 a)). Sensitive detectors in the visible spectrum allow the measurement of weak signals, even from single molecules in the observation volume.[14, 19]
Fluorescence properties like signal strength, wavelength, etc. differ between available fluorescent molecules in the visible spectrum. Generally, the fluorescent label should be bright to achieve a high signal to noise ratio, show no blinking, to achieve consistent photon emission over time, and be photostable to allow data acquisition without any bleaching events. Most prominent labels in cell biology are fluorescent proteins, quantum dots and organic fluorophores.[20] In this thesis, the organic dye ATTO 647N was generally applied (see Figure 1.1 b)), because of the convenient labeling of probes via NHS ester reactions,[10] the large molecular brightness and the photostability.
The molecular brightness p_{MB} [21] of fluorescent emitter is defined in this thesis, as the probability to detect a photon from a single molecule in a single excitation cycle. This definition is convenient for pulsed laser excitation and therefore for describing my results in the following sections.

$$p_{\mathrm{MB}} = \frac{I(x,y)}{h\nu \cdot \mathrm{LF}} \cdot \sigma_{\mathrm{abs}} \cdot \Phi_{\mathrm{f}} \cdot \eta_{\mathrm{det}} = \mathrm{E_{ph}}(x,y) \cdot \sigma_{\mathrm{abs}} \cdot \Phi_{\mathrm{f}} \cdot \eta_{\mathrm{det}} \tag{1.2}$$

In equation (1.2) I is the local laser power in [W/cm^2], $h\nu$ is the energy of the photons in [J], LF is the repetition rate of the laser in [Hz], σ_{abs} the absorption cross-section in [cm^2], Φ_{f} the quantum yield, η_{det} the detection efficiency of the setup and $\mathrm{E_{ph}}(x,y)$ is the energy per laser pulse in [photons/cm^2].
For a better understanding, the equation can be split into three parts. The local pulse energy $\mathrm{E_{ph}}(x,y)$ multiplied by the absorption cross-section σ_{abs} describes the probability of the molecule to become electronically excited. The Quantum Yield Φ_{f} is the efficiency of the fluorescent transition to emit a fluorescence photon by relaxation from the excited state and is defined as:

$$\Phi_{\mathrm{f}} = \frac{\text{number of emitted photons}}{\text{number of absorbed photons}} \tag{1.3}$$

Finally, the detection efficiency η_{det} describes the probability to measure an emitted fluorescent photon at the detector.
The ATTO 647N dye shows a molar absorption cross-section of about $2.5 \cdot 10^{-16}\,\mathrm{cm}^2$, a Quantum Yield Φ of 65% and the absorption and emission maxima at 644 nm and 669 nm, respectively.
The photostability of organic dyes is dependent on experimental parameters, like measurement buffer or laser power.[22] The photostability is in the range of seconds for ATTO 647N in phosphate buffered saline (PBS) buffer. There exist different buffer systems which increase the photostability by orders of magnitude and have been optimized for individual emitter.[23, 24, 25] ROXS has shown to work best with ATTO 647N and is therefore generally applied in this work. The working principle of ROXS is shown in Figure 1.2.

The fluorescence emission ($\mathrm{k_{fl}}$) is the transition from the excited electronic state $\mathrm{S_1}$ to the ground state $\mathrm{S_0}$. The rotational and vibrational states relax very fast and have no

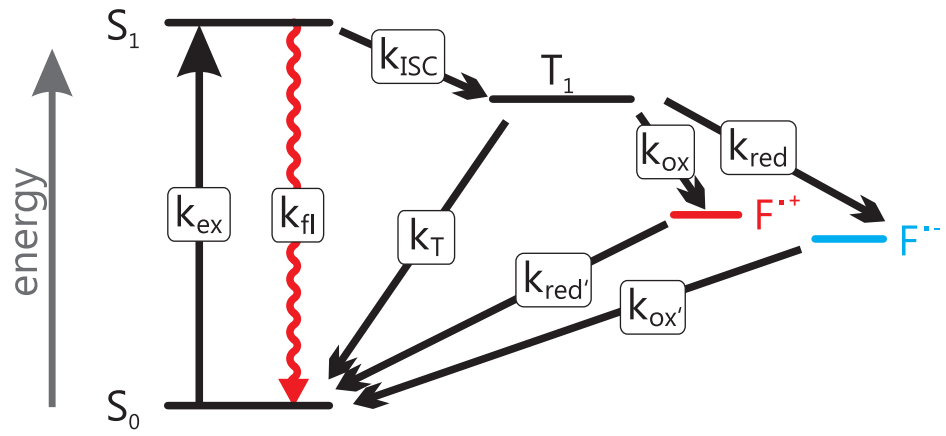

Figure 1.2.: Jablonski diagram of an organic fluorophore depicting the ROXS concept. The electronic S_1 is populated upon photon absorption (k_{ex}). The electronic S_1 state is depleted by fluorescence emission (k_{fl}) and intersystem crossing (k_{ISC}). The long living triplet state T_1 is effectively depleted via electron transfer by an oxidizing (k_{ox}) or a reducing (k_{red}) agent. The radical state $F^{\cdot+}$ or $F^{\cdot-}$ is then reduced ($k_{red'}$) or oxidized ($k_{ox'}$) by the respective agent and transfered to the ground state S_0. Thereby, the slow triplet depletion rate k_T is circumvented.

importance here. A competing transition is the intersystem crossing (k_{ISC}) to the T_1 state. The transition is like the reverse transition to S_0 (k_T) spin forbidden. Hence, the triplet lifetime is generally long (about 27 ms for ATTO 647N [20]).
The basic idea of ROXS is the effective depletion of the triplet state and therefore minimizing the time of the fluorescence molecule residing in the triplet state. The long living triplet state prevents fluorescence emission and is an initial state for photobleaching pathways.[26] Oxygen is known as a very effective triplet quencher, however the radical form promotes bleaching and is generally removed from stabilizing buffers.[27, 26] There are various other reducing and oxidizing agents, each with their individual reduction and oxidation potential.[23] The triplet state is reduced or oxidized to a radical ion forming the state $F^{\cdot+}$ or $F^{\cdot-}$, respectively. The radical ion states are rapidly depopulated to the singlet ground state S_0, by the equivalent oxidizing ($k_{ox'}$) or reducing agent ($k_{red'}$). For the ATTO 647N dye a mixture of ascorbic acid (AA) and 1,1'-Dimethyl-4,4'-bipyridinium dichloride (MV) have been found to effectively prevent blinking and improve photostability of fluorescence emission.[23]
The superior signal and selectivity in fluorescence spectroscopy has been applied in microscopy. Taking advantage of spatial resolution in light microscopy and the sensitivity of fluorescence detection, this combination is an indispensable tool in cell biology [9] and many other scientific fields today, where dynamic information with high specificity is required.

The resolution is limited in fluorescence microscopy by diffraction (see Figure 1.3). Even the signal of a point source is smeared out by diffraction to a broad signal on the

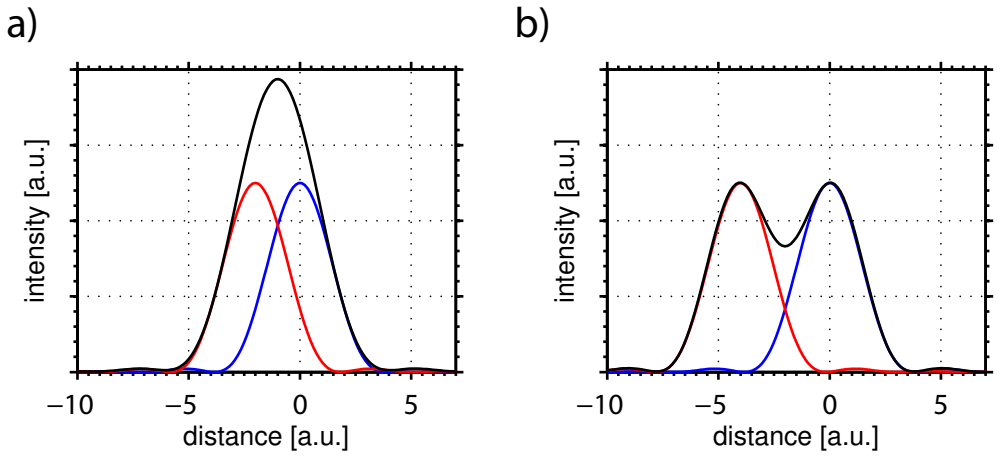

Figure 1.3.: Two distinct molecules cannot be resolved to arbitrary distances by light microscopy. Due to diffraction, the signal on the detector is broadened and the individual signals cannot be separated below the resolution limit. The overall signal could also originate from a single emitter with twice the brightness. In a), the two molecules cannot be resolved because they are closer than the resolution limit. The superposition of both PSFs shows no features of the two underlying PSF's anymore. In b), the resolution limit is depicted. Here, the first zero crossing of the red PSF is located below the peak of the blue PSF. The superposition of the two molecules shows a dip in intensity.

detector, the point spread function (PSF). This implies that two fluorescent emitters cannot be distinguished if their distance Δx is less than the resolution limit, which was first defined by Abbe:[28, 29]

$$\Delta x = \frac{0.61\lambda}{\mathrm{NA}} \approx \frac{\lambda}{2n_{\mathrm{ref}} \sin \alpha_{\mathrm{obj}}} \tag{1.4}$$

λ is the wavelength of the detected light and NA is the numerical aperture which depends on the refractive index n_{ref} of the media between specimen and the front lens and the opening angle α_{obj} of the lens. Below the resolution limit, about 250 nm in a typical microscope setup, several fluorescent molecules appear as one single emitter with high intensity. A direct approach of counting, by discerning single entities in space, is not feasible anymore (see Figure 1.3). The size of a fluorescent molecule is few nm and therefore many emitters can reside in a resolution limited spot. However, in fluorescence microscopy several different approaches have been developed to estimate the number of observed molecules beyond the limitation in resolution.

1.1.2. Intensity Reference Approaches

Fluorescence spectroscopy is not inherently a quantitative approach. An obvious measure for the observed number of emitters is the fluorescence intensity. Its use though,

to count the number of emitting molecules is not as straight forward as one might expect. The fluorescence intensity of n emitters can be larger than the intensity of n+1 emitters, since the molecular brightness (MB) p_{MB} depends on environmental parameters (see equation 1.2). In experiments, these parameters can be affected in a non-controllable manner. For example, the excitation intensity may vary locally. The quantum yield of individual emitters can be altered by the microenvironment due to solvent effects (viscosity, pH) as well as in presence of fluorescence quenchers or conjugated molecules.[30, 31]
The fluorescence intensity can be measured very fast and is inherently obtained in fluorescence microscopy. Thus, different methods have been developed to estimate the number of emitting dyes. A straight forward approach for this is to measure the mean intensity of a calibration standard with a reliable and known number of labels. The standard should be acquired on the specific setup with the same experimental conditions, preferably together with the experiment of interest. The fluorescence images then can be referenced by the intensity standard and a simple estimation of numbers can be obtained. The method is highly sensitive to the robust preparation of the standard sample and to its photophysics. The approach is used in samples with large emitter numbers, for example in abundant protein expression.[32, 33, 34, 35, 36, 37] On the single-molecule level, this approach can be applied by acquiring the probability distributions of photon emission for different label numbers in reference to the data of single molecule emission. By this, a reliability function can be calculated, assigning the measured intensity to the number of emitters. Because of broad intensity distributions for emitter numbers larger than 5, however, no unambiguous assignment can be found. The method has been applied to identify up to 4 emitters in experiments.[38]

1.1.3. Intensity Fluctuation Based Approaches

In 1972, Magde et.al. [39] introduced fluorescence correlation spectroscopy (FCS). In FCS the intensity fluctuations due to molecules diffusing in and out of the focal volume are measured. Because the diffusion time is in the order of ms, the fluorescent signal needs to be acquired with high time resolution. By using avalanche photo diodes (APDs) for example, which are read out by time correlated single photon counting (TCSPC) devices, the photons can be registered with ps resolution. The diffusion time of emitters can be determined by correlation of the acquired photon times.
FCS is widely applied for diffusion measurements, but methods have been developed, which can estimate the mean number in the focal volume from the same data. Methods like photon counting histogram [40] or fluorescence intensity distribution analysis [41] look at the accumulated photon emission statistics. In these methods the number of emitters and their mean molecular brightness can be estimated from the additional broadening of emission statistics by intensity fluctuations.
The photon emission statistics of steady, single emitters follows poissonian statistics.[8] Therefore, the photon counts per time bins arriving at the detector $p(\mathrm{W})$ are also Poisson distributed. Put into a solution the emitters are diffusing through the Gaussian excitation volume and the number of observed particles fluctuates, which broadens the detected distribution because of the increased variance.

The detection process in single photon detectors, like APDs and photomultiplier tubes (PMTs) exploits photo-induced charges in the detector material. The signal is then subsequently amplified to yield an electronic signal. The process has been described semi-classically and the resulting photon counting statistics has been deduced to [42]

$$p(k) = \int_0^\infty Poi(k, \mathrm{W}) p(\mathrm{W}) d\mathrm{W} = \int_0^\infty \frac{\mathrm{W}^k \, \mathrm{e}^{-\mathrm{W}}}{k!} p(\mathrm{W}) d\mathrm{W} \tag{1.5}$$

where k is the average number of photons detected. Therefore the probability to detect k photons p(k) is broadened by the poissonian photon detection process, generally referred to as "shot noise". By modeling the confocal excitation volume, the fluorescence intensity $p(\mathrm{W})$ can be replaced by the photon emission probability for single molecules $p^{(1)}(k)$. The photon count distribution of n particles $p^{(n)}(k)$ can then be described as the convolution of $n \times p^{(1)}(k; V_0, p)$

$$p^{(n)}(k) = \underbrace{p^{(1)} \otimes \cdots \otimes p^{(1)}(k; V_0, p_{\mathrm{MB}})}_{n\,times} \tag{1.6}$$

where V_0 is the modeled confocal volume and p_{MB} is the molecular brightness. The experimentally acquired photon count statistics can be fitted by the theoretical distribution and the mean number of observed particles is estimated. The result is the average number over several molecules. A slightly different and faster approach has been made by acquiring the photon counting statistics of a single dye molecule $p^{(1)}(k)$ experimentally with similar results.[43] These methods have been applied measuring the concentration of molecules in solution,[40] but also the aggregation state of proteins up to 3 molecules has been identified.[44]

The idea to analyze intensity fluctuations has been modified in the Number&Brightness method for measurements in microscopic images.[45] Here, not the complete photon emission statistics is acquired, but only the first two statistical moments, the mean and the variance, are observed. The estimated number of fluorophores n and the molecular brightness p_{MB} are derived from considerations about the dependence of both mean $\langle k \rangle$ and variance of the fluorescence emission σ^2 on the mean number of particles and their brightness.[46]

$$p_{\mathrm{MB}} = \frac{\sigma^2}{\langle k \rangle} \qquad n = \frac{\langle k \rangle^2}{\sigma^2} \tag{1.7}$$

The necessary data can be acquired much faster and the computational effort to analyze a complete image is highly reduced. This method has been applied to quantify protein aggregation with spatial resolution up to cluster sizes of about 15.[47, 48] Nevertheless, as the method derives the estimates only from the first two statistic moments it might be considered as vague. The estimations of the number of particles and molecular brightness in solutions were confirmed by PCH,[45] yet, a measurement of a reliable probe with large number of emitters is missing. All fluctuation methods require the diffusion of emitter numbers inside the focal volume. No information about immobile emitters can be obtained and the estimations only give the average number of labels in the focal volume during data acquisition and therefore have to be interpreted with care.

1.1.4. Time Resolved Approaches

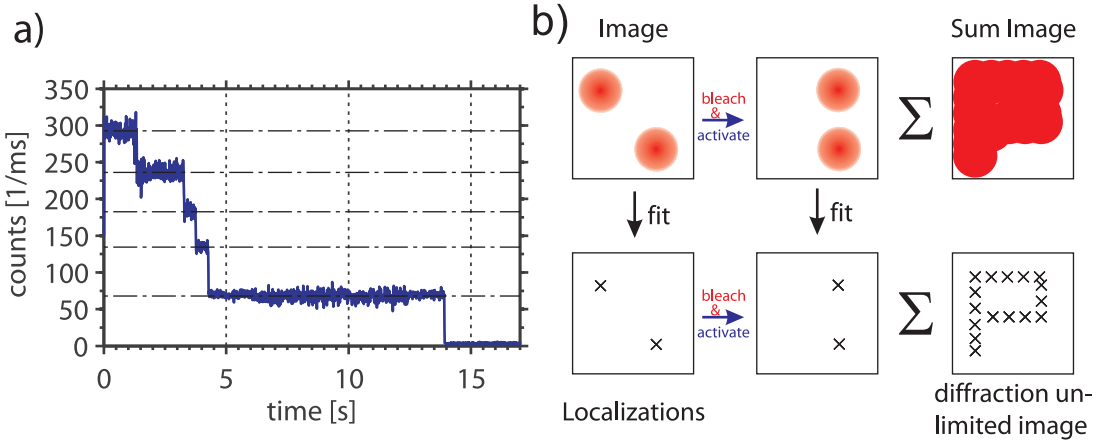

Figure 1.4.: a) Fluorescence transient with five consecutive bleaching steps (horizontal grid lines) indicating five initial emitters. The drops in intensity of 55 kHz, 51 kHz, 49 kHz, 69 kHz and 68 kHz are not equally spaced. b) PALM principle: By activation of a subset of photo-activatable fluorescent proteins, single molecules can be observed until photobleaching occurs. The point spread functions of these single emitters are fitted and their maxima are localized. By accumulating all localization information, an image with 10-fold resolution can be obtained, which shows more details than the sum image.

Other quantitative methods separate the molecules in time and counting is achieved either by observation of consecutive bleaching events,[49, 50] or by application of photo-activated localization microscopy (PALM).[51, 52, 53]
Bleaching step (BS) analysis observes the consecutive drops in fluorescence intensity due to photobleaching (see Figure 1.4 a)). As long as the intensity drops are well separated in time, they can be identified in the fluorescence transient and and a number estimate is obtained. The bleaching steps can however be disguised by complex photophysics, for example blinking or molecular states with different molecular brightness, or by synchronous bleaching of multiple fluorescent emitters. The probability for these events scales with the number of molecules to be counted. Nevertheless, bleaching step analysis could be successfully applied to observe protein clusters of five in the cell membrane.[54]
In a similar manner this approach can directly be applied in PALM (see Figure 1.4 b)). PALM circumvents the resolution limit by observing subsequently a subset of single molecules in time until photobleaching. The diffraction limited signal on the detector, the PSF, is known and the location of the emitting molecule can be determined with the localization precision.[55]
For application in microscopy the observation of single fluorescent emitters in the resolution limited excitation volume has to be ensured, while the other residing molecules must not fluoresce. Photoactivatable fluorescent proteins can be switched stochastically by light with short wavelength from a dark state to an emissive state.[56, 57] The

photo-activation rate hereby is dependent on the laser power and should be chosen low enough to ensure activation of only a sub-population of single fluorophores. The emissive fluorescent proteins are then observed until photobleaching occurs and a new subset is activated. By cycling this process many times, a complete image of single molecule localizations can be obtained with the localization resolution (see Figure 1.4). By counting the number of bleaching events of fluorescent emitters at a single spot, this method can be quantitative. However, each molecule has to be observed exactly once and without blinking. Therefore, many activation-bleaching cycles have to be run at low activation intensity and over a long time period to ensure the photoactivation of each molecule.
Acquiring PALM images has been used to analyze clusters of up to a few hundred fluorescent emitters.[58, 59] But data acquisition is time intensive, as the acquisition time scales with the number n and the switching rate, which has to remain low to assure single molecule observation. Like with bleaching step analysis, it is inherently not possible to obtain dynamics due to the destructive character of the methods, i.e. the measurement cannot be repeated for the same sample.

1.1.5. Resonance Energy Transfer

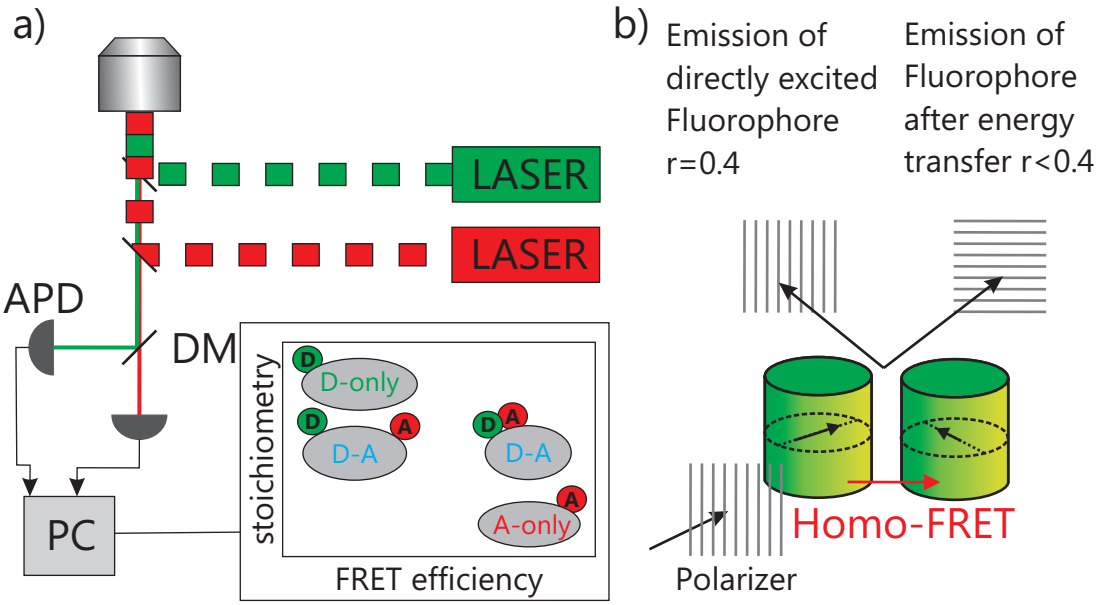

Figure 1.5.: a) Scheme of alternating laser excitation. The interleaved red and green excitation pulses allow the detection of FRET and Stoichiometry at the same time. Species with different label numbers and conformations can be differentiated in the S-E histograms (see inset).[60] b) Principle of fluorescent anisotropy measurements. The polarized excitation light is depolarized by the absorption and emission process of a single molecule. Upon an additional energy transfer in Homo-FRET the depolarization increases further.

A tool to observe distances between two fluorescent emitters is Förster energy transfer (FRET).[61] The energy of an excited fluorescent emitter (donor) is transferred via dipole-dipole coupling to a nearby molecule (acceptor). The FRET rate k_{FRET} is highly dependent on the distance R:

$$k_{FRET} = \frac{1}{\tau_{\mathrm{D}}} \left(\frac{R_0}{R} \right)^6 \tag{1.8}$$

$$R_0^6 \propto \frac{\kappa^2 \Phi_D}{n^4} \Gamma \tag{1.9}$$

Here, τ_{D} is the lifetime of the donor, R_0 is the Förster distance for a particular donor-acceptor pair, defined as the distance at which FRET efficiency is 50%. κ is the dipole-dipole orientation factor, Φ_{D} is the quantum yield of the donor fluorophore, n is the refractive index and Γ is the spectral overlap between donor and acceptor. The overlap between fluorescence excitation and emission spectra can be small for identical fluorophores (homoFRET) due to the Stokes-shift. By choice of a suitable FRET-pair of a donor and acceptor, the spectral overlap can be maximized. The donor emission F_{donor} is then red-shifted compared to the acceptor emission F_{acceptor} (heteroFRET) and the FRET signal can be detected separately from donor emission. The FRET efficiency E_{FRET} is defined as:

$$E_{\mathrm{FRET}} = \frac{F_{\mathrm{D_{ex}}}^{\mathrm{A_{em}}}}{F_{\mathrm{D_{ex}}}^{\mathrm{A_{em}}} + F_{\mathrm{D_{ex}}}^{\mathrm{D_{em}}}} \tag{1.10}$$

The detection of FRET signal indicates the proximity of FRET partners and can be used to observe dimerization.[62] Higher oligomers cannot be identified because of the binary signal output.
But methods have been developed which can probe the stoichiometry by alternating laser excitation (ALEX [63]) or pulsed interleaved excitation (PIE [64]). Thereby the donor and the acceptor fluorophores are excited in alternative manner and a stoichiometry term can be calculated from acquired intensities:

$$S = \frac{F_{\mathrm{D_{ex}}}^{\mathrm{A_{em}}} + \gamma F_{\mathrm{D_{ex}}}^{\mathrm{D_{em}}}}{F_{\mathrm{D_{ex}}}^{\mathrm{A_{em}}} + \gamma F_{\mathrm{D_{ex}}}^{\mathrm{D_{em}}} + F_{\mathrm{A_{ex}}}^{\mathrm{A_{em}}}} \tag{1.11}$$

$F_{\mathrm{D_{ex}}}^{\mathrm{A_{em}}}$ is the fluorescence intensity of the acceptor upon donor emission, $F_{\mathrm{D_{ex}}}^{\mathrm{D_{em}}}$ is the fluorescence intensity of the donor upon donor emission, $F_{\mathrm{A_{ex}}}^{\mathrm{A_{em}}}$ is the fluorescence intensity of the acceptor upon acceptor emission and the factor γ corrects for crosstalk between donor and acceptor. Through the stoichiometry the number ratio of acceptors and donors is obtainable also for higher oligomers [65](see Figure 1.5). This cannot be used to estimate absolute numbers from the fluorescence signal, though.
In contrast, the cluster size of fluorescent molecules can be obtained by observation of homoFRET in fluorescence anisotropy imaging measurements (FAIM).[66, 67] Fluorescence absorption is sensitive to the polarization of the excited light, as it couples via the dipole moment of the fluorescent dye. The detected anisotropy r_{homoFRET} is generally defined as:

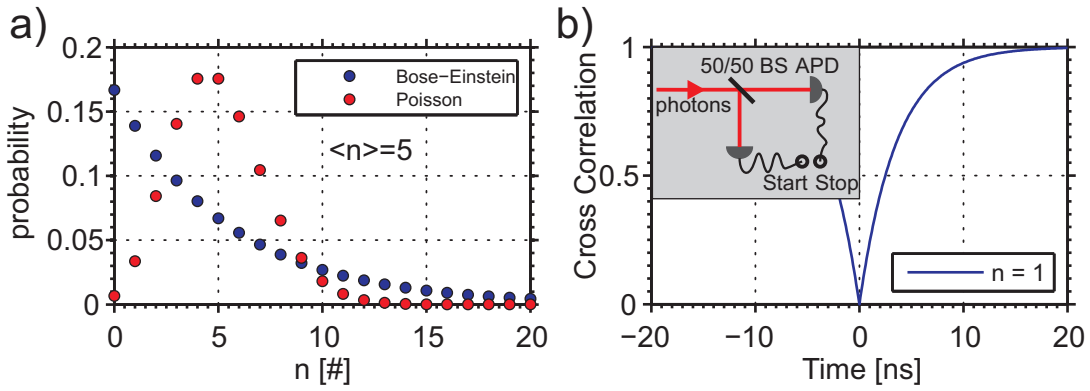

Figure 1.6.: a) Photon counting distributions for different emitter types. The classical thermal emission shows Bose-Einstein statistics, while the quantum emitter follows a Poisson distribution. b) Fluorescence cross correlation of fluorescence emission from a single molecule. In the inset a Hanbury-Brown Twiss setup is shown, by which the inter-photon times can be measured.

$$r_{\text{homoFRET}} = \frac{I_{\parallel} - GI_{\perp}}{I_{\parallel} + 2GI_{\perp}} \tag{1.12}$$

Hereby $I_{\parallel}$ is the detected signal parallel to the excitation polarization and $I_{\perp}$ perpendicular to it. The factor G is a calibration factor for the different sensitivity of the detector to parallel or perpendicular light.
By FRET the polarization of the signal is reduced, because energy is transmitted in an additional dipole-dipole interaction and therefore the distributions of orientations is wider. The depolarization dependence on the cluster size and the inter-fluorophore distance has been derived by Runnels et.al..[68] Nevertheless, there are some inherent limitations to that method. FAIM requires that the emitters are not perfectly aligned, because by this the polarization would remain. Even a correlation between the emitter orientation prevents application of the proposed theory to count clusters. Additionally, because of diffraction limited microscopy, the obtained anisotropy is accumulated from all molecules and clusters inside the observation focus. The sizing relation may therefore give only an average value.[69] HomoFRET has since been used to measure clusters up to four emitters, because the change in anisotropy diminishes rapidly with numbers.[70, 71, 72, 62]

1.1.6. Photon Antibunching based Approaches

The photon-number statistics of light is dependent on the process of emission.[8, 73] If the photon source is thermal and emits black body radiation, the occupied energy levels in thermal equilibrium are described by the Boltzmann distribution:[29]

$$P\left(E_n\right) \propto \mathrm{e}^{\left(-\frac{E_n}{kT}\right)} \tag{1.13}$$

E_n is the quantified energy level, k_B is the Boltzmann's constant and T the temperature. If we further use the energy quantization relation from the resonator model $E_n = \left(n + \frac{1}{2}\right) h\nu$, with h as Planck's constant and ν as the resonator frequency, we can write the probability distribution of finding n photons as

$$P(n) = \frac{1}{\langle n \rangle + 1} \left(\frac{\langle n \rangle}{\langle n \rangle + 1} \right)^n \tag{1.14}$$

The probability distribution $P(n)$ of the Bose-Einstein statistics is shown in Figure 1.6 a). The average number of excited molecules $\langle n \rangle$ is given by

$$\langle n \rangle = \frac{1}{\exp(h\nu/kT) - 1} \tag{1.15}$$

The variance of the distribution can be calculated to

$$\sigma_n^2 = \langle n \rangle + \langle n \rangle^2 \tag{1.16}$$

For coherent light the emission statistics are different. When we assume a constant mean photon flux J [photons/s], the average number of detected photons $\langle n \rangle$ in a time interval t_bin is

$$\langle n \rangle = J t_\mathrm{bin} \tag{1.17}$$

To obtain the number statistics we need the probability to find n photons in equally spaced time bins. As long as the detection events are independent, this is a Poisson process and the distribution is poissonian (see Figure 1.6 a)):

$$P(n) = \frac{\langle n \rangle^n \exp\left(-\langle n \rangle\right)}{n!} \tag{1.18}$$

The variance σ of the Poisson distribution is given by

$$\sigma_n^2 = \langle n \rangle \tag{1.19}$$

Both phenomena show a variance of at least the Poisson variance, but quantum mechanical processes exist, which reduce the randomness in the photon stream and show a lower variance. As a measure the Mandel parameter Q [74] can be introduced and describes the similarity to Poissonian statistics:

$$Q = \frac{\langle n^2 \rangle - \langle n \rangle^2}{\langle n \rangle} - 1 \tag{1.20}$$

The Mandel parameter is zero for poissonian statistics and positive for chaotic light, like black body radiation. This is also called photon bunching, because of the low order parameter the photons generally arrive in packs at the detector. If the Mandel parameter is $-1 \leq Q < 0$, the statistics are sub-poissonian and the photon stream shows photon antibunching. In case of $Q = -1$ the photons are equally spaced in the photon stream.
The most convenient way to measure the inter-photon times is by cross-correlation

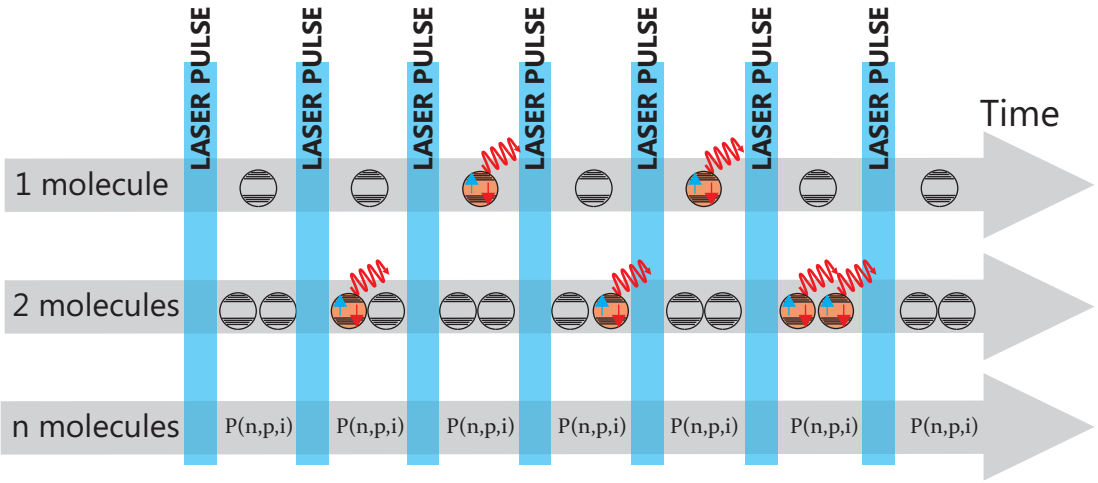

Figure 1.7.: The detection probability of mDE is dependent on the number of molecules residing in the focal volume. A single molecule emits only a fluorescent photon with its molecular brightness p_{MB}. Two molecules will have a certain probability to emit 2 simultaneous photons of p_{MB}^2. The detection probability $\mathrm{P}(n,p_{\mathrm{MB}};i)$ for i simultaneous photons out of n molecules is described in equation (1.24).

$g^{(2)}(\tau)$ of signals from two detectors in an Hanbury-Brown Twiss (HBT) setup [75] (see Figure 1.6 b)).

$$g^{(2)}(\tau) = \frac{\int I(t)I(t+\tau)dt}{\int I(t)^2 dt} \tag{1.21}$$

In a HBT detector scheme the incoming photon stream is split by a 50/50 beamsplitter to two detectors. By calculating the cross-correlation, the Mandel parameter is directly accessible from $g^{(2)}(0)$

$$g^{(2)}(0) = 1 + \frac{Q}{\langle n \rangle} \tag{1.22}$$

Therefore, the cross-correlation shows a value of 1 for Poisson statistics and for antibunching a value of 0 at lag times τ zero.
At first the photon antibunching effect has been observed in fluorescence spectroscopy in 1977 [76] and later with single fluorescent molecules.[77] Photon antibunching occurs, because the fluorescent molecules are single photon emitters. Simplified, a fluorescent molecule undergoes mostly transitions between two electronic states, the ground state S_0 and the excited state S_1. Upon absorption of a photon the molecule is promoted into to the excited state and resides there for approximately the fluorescence lifetime. By emitting fluorescence the molecule relaxes to the ground state and is available for excitation again (see Figure 1.1). Here, we make the assumption that the molecule cannot be further excited from the excited state S_1, which is justified only for low laser intensities. But, as we generally observe only the emission from the S_1 state, we are not able to recognize higher order excitation, except by an increased bleaching rate.[26]

Since the quantum system can solely occupy a single state at a time, it synchronizes the fluorescent emission and increases the ordering of emitted photons. Therefore, the second order correlations of single molecule fluorescence emission show the remarkable photon antibunching dip at $g^{(2)}(0)$. By increasing the number of fluorescent emitters n, the antibunching dip diminishes by $1 - \frac{1}{n}$. This approach has been used to prove the observation of single molecules.[77, 78, 79]
With pulsed laser excitation the photon antibunching can be seen from a stochastic point of view (see Figure 1.7). Each laser cycle can be considered as a trial to probe the occurrence of multiple detection events (mDE). For a single emitter the probability for mDE should approach zero and rises with emitter numbers. Photon antibunching with pulsed laser excitation, namely coincidence analysis, has since been used to count up to 2 molecules.[80, 81, 82, 83]
It should be noted, that all pulsed laser experiments apply an excitation scheme with

$$\tau_{\text{Laser Pulse}} \ll \tau_{\text{Lifetime}} \ll \tau_{\text{Laser Frequency}} \tag{1.23}$$

where the pulse duration $\tau_{\text{Laser Pulse}}$ is smaller than the fluorescent lifetime τ_{Lifetime} and the laser repetition $\tau_{\text{Laser Frequency}}$. Thereby, it is avoided that single fluorescent dye emits 2 photons in a single laser cycle.[84]
Following the idea of mDE, a different method was introduced by counting by photon statistics (CoPS).[85] An analytical model was developed that describes the probabilities of mDE in dependence of the emitter number n and the mean molecular brightness p_{MB} in the observed volume. This dependency can be described by a recursive and piecewise formula:

$$P\left(n, p_{\text{MB}}; i\right) = \binom{m}{i} \left[\begin{array}{c} \left(1 - \left(\frac{m-i}{m}\right) p_{\text{MB}}\right)^n \left(1 - \left(\frac{m-i}{m}\right) p_b\right) \\ - \sum_{k>0}^{i-1} \frac{\binom{i}{k}}{\binom{m}{k}} P\left(n, p_{\text{MB}}; k\right) \end{array} \right] \tag{1.24}$$

m denotes the number of detectors and i the number of mDE. The background is modeled as a weak fluorophore with a molecular brightness of p_b.
CoPS is a quasi-instantaneous method, because the time resolution depends only on the accumulation of converged statistics and not on photo processes such as bleaching or switching. It has been successfully applied in experiments with a DNA sample labeled with up to five dyes.[86]

1.1.7. Comparison of Existing Methods

We have seen that there are several different methods to obtain quantitative information in single-molecule fluorescence microscopy. They are based on different approaches and show individual limitations and advantages. In Table 1.1 the methods are compared in their most important features.
Most approaches can measure the number of emitters from the fluorescent signal only, however, the intensity based approaches and the intensity fluctuation based approaches

require prior calibration of measurements. This complicates data acquisition in experiments.
The time resolution of methods exploiting photophysical effects, like bleaching or switching, scales with the numbers to be observed and can range from seconds to hours. In contrast, fast methods based on the detection of fluorescence signal only, like intensity calibration or FRET/ALEX/PIE approaches, require only a few µs.
The comparison of the counting limit is not evident as standard samples with different numbers are missing. The methods have been applied to known protein oligomers and solution measurements. Most methods can measure clusters with less than five emitters, however first reports of higher numbers have been stated in N&B and CoPS. PALM is noteworthy, because it is not inherently limited by large numbers, rather by the time to measure sufficient activation and bleaching cycles.
The fluctuation based methods can measure to very large numbers and have been tested in solution measurements. They require diffusion of single molecules inside the focus volume and result in averaged estimates over several single molecules, though.
A very useful feature for molecular biology would be the spatial observation of emitter numbers over time. By measuring a large number of pixels, all methods could be quantitative, but the acquisition time of a single pixel limits the feasibility. Except for PCH, photon antibunching and CoPS, all methods have shown their capability to acquire images of numbers. To determine the stoichiometry over time non-invasive approaches are required. Therefore, methods which exploit bleaching effects cannot measure changes in stoichiometry.

1.2. Motivation

In the previous section we have seen many different methods to obtain stoichiometry from nanoscale environments by fluorescence spectroscopy. They differ highly in each category and no method provides a general solution. An optimal counting method would give an instantaneous result with high counting resolution and would be applicable over a wide range from single molecule counting in protein clusters to thousands in measuring protein expression levels. Additionally, the method should require minimal adaption of experimental conditions, require no prior calibration and allow obtaining number&brightness images over time.
As it can be seen in Table 1.1, there is by far no method which meets all requirements. The most difficult part is presumably the wide counting range. Most methods can reliably count clusters up to 5 emitters and some can also estimate very large numbers in solutions. First results [86] have shown though, that by CoPS it is possible to estimate numbers up to 15 emitters. Further investigations could not be conducted, because no reliable probe with arbitrary numbers between 5 and 100 was available. In this thesis I will present data of a new standard sample by which we could analyze the counting limit of CoPS.
Nevertheless, usually not only the counting limit is of interest, it is rather the counting resolution. In experiments we measure differently prepared samples and we are interested, if there is a change in stoichiometry between samples or not. The differences in observed emitter numbers and the reliability with which these differences can be

Table 1.1.: Table comparing recent quantitative approaches in fluorescence microscopy

method	calibration	typical time resolution	application limit	molecule averaging	invasive	2D	references
Intensity calibration	yes	$>$ few µs	up to 4 by a standard sample; few hundred in cell measurements	no	no	yes	[87, 33]
all photons emission calibration	yes	$\propto n/p_{\text{bleach}}$	up to 3 by oligomerization of fluorescent protein	no	yes	yes	[88]
PCH / FIDA	yes	min	concentration measurements range from nM to µM, up to 2 by protein oligomerization	yes	no	no	[41, 40, 89]
N&B	yes	s	concentration measurements range from nM to µM, up to 15 by cluster observation in cell experiments	yes	no	yes	[45, 47]
FRET	no	µs	protein-protein interactions	no	no	yes	
ALEX / PIE	no	µs	only ratio estimates	no	no	yes	[90, 63, 60]
homoFRET	no	s	up to 5 in protein aggregation	no	no	yes	[68, 71]
bleaching steps	no	$\propto n/p_{\text{bleach}}$	up to 5 in protein oligomerization	no	yes	yes	[49, 50]
PALM	no	$\propto n/p_{\text{bleach}} \cdot k_{\text{activation}}$	quasi unlimited	no	yes	yes	[59, 58]
photon antibunching	no	s	identification of single molecules	no	no	no	[76, 78]
Coincidence Analysis	no	s	up to 2 emitters	no	no	yes	[81, 82]
CoPS (2009)	no	s	up to 5 emitters, first results of 15 emitters	no	no	no	[86, 84]

quantified is of great interest to us. It is similar for time measurements. Knowing the time resolution could help to minimize acquisition time or allow conclusions about dynamics in the sample.
By characterization of the method, it can be applied to complex problems and still reliable results can be obtained. There are several biological problems in the number range between 5 and 15,[91, 92, 93, 94] which could not be investigated.
An advantage of CoPS is also the estimation of the numbers and the mean molecular brightness at the same time. Thus, not only changes in numbers could be observed, but also changes in the brightness, due to environmental or intramolecular effects.

2. Materials & Methods

In the first part of this chapter the optical setups will be described which have been used to acquire fluorescence data. Up to now a confocal microscope has been applied for the application of counting by photon statistics (CoPS). For measurements of CoPS in combination with stimulated emission depletion (STED) microscopy, a new detection device was built, in cooperation with Pit Bingen and Thorsten Staudt (AG Hell, DKFZ, Heidelberg), and it is described here. The necessary changes compared to a confocal setup are pointed out and the detection efficiency of each setup is analyzed. The application of CoPS requires high molecular brightness. Therefore, the achieved detection efficiency is generally of importance and measurements to compare the detection efficiency of individual setups will be presented.
The experimentally acquired data has been compared to simulations. The Monte Carlo (MC) simulations will be introduced and the modeled physical processes will be described. In the later parts the applied probes are described and the preparation of samples is presented. The last part will be about the computational implementation of the model function and the error estimation of a single fit. In further analysis a heuristic error distribution of CoPS is investigated.

2.1. Data Acquisition & Simulations

Before describing the setups, I want to define some variables and units, which are generally used during this thesis:

- The excitation laser in the setups are driven with different repetition rates (confocal = 20 MHz, STED = 18 MHz). Therefore the mean intensity has to be corrected to compare the photons per pulse. During the measurements the laser intensity was measured before the dichroic mirror and the objective. Additionally the beam focus has a Gaussian intensity profile and the intensity is largest in the center. In the simulations, this was not accounted for and a binary excitation profile has been assumed. I corrected for both effects and the laser excitation will be given in µW of the confocal setup.

- The fluorescence intensity will be generally given in kHz. When I describe the photon emission process I will sometimes refer to the probability of photon counts per laser cycle (cplc). For conversion the probability has to be multiplied by the laser frequency.

- The mean molecular brightness p_{cops} estimated by CoPS is generally given in photon counts per laser cycle and molecule (cplcm). In the Figures, when it is

plotted with the intensity, it is multiplied with the laser frequency and gives the mean photon emission of a single molecule at the laser frequency.

– The acquisition time to accumulate statistics of multi detection events (mDE) is generally referred to as t_{ac}.

2.1.1. Confocal Setup

A standard microscope in fluorescence microscopy is the so called confocal setup.[95] The principle is shown in Figure 2.1 a). The out of focus light is blocked in the excitation and detection beam path respectively by use of a pinhole. The detected light therefore originates from the confocal volume, which can be as small a few fL. To acquire microscopic images, the field of view (FOV) is scanned by the focal volume, either by moving the table or the laser focus. The resolution is calculated to:[7, 95]

$$\Delta x_{\mathrm{lateral}} = \frac{0.4\lambda}{\mathrm{NA}} \tag{2.1}$$

λ is the wavelength of light, and NA is the numerical aperture. The achieved resolution is a little bit better than in widefield microscopy because the confocal volume is the product of the excitation PSF and detection PSF. The z-Resolution calculates to

$$\Delta x_{\mathrm{axial}} = \frac{1.4\lambda n_{\mathrm{ref}}}{\mathrm{NA}^2} \tag{2.2}$$

n_{ref} represents the refractive index.

A confocal setup (see Figure 2.1 b)) has been used to acquire fluorescence information of the samples. The excitation source is a 635 nm pulsed picosecond laser diode (LDH-P-635, PicoQuant, Berlin, Germany). It can be operated at repetition rates of 10 MHz to 80 MHz (PDL800B, PicoQuant, Berlin, Germany). The excitation light passes an excitation filter centered at 635 nm (HQ 635/10, AHF Analysentechnik AG, Tübingen, Germany) and is then directed via a telescope (f=16 mm & f=60 mm) with a 100 µm pinhole into an inverted microscope (Zeiss AxioVert $S_1$00-TV, Oberkochen, Germany) using a dichroic mirror (DM) (F53-488, AHF Analysentechnik AG, Tübingen, Germany) to illuminate the back-aperture of a microscope lens (PlanApo 100 ×, NA 1.4, Olympus Corp., Japan). Fluorescence emitted by the sample is collected by the same lens and passes a telescope array (f=50 mm & f=50 mm) for confocal detection with a 100 µm pinhole.
The detection scheme represents an extended HBT array and is split into four beams of equal intensities using three 50:50 beam-splitter (BS). The fluorescence signal passes an emission filter (675/50, AHF Analysentechnik AG, Tübingen, Germany). Four avalanche photon diodes (APDs, SPCM AQR-13, Perkin-Elmer, Waltham, MA, USA), which are operated by 4 synchronized TCSPC-cards SPC 130 (Becker& Hickl, Berlin, Germany) connected to a NI SCB-68 Connector Block (National Instruments, Austin, Tx, USA) detect the photons. The microscope is equipped with a piezo-stage (Physik Instrumente (PI), Karlsruhe, Germany) operated by a controller (PI E501:00, PI) for positioning of the sample in the confocal observation volume with nanometer precision. Stage scanner and photon-counting cards are controlled by custom software modules in

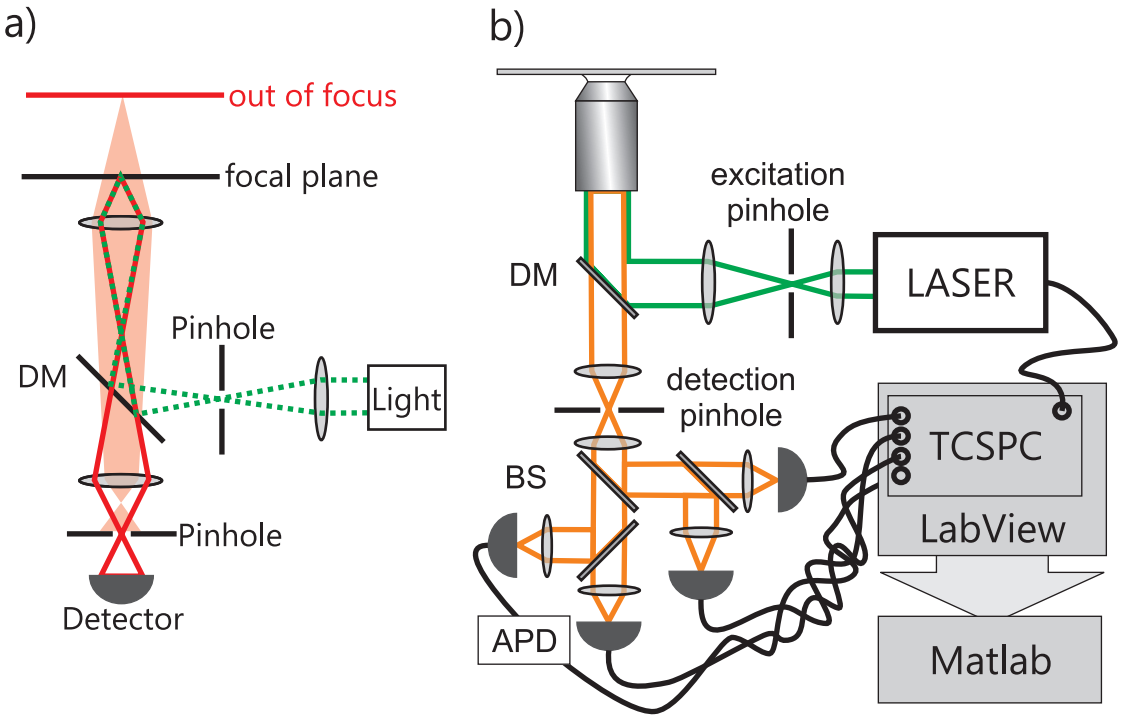

Figure 2.1.: a) Confocal principle: Mainly light from the excitation focus is directed to the detector. The out of focus light is not focused by the lenses at the detection pinhole. b) The confocal setup used for data acquisition. The excitation path corresponds to a confocal setup, while the detection pathway shows an extended HBT setup with an array of four APD. The TCSPC information of the photon stream is saved for later analysis.

LabView (LabView 7.1, National Instruments, Austin, Texas, USA) for synchronized data acquisition.
The microscope software enables the acquisition of images and the Pick & Destroy (PnD) approach.[81] Spots in the acquired image can be picked manually or by a intensity threshold with a peakfinding algorithm. The fluorescence transients of the registered spots are observed one by one with full control of the acquisition time.

During my thesis the microscope setup was under a constant construction and readjustment process. However, a major increase in detection efficiency was obtained by choice of a different objective lens (Zeiss Plan Fluar, 100 ×, 1.45 oil immersion), the removal of the tubus lens from the inverted microscope, removing the detection pinhole and a new fluorescence filter (685/70, AHF). During my thesis only surface immobilized probes have been investigated, so removing of the detection pinhole is justified. For convenience I will refer to the modified setup with Zeiss objective as Zeiss-confocal and to the setup with Olympus objective as Olympus-confocal. The experiments presented here are conducted on both setups. The measurements of Hyp5 and DNA origami have been run with the Olympus-confocal. The nucleotide labeled probe with 4 labels (NuP4) experiments have been accomplished with the Zeiss-confocal.

2.1.2. STED-CoPS Setup

2.1.3. Principle

In the introduction I have shown, that two nearby fluorescent emitters cannot be distinguished at arbitrary distances. The resolution is limited by diffraction to few 100 nm with visible light (see Figure 1.3). Recent methods have been developed to circumvent this barrier, for example localization microscopy (see in Figure 1.4) and reversible saturable optical fluorescence transitions (RESOLFT) microscopy.[96] The principle behind localization microscopy, especially PALM, is explained in 1.1.4. The STED principle and setup components will be explained briefly here, for more details about STED theory it is referred to the associated PhD thesis of Pit Bingen.[97]
The RESOLFT methods circumvent the diffraction limit by silencing the fluorescent emitters in the outer rim of the excitation profile. Thereby, it is assured that fluorescence emission arises from molecules in a spot smaller than the diffraction limited excitation profile (see Figure 2.2). To suppress the emission of fluorescent labels RESOLFT approaches take advantage of saturable molecular transitions. Fluorescence emission is a transition from the excited state S_1 to the ground state S_0. By depleting the S_1 state the fluorescence emission can be suppressed and the emitters are silenced.

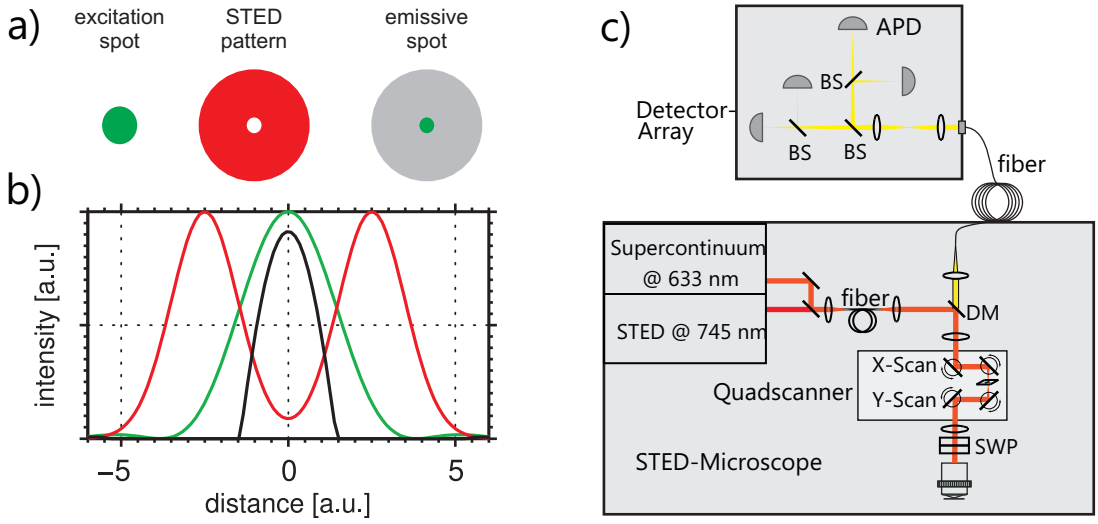

Figure 2.2.: a) Lateral intensity profile of the excitation beam (green), STED beam (red) and overlay. b) Scheme of the intensity profile overlay of the excitation (green,–), STED(red,–) and the resulting fluorescence excitation profile (black,-). c) Scheme of the STED-CoPS setup. The laser scanning STED microscope with excitation and STED laser requires the quadscanner to raster the sample. The beam profiles are generated in the chromatic segmented waveplate (SWP). The detector-array is connected via fiber coupling and shows a extended HBT scheme to observe mDEs.

In STED microscopy super resolution is achieved by confining the spatial probability of fluorescent labels to emit photons. This is ensured by overlaying the diffraction limited excitation profile, with a doughnut shaped depletion beam (see Figure 2.2 a). All molecules in the excitation laser beam might get excited, however, due to the intense STED beam, the molecules distant to the center are rapidly transferred to the ground state upon stimulated emission. The long wavelength photons can be spectrally separated and the fluorescence signal from the sub-diffraction volume can be observed.

2.1.4. Implementation

The STED setup used in this work has been built for parallel STED microscopy and is described in more detail in the associated PhD thesis.[97] During the process of data acquisition for CoPS-STED it has been converted to an easySTED setup [96] depicted in Figure 2.2 c).
As an excitation serves a supercontinuum source at 633 nm (SC450-20-2, Fianium, Southhampton, United Kingdom), which also procure the STED wavelength at 745 nm. The laser wavelengths are coupled into a common fiber to ensure spatially self-aligned beams. After passing the single-mode polarization maintaining NA=0.12 fiber (PM630-HP, Thorlabs, USA), the fiber output is collimated using a $f = 20\,\text{mm}$ lens. The beam is further focused into a custom-made beam-scanner (QuadScanner, described in more detail elsewhere Patent number: WO2010069987), consisting of four galvanometric mirrors (Cambridge Technology, USA), placed next to a commercial microscope (DMI 3000B, Leica Microsystems, Germany). The segmented waveplate (SWP) used as beam-shaping device (B. Halle, Germany) is placed just before the 1.46 numerical aperture 100× oil objective lens (Leica Microsystems, Germany). Most importantly, regardless of the input polarization, the SWP shapes the STED beam into a doughnut-shaped beam with a central zero intensity in the focal plane as required for reversible saturable (flurorescence) transitions (RESOLFT) methods while leaving the excitation wavelengths essentially unaltered. After passing the scan lens, the fluorescent beams are decoupled from the excitation path by crossing the bandpass filter, previously used in reflection. The maximal detection band is therefore limited by the bandpass filter to $\sim 650\,\text{nm}$ to 720 nm. Finally, additional shortpass (SP750, Semrock, USA) and bandpass (675/50, Semrock, USA) interference filters are placed in the detection path to further isolate the fluorescence from reflected excitation and STED light. The fluorescence signal is coupled into a multimode fiber (NA 0.275, Core ⌀ 62.5 µm, M31L01, Thorlabs, USA) and transmitted to the CoPS detection setup. The fluorescence signal is first collimated using a $f = 20\,\text{mm}$ lens and then focused by an $f = 200\,\text{mm}$ lens to 4 APDs (SPCM-AQRH-13/15, Perkin-Elmer, USA) in an extended HBT arrangement using three 50:50 beam-splitter. The read-out of the APDs is processed by a synchronized, four-channel TCSPC module (HydraHarp 400, PicoQuant, Germany). For the reconstruction of images, synchronization signals (line start/stop, frame clock) from the FPGA board, controlling the quadscanner, are looped through. Data read out and image construction is conducted by home-built MATLAB (Mathworks, Natick, Massachusetts, USA) and C++ (Visual C++, Redmond, USA) code.
For scanning a fluorescent sample in axial direction and reducing thermal drifts, the

sample was clamped directly to the objective lens by a home-build sample holder with an integrated linear piezo-electrical actuator (PI, Karlsruhe, Germany) for controlling the axial position of the sample. Scanning as well as data processing of the collected signal was controlled using a FPGA board (PCI-7833R, National Instruments, USA) and self-made scanning software (LabVIEW, National Instruments, USA) written by Johann Engelhardt (AG Hell, DKFZ, Heidelberg).

2.1.5. Brightness Comparison

The fluorescence signal from a single molecule can be characterized by the so-called molecular brightness.[21] In this work, the molecular brightness p_{MB} is defined as the probability to detect a photon from a single emitter in one laser cycle. In a microscope setup with pulsed laser excitation it can be defined as following:

$$p_{\mathrm{MB}} = \frac{I(x,y)}{h\nu \cdot \mathrm{LF}} \cdot \sigma_{\mathrm{abs}} \cdot \Phi_{\mathrm{f}} \cdot \eta_{\mathrm{det}} = E_{\mathrm{ph}}(x,y) \cdot \sigma_{\mathrm{abs}} \cdot \Phi_{\mathrm{f}} \cdot \eta_{\mathrm{det}} \tag{2.3}$$

I is the local laser power in [W/cm^2], $h\nu$ is the energy of the photons in [J], LF is the repetition rate of the laser in [Hz], σ_{abs} the absorption cross section in [cm^2], Φ_{f} the quantum yield, η_{det} the detection efficiency of the setup and $E_{\mathrm{ph}}(x,y)$ is the local pulse energy in [photons/cm^2].
The molecular brightness p_{MB} is influenced by many processes. The number of absorption processes are obviously dependent on p_{MB} and can be adjusted in experiments by the applied laser power. The quantum yield Φ_{f} (see equation (1.3)) describes the efficiency of the fluorescent transition and is a reporter of the molecular environment and photophysical processes.[10] The detection efficiency η_{det} of the setup is dependent on the numerical aperture $\mathrm{NA} = n_{\mathrm{ref}} \sin(\Theta)$ of the objective lens, the refractive index of the immersion media n_{ref}, the opening angle of the objective Θ, the transmission of all optical elements $\mathrm{T}_{\mathrm{opt}}$ and the detection efficiency of the APDs $\eta_{\mathrm{APD}}(\lambda)$ at the desired wavelength.

$$\eta_{\mathrm{det}} = (1 - \cos(\Theta))\mathrm{T}_{\mathrm{opt}}\, \eta_{\mathrm{APD}}(\lambda) \tag{2.4}$$

The parameters for the detection efficiency η_{det} are all properties of the electronic and optical elements. The APDs are currently the most sensitive detectors with TCSPC abilities. They achieve a detection efficiency of about about 70% at wavelengths of 600 nm to 700 nm. A series of optical elements is necessary to guide and shape the beam in the setup, however each additional optical element is reason for losses. The fluorescence emission of freely rotating molecules is isotropic. The solid angle of the objective describes the amount of photons accumulated by the lens. A typical value for the opening angle Θ of oil immersion objectives is 73°(Zeiss) and 71° (Olympus). They can therefore collect 35% and 34% of all emitted photons, respectively. By considering only the collection efficiency and the detection efficiency of the APD the best detection efficiency one can achieve is about 24%. Yet, the detection efficiency can also be determined in experiments.

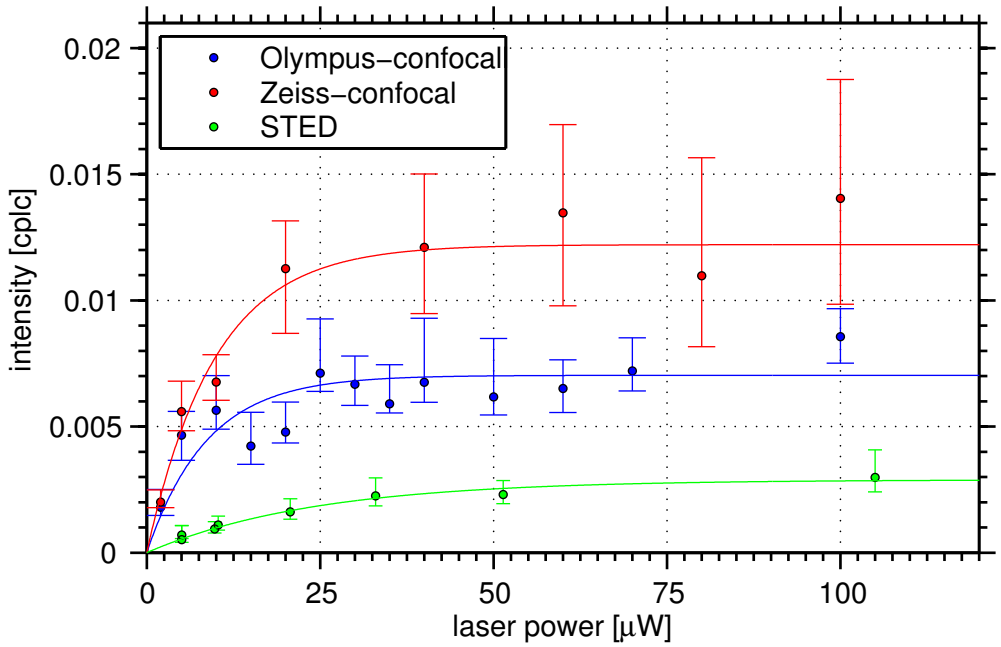

Figure 2.3.: Saturation curves of single ATTO 647N molecules at the different setups used during this thesis. The data is fitted by a saturation function $A\,(1-\exp(-cx))$ to estimate the saturation intensity A.

To test the efficiency of our setup, I measured the saturation curve of single molecules of ATTO 647N which have been immobilized via streptavidin-biotin binding to a single-molecule surface (for the protocol see section 2.3). Fluorescence images have been acquired at increasing laser power. The fluorescence emission rises in a non-linear manner due to the saturation effect. By analysis of the images, the intensity of single spots can be determined and can be calculated in reference to the laser repetition rate. In Figure 2.3 the evolution of the fluorescence signal is shown. The box plot indicates the median and the central 68% of the data. The fluorescence signal is increasing up to a laser power of 20 µW for the confocal setups and about 50 µW for the STED setup. The saturation value is dependent on the individual setups and saturates for the Zeiss-confocal at 1.3%, for the Olympus-confocal at 0.8% and for the confocal STED setup at 0.3%. The fluorescence signal of a single molecule of ATTO 647N can therefore be estimated to 260 kHz, 160 kHz and 60 kHz at 20 MHz laser excitation.
Nevertheless, the high laser powers required to achieve saturation are reason for photobleaching [20, 26] and should be avoided in quantitative methods. In the experiments the laser power was set to a minimal level to achieve a sufficient signal to noise ratio but to avoid photobleaching effects at measurements timescales. With CoPS, both the number of fluorophores and the mean molecular brightness can be estimated at the same time. Therefore, one can analyze and compare the different probes and setups directly in their individual molecular brightness.

In Figure 2.4 the mean molecular brightness estimated by CoPS in different experi-

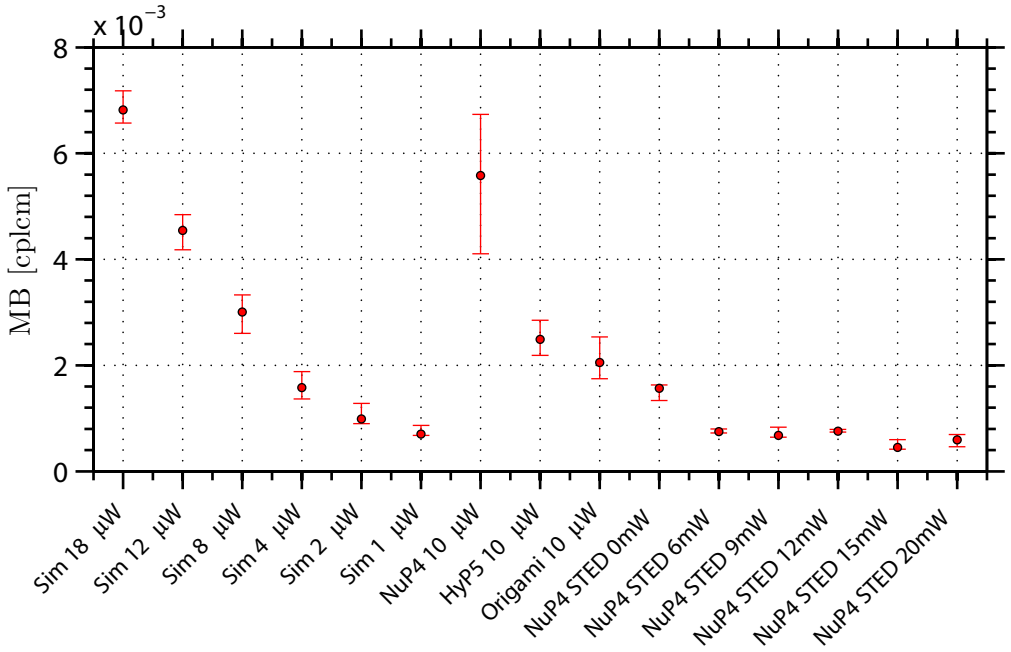

Figure 2.4.: Individual mean molecular brightness of different samples and setups is displayed as a box plot. The median and the central 68% of the data are indicated by the center and error bars. The first 6 entries represent CoPS analysis of simulated data of emitter. The NuP4 probe has been acquired at the Zeiss-confocal. The HyP5 and DNA origami sample has been measured at the Olympus confocal. The entries marked by STED, show the estimated molecular brightness of NuP4 on the STED-CoPS setup. The excitation intensity has been 9 µW and STED intensity is increasing from left to right.

ments is shown. The center of the box plot displays the median of the distribution and the error bars indicate the central 68% of the data. The first 6 data points are acquired by simulation and show a decay in the molecular brightness due to the decrease in excitation power. The NuP4 probe was obsereved at the Zeiss-confocal and shows a molecular brightess of $5.6 \cdot 10^{-3}$ cplcm with an wide spread distribution. The HyP5 sample and DNA origami have been measured at the Olympus-confocal and the molecular brightness is estimated to $2.5 \cdot 10^{-3}$ cplcm and $2.1 \cdot 10^{-3}$ cplcm. The achieved molecular brightness at the STED setup is slightly lower. The molecular brightness of the NuP4 sample in the confocal case is $1.6 \cdot 10^{-3}$ cplcm and decreases by application of the STED beam to about $4 \cdot 10^{-4}$ cplcm to $8 \cdot 10^{-4}$ cplcm.
It is reasonable to see that the most prominent changes in molecular brightness appear by use of different microscopes. The detection efficiency among the three detection setups as well as the molecular brightness varies by a factor of four.
The large variations can also be explored in the saturation measurements of single ATTO647N molecules in Figure 2.3. The probability to detect a photon from a single emitter at the same excitation power is $4 \cdot 10^{-3}$ cplc, $2 \cdot 10^{-3}$ cplc and $1 \cdot 10^{-3}$ cplc for the Zeiss-confocal, Olympus-confocal and the STED setup, respectively. The estimated

molecular brightness from CoPS mirrors the relative results very well, however, they have been obtained by probes with several dyes attached.

2.1.6. Monte Carlo Simulations

Monte Carlo simulations are named after a famous casino in Monaco,[98, 99] as they rely on stochastic processes as much as gambling does. Those simulations are a method that is often applied in mathematics and physics, when complex systems with numerous degree of freedoms are considered and it is impractical to compute an exact result. Using random numbers, the probability distribution of a physical process can be sampled and several successive physical processes can easily be combined. Running the model numerous times, the simulated experiments probability density function is sampled.
By making assumptions about the probability distribution of high level processes, the simulated data can be obtained directly. However, the assumptions may approximate in some way and the experimental error might be underestimated. Dependent on the complexity of the problem, the simulations can attribute for the basic physical processes.

A scheme of the MC simulations applied in this work is depicted in Figure 2.5. The fluorescence transients are modeled starting the absorption and emission process of single molecules. All measurements presented in this thesis, have been performed by simulation of the dye ATTO 647N (absorption coefficient $1.5 \cdot 10^5\,\mathrm{L/molcm^2}$, Quantum Yield 65%, lifetime 3.5 ns).[100] The triplet state lifetime is of minor importance because the ROXS buffer efficiently deplet this state (see section 2.4). For simulations the mean fluorescence intensity I of a single molecule of ATTO 647N was calculated with equation (2.3)

$$\mathrm{I} = p_{\mathrm{mb}}\mathrm{LF} \tag{2.5}$$

The detection efficiency of the setup has been estimated to about 15% (see the detailed considerations in section 2.1.5), the background was modeled with a brightness of $5 \cdot 10^{-5}$ cplcm. The number of acquired photons is then randomly distributed to a series of laser cycles with equal probability (Figure 2.5, $1 \rightarrow 2$). The process is repeated for each of n simulated molecules and for the background. All emitted photons are accumulated in a photon emission trace and the individual photons are randomly attributed to one of the four APDs. In case of two photons arriving at a single detector in a single laser cycle, the earlier photon is accounted for and other photons are discarded, because of the detector dead time. The data of "detected" photon arrival times is stored for later analysis.

2.2. Quantitative Probes

To analyze the performance of a quantitative method, reliable standard probes are necessary. The most important feature of the probe is the possibility to observe a well defined number of labels with the least possible variation within the probe. In this

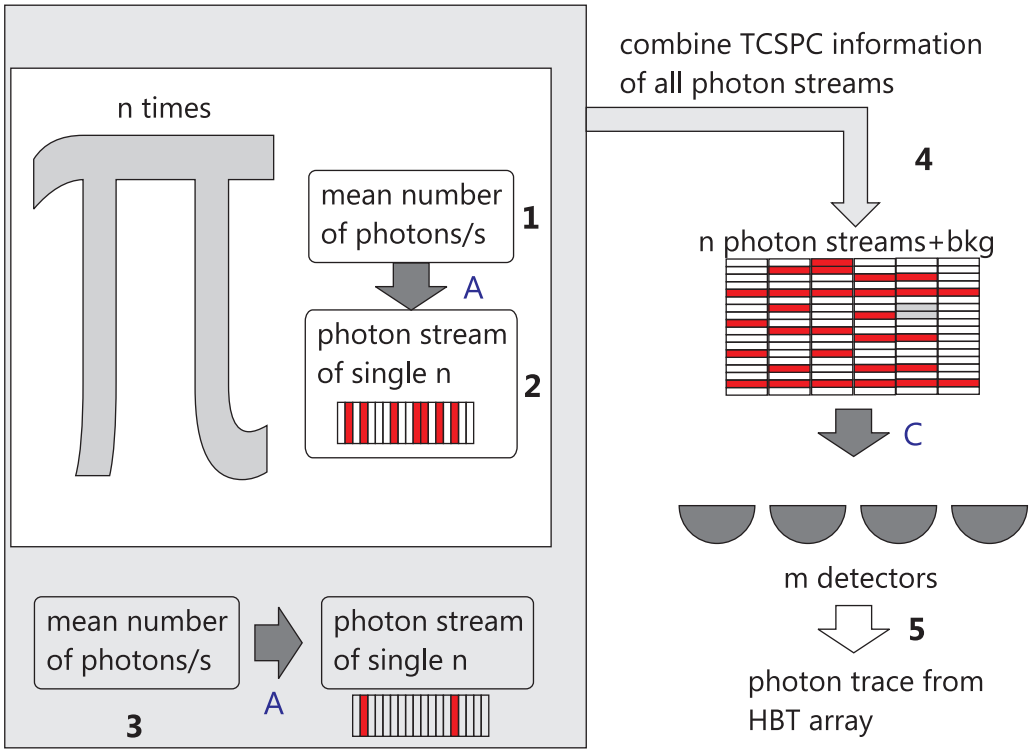

Figure 2.5.: Scheme of the Monte Carlo Simulations. The mean number of emitted photons is calculated from equation (2.5). The summed photons for each emitter are randomly distributed to the a series of laser cycles in a MC process A. The background (3) is modeled with as a weak fluorophore. All laser cycles are accumulated (4) in a single array and distributed to the m detectors (5). Each photon is assigned to a detector 1,...,m in a MC process C. If two or more photons are assigned to the same detector in a single cycle, the first one will be registered and all the other ones will be dismissed. The fluorescence transient is stored to hard disk (5).

thesis three different samples were applied: a hybridization DNA sample with five attached labels (HyP5), a DNA sample with four labels attached to the DNA nucleotides (NuP4) and DNA origamis. In this section the details of each sample are explained.

2.2.1. NuP4 Probe

The NuP4 probe in Figure 2.6 a) consists of a single stranded DNA (ssDNA) with 4 labels of ATTO 647N (ATTO Tec, Berlin, Germany) covalently linked to nucleotides. The ssDNA with 94 bases (5'-T**U**G GGA TAG GGG TCC TCC TCG TTT TGG GA**U** AGG GGT CCT CCT CGT TTT GGG ATA GGG G**U**C CTC CTC GTT TTG GGA TAG GGG TCC TCC TCG **U**T-3', Biomers, Ulm, Germany) has four uridines **U** in the structure, each labeled with an ATTO 647N molecule (ATTO Tec). The label is covalently bound to the 2'-O-Propargyl compound of the uridine ribose. The reverse

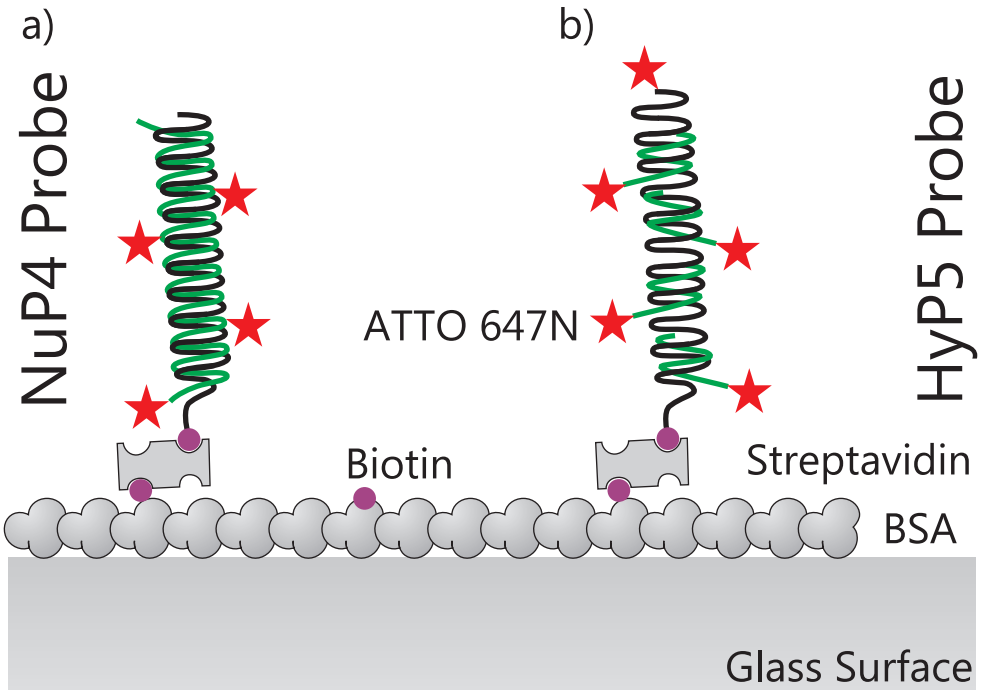

Figure 2.6.: a) The NuP4 probe consists of a long ssDNA strand (green) with four nucleotides with covalently bound ATTO 647N (red). By hybridization with another ssDNA (black) labeled with a biotin (violet), the probe can be immobilized to the singe-molecule surface. b) The HyP5 probe consists of four small ssDNA strands labeled with ATTO 647N (green) and a long ssDNA modified with biotin and ATTO 647N (red). By hybridization, each probe can have up to 5 emitters. The biotin allows immobilization of the probes to singe-molecule surfaces

strand (5'-AAC GAG GAG GAC CCC TAT CCC AAA ACG AGG AGG ACC CCT ATC CCA AAA CGA GGA GGA CCC CTA TCC CAA AAC GAG GAG GAC CCC TAT CCC AA-3', Sigma Aldrich, Taufkirchen, Germany) is modified on the 3' end with a biotin for immobilization to singe-molecule surfaces. Both ssDNA strands are mixed in equal concentrations and hybridized by heating up to 90 °C for 5 min. The sample is then cooled slowly by driving a gradient of $-2\,^{\circ}\,\mathrm{min}^{-1}$ to room temperature in a thermocycler (PTC-100, MJ Research, Ramsey, MN, USA).

2.2.2. HyP5 Probe

The HyP5 probe in Figure 2.6 b) was already subject of previous investigations.[86, 84] The probe consists of a long ssDNA with 94 bases (5'-AAC GAG GAG GAC CCC TAT CCC AAA ACG AGG AGG ACC CCT ATC CCA AAA CGA GGA GGA CCC CTA TCC CAA AAC GAG GAG GAC CCC TAT CCC AA-3', Sigma Aldrich). The 5' end is amino modified for labeling with a fluorescent dye. The 3' end is biotinilated for immobilization of the sample to a surface. The nucleotide pattern was designed in that manner that four smaller oligonucleotides can hybridize and result in five emitters per

probe. A 24 bases DNA was purchased with a complementary pattern (5'- TTG GGA TAG GGG TCC TCC TCG TT-3', Sigma Aldrich). The 5' end is amino-modified for later labeling with a fluorescent dye. The probes measured in this work have been labeled with ATTO 647N (ATTO Tec, Siegen, Germany) via NHS Ester by a standard protocol provided by ATTO Tec. Labeled probes have been purified by HPLC and the degree of labeling for each has been determined by absorption spectroscopy. The degree of labeling was estimated to 97% for the long ssDNA and to 151% for the short ssDNA. The dye and its position are identical to the NuP4 sample.

2.2.3. DNA origami Probe

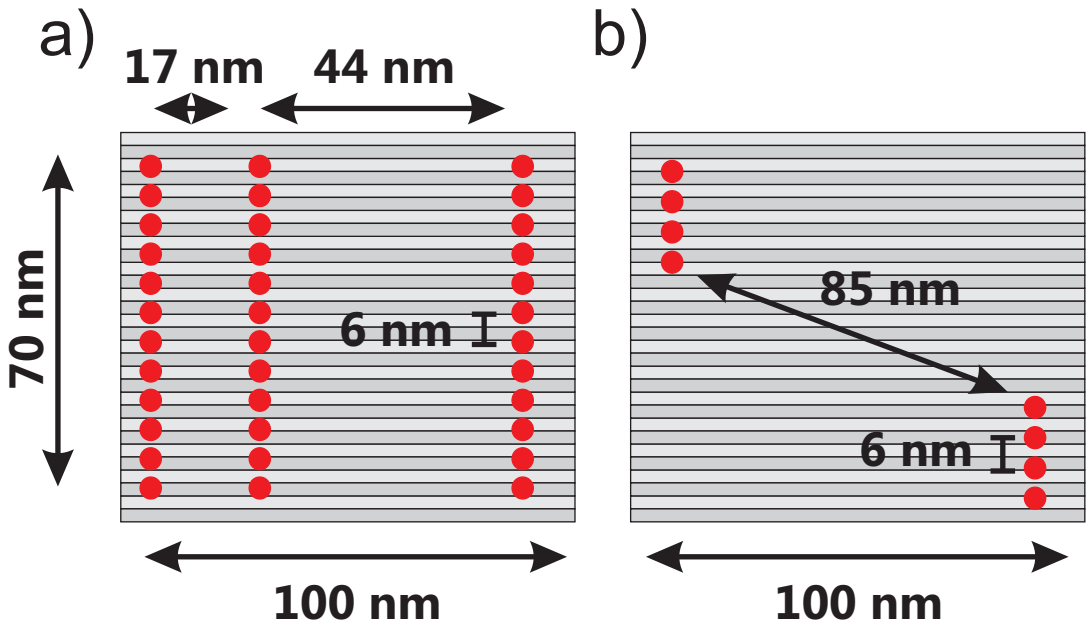

Figure 2.7.: a) DNA origami with 36 labels. b) DNA origami with 2x4 labels arranged in a spatial structure, which can be resolved by STED microscopy.

The DNA origami measured in this thesis were kindly provided by Jürgen Schmied (AG Tinnefeld). The DNA origamis used for the experiments are equal to the rectangular DNA origamis already published.[101] Detailed sketches of DNA origamis can be found in the Appendix section C. Unmodified and modified staple strands were purchased from MWG (Munich, Germany) or IBA (Göttingen, Germany) at a concentration of 100 µM and were used without further purification. DNA origamis were formed with a molar ratio of 1:30 between the viral and the unmodified staple strands and 1:100 between the viral DNA and the modified staple strands. For preparation of the scaffold strand *Escheria coli* strain K91 was infected with the M13mp18 phage p7249. After amplification, the phage particles were separated, purified and their single stranded DNA was extracted and purified similar as described before.[102] The concentration of phage DNA was adjusted to 100 nM.
For folding of the scaffold strand with modified and unmodified staple strands, they

were diluted in 1xTAE buffer containing 12.5 mM $MgCl_2$. The rectangular DNA origamis involves the same sequences as published in the Supporting Information of Rothemund.[101] The rectangles were immobilized on a bovine serum albumin (BSA)-biotin-streptavidin surface via the biotin modified oligonucleotides shown in Table 2.1. The biotins are located on the opposite side of the DNA origamis compared to the dyes.

r1t14f	Biotin - ATA GAA AAA GCC TGT TTA GAA GGC CGG
r7t2e	Biotin - GCG ACC AGG CGG ATA AGT GAA TAG GTG
r-7t2f	Biotin - TAG CTT TTG CGG GAT CGT CGG GTA GCA
r-7t22f	Biotin - TTT AAC GTC AAA GGG CGA AGA ACC ATC
r7t22e	Biotin - CAG TCA CCT TGC TGA ACC TGT TGG CAA

Table 2.1.: Biotin modified oligonucleotides used for immobilization of the rectangular DNA origamis on a BSA-biotin-streptavidin surface.

The hybridization was carried out in an Eppendorf (Hamburg, Germany) thermocycler starting with denaturation (95 °C for 30 s) followed by controlled annealing (cooling to 20 °C in 0.1 °C steps every 6 s). After folding the excess of staple strands was removed by filtration using Amicon (Schorndorf, Germany) Ultra-0.5 ml Centrifugal filters (100000 MCO) according to manufacturer's instructions. The DNA origamis solution was washed three times with 1xTAE + 12.5 mM MgCl2 buffer and concentrated to a final volume of 20 µl with a concentration of about 10 nM.
In order to avoid dimerization of DNA origamis, oligonucleotides corresponding to border columns were omitted. The distance between two dye-molecules within the same column was 12 nm for the samples with 6 and 18 dye molecules and 6 nm for the sample with 36 dye molecules.[101] Samples with 6 nm and samples with 12 nm distance have been measured for DNA origamis with 12 dye molecules.

2.3. Single Molecule Surfaces

For the observation of the same single molecule, the probe needs to be immobilized. A standard protocol of BSA-biotin surfaces could be applied for the confocal microscope. Because the BSA surface showed increased autofluorescence by STED illumination, the samples for the STED measurements are immobilized by an unspecific binding.

2.3.1. Confocal Samples

In order to immobilise of the probes for confocal microscopy an eight chamber cover glass Lab-Tek^{TM}(Fisher Scientific, Waltham, Massachusetts, USA) was first cleaned with hydrofluoric acid (0.1 %, Sigma-Aldrich) twice for 30 seconds. After rinsing with MilliQ grade water, the surface of the chambers was incubated with a mixture of bovine serum albumin (BSA) and biotinylated BSA at a ratio of 20:1 for 30 min (both Sigma-Aldrich, Germany). By washing with phosphate buffered saline (PBS, Sigma-Aldrich)

remaining free proteins were removed and the surface was subsequently treated with recombinant Streptavidin (Sigma-Aldrich) for 30 min. Then the surface was washed three times with PBS. For a convenient density of probes per area a 0.5 nM solution of the hybridized sample is incubated for 10 min. This means that at least several probes are immobilized in the image area, but still in a spatial distance greater than twice the resolution limit, so that they can be observed individually.

2.3.2. STED Samples

In STED samples the use of BSA proteins needed to be avoided because of the activation of autofluorescence by the STED beam. The immobilization was achieved by unspecific binding to poly-L-lysine coated surfaces.
Glass slides (Roth, Karlsruhe, Germany) have been cleaned with hydrofluoric acid (0.1 %, Sigma-Aldrich) twice for 30 seconds. After rinsing with MilliQ grade water and drying with compressed air, the surface of the chambers was incubated with a 0.01% poly-L-lysine solution (Sigma-Aldrich) for 15 min. The surface was rinsed with MilliQ grade water and dried afterwards. A 0.5 nM solution of the hybridized sample is incubated for 10 min to achieve a convenient probe density of immobilized probes (see confocal samples).

2.4. ROXS Buffer

The ROXS buffer applied in this thesis is a degased 5xPBS buffer containing 300 mM glucose (all chemicals were purchased from Sigma-Aldrich) and 12.5 % (v/v) glycerin. Shortly before measurement reducing and oxidizing agents are added to their final concentration of 1 mM MV, 1 mM AA, 1 mM TCEP, 2 Units/µl glucose oxidase and 250 Units/µl catalase are used as enzymatic oxygen and scavenging system. The solution is carefully mixed and then filled into the Lab-Tek chamber. Afterwards the chamber is sealed with Parafilm®(Brand, Wertheim, Germany) to avoid mixing with atmospheric oxygen. In case of the STED sample, a cover slide with indentation (Bresser, Rhede, Germany) was filled with ROXS buffer. A glass slide was put atop and the chamber was sealed with nail polish.

2.5. CoPS Analysis

As described in the introduction, the number of emitters and the molecular brightness can be determined from accumulated mDE statistics by CoPS. For CoPS, the fluorescence signal has to be detected with a suitable setup, with pulsed laser excitation and with an extended HBT detection array of synchronized APDs. By acquiring fluorescence transients in the previously described PnD approach, time is reduced. Only the registered spots of interest are sequentially observed and surrounding pixels are avoided. However, the method is not limited to fluorescence transients and can also be

applied in imaging.
In this section I will describe the implemented algorithm to obtain the quantitative information from the mDE statistics and I will describe the changes I made to improve the robustness of the analysis. During the thesis I could observe the error distribution of CoPS in experiments and in simulations. I will show the appearance of the distribution in different experiments and investigate the probability function.

2.5.1. Computational Implementation

CoPS analyzes the signal from a fluorescent spot over time to obtain numbers and mean molecular brightness. The photon stream acquired by either the confocal or STED setup is saved in the manufacturers file format with the required TCSPC information and detector channel. For each setup an I/O routine has been implemented and therefore all data could be analyzed by the same software.

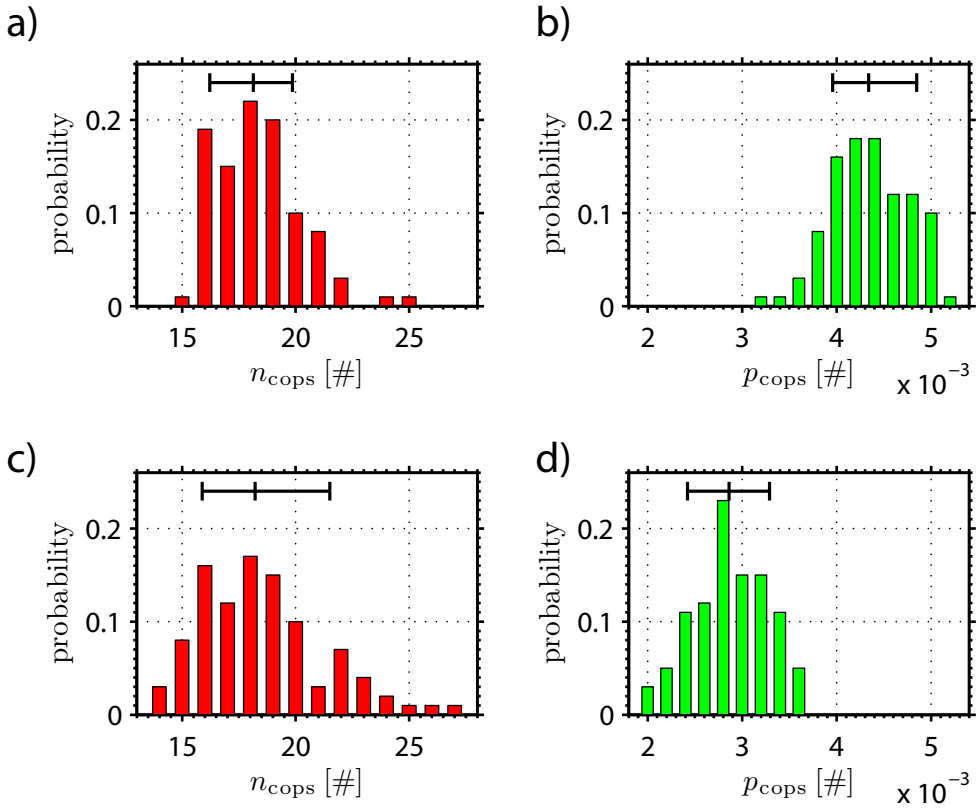

Figure 2.8.: Bootstrapping results from a single analysis window of 18 simulated emitters (a),b)) and from 18 labels attached to a DNA origami (c),d)). The estimated numbers are shown in red, the mean molecular brightness is shown in green. The box plot atop of distributions indicates the median and the central 68% of the data. (100 botstrap cycles, $5 \cdot 10^6$ laser cycles)

The software acquires the TCSPC data for the analysis window from file and calculates the mDE events. The mDE events are accumulated in a histogram showing the probability of 0, 1, 2, 3, 4 photon detection event. The CoPS model (see equation (2.6))[86] is then fitted by a least-square estimation with the Levenberg-Marquardt algrithm to the mDE probabilities. The the number n_{cops} and mean molecular brightness p_{cops} are obtained.

$$P(n,p;i) = \binom{m}{i} \left[\begin{array}{c} \left(1 - \left(\frac{m-i}{m}\right) p\right)^n \left(1 - \left(\frac{m-i}{m}\right) p_b\right) \\ - \sum_{k>0}^{i-1} \frac{\binom{i}{k}}{\binom{m}{k}} P(n,p;k) \end{array} \right] \tag{2.6}$$

m denotes the number of detectors and i the number of mDE. The background is modeled as a weak fluorophore with a molecular brightness of p_b.
In this step I implemented bootstrapping algorithm [103, 104] as it increases the robustness of the fit and allows estimations of errors. The bootstrapping method is a statistical method and can be attributed to the class of resampling methods.[105, 106] The underlying principle, is to provide repeated simulated observations from a single data set. In this work, different mDE statistics for fitting are acquired from a random subset (75%) of all laser cycles in the analysis bin. By repeating the process for 100 times, the fitting distribution from the bin is obtained.
In Figure 2.8 the bootstrapping results from CoPS analysis of simulated data with 18 emitter at an excitation power of 12 µW (a), b)) and of a DNA origami with 18 labels attached at 10 µW is shown (c), d)). The values for the number estimates are 18±2 for simulated and 18±3 for the DNA origami data. The median values for the brightness are $(4.3 \pm 0.4) \cdot 10^{-3}$ cplcm for the simulated data and $(2.9 \pm 0.4) \cdot 10^{-3}$ cplcm for the experimental data.
By bootstrapping a distribution of results is obtained, which is centered around the dedicated value. The width of the distribution is slightly enlarged for the experimental data and mirrors the precision of a single estimate by CoPS in a single analysis window. The estimate become more robust as the extreme results are not considered, but the median of the distribution is the result in number. By obtaining the width of the distribution an adequate error estimate is available.
The precision of CoPS is determined by the difference of mDE statistics for different dye numbers and mean molecular brightness. The difference between one and two molecule is indicated by the existence of a certain probability for 2DE. The difference is decreasing with increasing number. This can be visualized by illustrating the parameter space of the fit.

The parameter space shows the χ^2 between the experimental data and the model function (equation (2.6)) for varying model parameter n and p_{cops}. In Figure 2.9 a) the parameter space for the mDE statistics from 18 simulated emitters at 8 µW is shown. The black circles are obtained in the bootstrapping process from Figure 2.8 and estimation by CoPS is determined to 18±2 emitters with a mean molecular brightness of $(4.3 \pm 0.4) \times 10^{-3}$ cplcm. The parameter space shows a curve with a low χ^2. Along the minimal line, the differences in χ^2 are relatively low. In the axes b) and c) I have

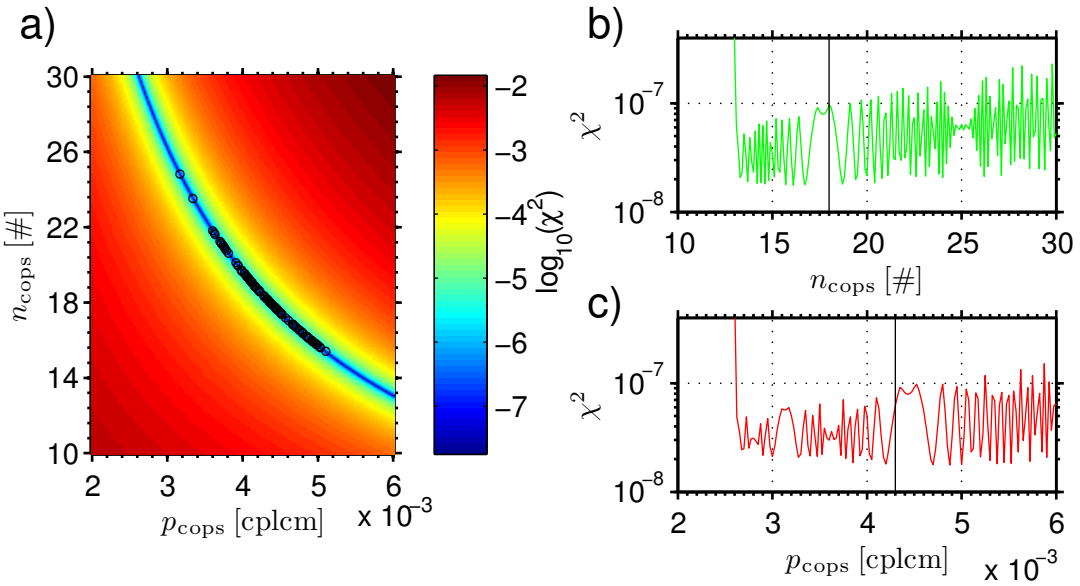

Figure 2.9.: a) The logarithmic parameter space of the CoPS model function to mDE statistics from 18 simulated emitters with 12 µW. The black circles indicate the bootstrapping result from Figure 2.8 with estimated 18±2 emitters with a mean molecular brightness p_{cops} of $(4.3 \pm 0.4) \times 10^{-3}$ cplcm. b) The minimum projection of χ^2 by varying number n_{cops}. c) The minimum projection of χ^2 by varying mean molecular brightness p_{cops}. The solid black line indicates the estimation by CoPS.

plotted the projection of the χ^2 minimum for the numbers and for the mean molecular brightness, respectively. The parameter space is highly complex and shows many local minima, which can influence the precision of fitting and broaden the resulting distribution of n_{cops} and p_{cops}.

2.5.2. Fitting Distribution

The exact distribution of label numbers n_{cops} and the mean molecular brightness p_{cops} is not exactly known. They cannot be described analytically easily, because they depend on the parameter space of the nonlinear fit and of experimental probability distributions, like shot noise, variances in quantum yield, etc. However, in the experiments probability distributions for n_{cops} and p_{cops} are achieved, which can be described very well by the log-normal distribution. By looking at the estimated numbers from different experiments in Figure 2.10, 6 different experiments are depicted. In the left column a), c), e) the probe have only few labels attached and in the right column b), d), f) the estimations are applied to 18 emitters. In the axes a) and b) simulated data with a mean molecular brightness of $3 \cdot 10^{-3}$ cplcm are shown. In axes c) and d) the mean molecular brightness is increased to $5.6 \cdot 10^{-3}$ cplcm for the NuP4 sample and $6.8 \cdot 10^{-3}$ cplcm for the simulated 18 emitter. In the bottom row, the DNA origami

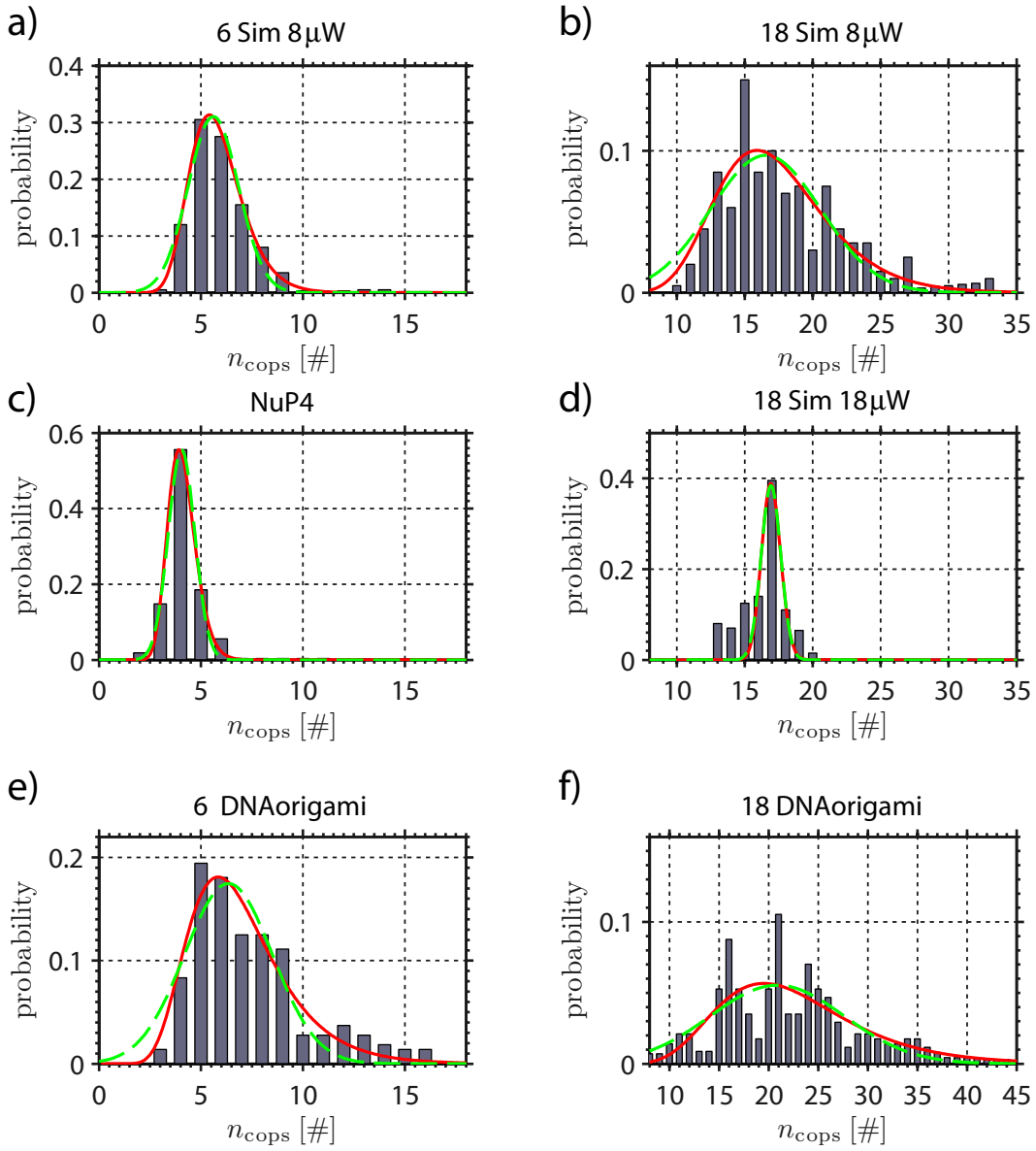

Figure 2.10.: Observed error distributions from CoPS analysis of several samples (gray) fitted by a normal distribution (green,–) and a log-normal distribution (red,-). a) 6 Simulated emitters and b) 18 simulated emitters (both at 8 µW) c) NuP4 probe at 10 µW d) 18 simulated emitter at 18 µW e) and f) 6 and 18 labels of ATTO 647N attached to DNA origami at 10 µW

data show only a mean molecular brightness of $2.1 \cdot 10^{-3}$ cplcm. Each distribution is approximated by a log-normal (red,-) and a normal (green,- -) probability distribution. The data acquired by medium and low mean molecular brightness (row 1 and 3) show a non-symmetric distribution with a tail to longer numbers. Compared to this behavior, the distributions with a higher molecular brightness in c) and d) show very narrow

distributions and the difference between the log-normal and normal distribution fit is negligible.
To quantify the results, a one-sided Kolmogorov-Smirnov test (ks-test),[107, 108] implemented in MATLAB, was applied. The one-sided ks-test is a non-parametric test and calculates the largest difference between the cumulative distribution function (cdf) of the data and the cdf of the reference distribution. The null hypothesis states that the distribution is drawn from the reference distribution and is rejected otherwise. The p_{ks}-value in statistical testing describes the probability to obtain a distribution like the test distribution, by considering the null hypothesis as true.[106] I tested the acquired distribution against the normal distribution and the log-normal distribution. The α value, when to dismiss the null hypothesis, has been set to 5%. The acquired values are listed in Table 2.2.

	normal		log-normal	
sample	H0	p_{ks} [%]	H0	p_{ks} [%]
6 Sim 16	ϟ	1.4	0	51
18 Sim 16	ϟ	0.4	0	52
6 Sim 16	ϟ	0.3	0	22
NuP4	ϟ	0.3	ϟ	0.04
18 Sim 36	0	29	0	8
18 DNA origami	0	8	0	16

Table 2.2.: Kolmogorov-Smirnov tests for acquired distributions in Figure 2.10 to originate from normal or log-normal distributions. The α value has been set to 5% and the ϟ symbol indicates the rejection of the null hypothesis.

The normal distribution is rejected for all observed experiments except for the DNA origami with low molecular brightness. In contrast, the log-normal distribution is only rejected for the NuP4 sample. The resulting distribution spans here only over a single bin and applying any fit is probably not reasonable at all. Generally, considering the data, the error distribution of CoPS only appears in low MB data and is of log-normal form.
The log-normal distribution is known to represent frequency statistics [109, 110] and has been applied to fit fluorescence intensity data.[43] The log-normal probability density function depends on two variables. The location parameter μ and the shape parameter ω:

$$\mathrm{PDF}(x \,|\, \mu, \omega) = \frac{1}{x\omega\sqrt{2\pi}} \mathrm{e}^{-\frac{(\ln(x)-\mu)^2}{2\omega^2}}, \qquad x > 0$$

From the parameters of the log-normal fit, the mode, median and sigma can be calculated. The mode is the most probable value in the probability distribution. The median gives the value which separates the distribution in equal parts. We define sigma as measure for the distribution width similar to that of the normal distribution by half of the 68% confidence interval. The mode, median and sigma are connected to the parameters as follows:

$$\text{mode} = e^{\mu-\omega^2} \qquad \text{median} = e^{\mu} \qquad \text{sigma} = \frac{1}{2}(e^{\mu+\omega} - e^{\mu-\omega})$$

The mode of the log-normal fit to our data describes the expected number of labels well. For a log-normal distribution the median is always larger than the mode.

3. Experiments & Results

In this chapter I will describe several experiments which have been conducted to analyze characteristics of CoPS. In the introduction I reviewed many different approaches to obtain quantitative data in fluorescence spectroscopy. But observing their individual performance is difficult because reliable standard samples are missing. However it is a prerequisite to obtain reliable results in complex environments.
In section 3.1 experiments with the single stranded DNA (ssDNA) standard probe HyP5, applied in previous investigations [86] are described. By measuring the number of labels (NOL) distributions with bleaching step (BS) analysis and CoPS, it is noticed that the NOL depends on the preparation process and therefore not suited as counting standard. By introducing a new standard probe NuP4, the error prone steps in probe preparation could be circumvented and a more narrow NOL distribution could be achieved. By observing the NOL distribution with different probes and with small deviations in emitter numbers, the error distribution of CoPS can be explored and the observation of the minimal requirements and acquisition time is accomplished.
Previous simulations by Ta et.al. [85] showed the possibility to count up to 50 molecules by CoPS. To inquire the resolution and error of CoPS, simulations of various numbers of molecules and molecular brightness have been conducted. The results are presented in section 3.2. By modeling a probe without photobleaching and stable emission, simulated fluorescence transients are obtained. As the transients show no deviation in numbers and a stable fluorescence emission, the error distribution of CoPS can be determined. By simulated traces, the time and number resolution and the dependency on molecular brightness is explored.
To compare the simulations with experiments a different probe is used. DNA origamis (explained in detail in section 2.2.3) can be labeled with large numbers of emitters. With this probe it is possible to conduct the same experiments as in simulations and observe the differences. In experiments, the time and counting resolution and the counting limit is observed and the minimal requirements to apply CoPS are identified.
CoPS deals with photon detection only and can therefore be combined with STED microscopy (see section 2.1.3). In section 3.4 of this chapter, the application of STED-CoPS is shown. In cooperation with the group of Prof. S. Hell (DKFZ, Heidelberg), we designed and built a setup to acquire fluorescence transients from a non diffraction limited spot for the application of CoPS. We analyze the feasibility and limits of STED-CoPS with standard samples and DNA origami with spatial arrangement of label positions.

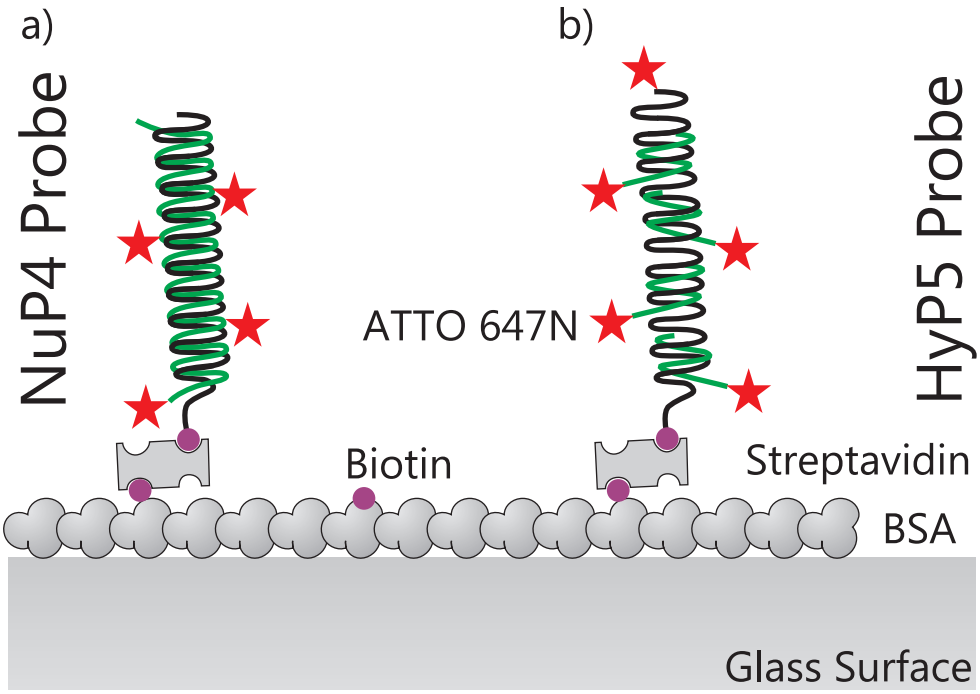

Figure 3.1.: a) The NuP4 probe consists of a long ssDNA strand in which four nucleotides are covalently bound to ATTO 647N (green). By hybridization with another ssDNA (black) labeled with a biotin (violet), the probe can be immobilized to the singe-molecule surface (see section 2.3). b) The HyP5 probe consists of four small ssDNA strands labeled with ATTO 647N (green) and a long ssDNA modified with biotin and ATTO 647N (red). By hybridization, each probe can show up to 5 emitters. The probe can be immobilized to singe-molecule surfaces by biotin-streptavidin bindings.

3.1. Single Molecule Counting

For the evaluation of quantitative methods at the nanoscale a fluorescence standard probe is necessary. To estimate the precision and bias of the method, the NOL per probe should be precise. In previous work by Ta et.al.,[86, 84] CoPS has been applied to a DNA hybridization probe with five dyes (HyP5, see Figure 3.1). The probe preparation is complex and prone to deviations in the actual number of attached labels. The NOL distribution attached to a single HyP5 is explored in section 3.1.3 To observe the error in experiments with less influence of probe preparation, a standard sample with a narrower NOL distribution has to be used. In the NuP4 probe, the stochastic hybridization process has been circumvented and the labels are covalently bound to one single ssDNA. By use of the NuP4 probe, the time resolution of CoPS can be investigated.

3.1.1. Standard sample

The well-defined stoichiometry of the NuP4 probe is achieved by omitting the stochastic hybridization process and labeling ssDNA. The fluorophor is covalently bound to a nucleotide and directly incorporated in the DNA (see Figure 3.1 and section 2.2.1). By hybridization with a biotinilated reverse strand, the probe is immobilized to a single-molecule (SM) surface. The label stoichiometry can be determined by acquiring fluorescence transients with two independent methods, BS analysis and CoPS.
In this experiment I acquired fluorescence transients by PnD [81] of single NuP4 probes with four attached molecules of ATTO 647N. In a short overview scan the coordinates of individual probes are registered and each spot is observed sequentially until complete photobleaching of all emitters in the spot occurs (more details in section 2.1.1).

In Figure 3.2 a) a fluorescence transient (blue, left axes) of a NuP4 probe is shown. Four large intensity drops of about 200 kHz are visible at 3.1 s, 5.4 s, 18.4 s and 20 s and some smaller steps and one intermittence can be found at 7.7 s, 15.2 s, 17.7 s and 14.8 s, respectively. Between 20 s and 22.6 s the intensity is very low with 15 kHz. It is still above the background of about 4 kHz, though. At 21.2 s another drop in intensity occurs by about 4 kHz, which is better visible in the logarithmic plot of the 1DE (blue) in axes b). At 22.6 s the intensity is rising again to about 90 kHz.
The large drops in intensity during the transient can be attributed to photo-bleaching. The small steps of few kHz appear random and sometimes increase or decrease the count rate. The process is unclear, but maybe these are quenching effect of the local environment. It is also interesting to note that the fluorescence signal reappears at 22.6 s, because all emitters have already been "photobleached". Obviously, a large fluorescent drop in intensity does not necessarily indicate a bleaching event. The fluorescence intensity may be inhibited (e.g. quenching, long triplet state, etc.) and recover after a while.[22] From previous publications it is known that the ATTO 647N dye possess different emissive states [111] and can cycle between them. This behavior complicates BS analysis, since switching between states might be recognized as bleaching events.
The estimates of number n_{cops} and brightness p_{cops} by CoPS give a slightly different view. The estimates do not exploit a photophysical effect, but rather estimate n_{cops} and p_{cops} by analyzing the accumulated mDE statistics (see Figure 3.2 b)). The mathematical model, described in equation (1.24), is fit to the mDE statistics of about 250 ms by a nonlinear regression algorithm (see the details in section 2.5).
Number estimates by CoPS (red, right axes) indicate the initial four emitters and follow the intensity drops due to bleaching events in the fluorescence transient. However, after the fourth intensity drop at 20 s, the number estimate is not decreasing to zero and still calculated to be one. Instead, the mean molecular brightness (green, left axes, in kHz) is decreasing at 20 s. In the end it even shows a rise in fluorescence intensity again at 22.6 s.
CoPS does not only evaluate the number of emitters, but also assess inherently the mean molecular brightness of the emitters. Therefore, CoPS can analyze numbers despite the photophysics of dyes and photophysics despite the numbers.
In Figure 3.2 b) the probabilities for 1DE (blue) and 2DE (red) acquired in one analysis window are plotted for the fluorescence transient shown in a). Higher mDE have

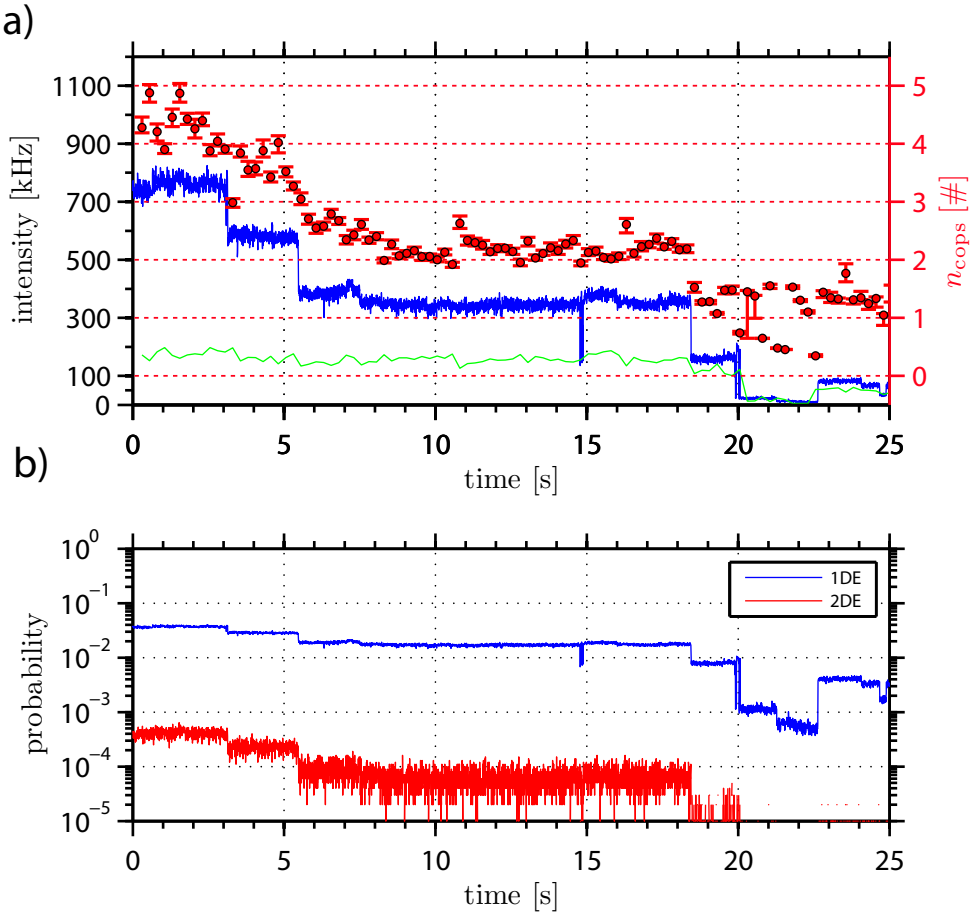

Figure 3.2.: a) A fluorescence transient of NuP4 (blue, left axes) was acquired at 10 µW and 20 MHz laser frequency. The four drops in intensity indicate the number of emitters. CoPS analysis identifies the number of molecules n_{cops} (red, right axes) and the mean molecular brightness p_{cops} (green, left axes, in kHz) in a single analysis period t_{ac} of 250 ms. The red axes are offset for better visualization. b) The probabilities of 1DE and 2DE for the fluorescence transient during single analysis windows t_{ac} of 250 ms from a) are shown.

not been measured during this transient, because the detection probability of 3 photon detection events (3DE) and 4 photon detection events (4DE) rises to observable values only at larger numbers or brighter molecules (see Figure 4.1). The acquired 2DE are less probable than 1DE by about 2 orders of magnitude. This is expected because the probability for 2 photons emitted in a single laser cycle scales with p^2_{exp}.[84]
The bleaching events can be recognized as drops in the mDE probabilities and at 20 s. When the fluorescent intensity vanishes, there is no recognizable probability for 2DE anymore. CoPS will therefore always predict a single fluorophore with low molecular brightness, as long the signal is above background.

CoPS analyzes the appearance of mDEs and thus, depends essentially on the detection of them during an analysis window (this will be discussed in detail in section 4). In order to make a significant estimate, the probability of acquiring 2DE has to be reasonable high. This can either be achieved by prolonging the acquisition time or by increasing the molecular brightness.

3.1.2. Characterization of CoPS

In equation (1.2) we have seen that the molecular brightness is dependent on the laser power. Thus, CoPS estimates depends on the laser power, too. Several SM surfaces of NuP4 at different excitation intensities of 2 µW, 5 µW, 7 µW and 10 µW have been observed and by PnD 401, 211, 200 and 233 transients could be accumulated, respectively. In each transient the number and the brightness are evaluated for the first analysis window. Thereby the bleaching effect is minimized and the unaltered label number is measured. By changing the size of the analysis interval t_{ac}, the minimal observation time could be investigated.
The estimated numbers n_{cops} from each sample can be summarized in their probability distribution. But the intrinsic estimation variance of CoPS estimates is not known analytically (see section 2.5.2). To characterize the distributions in a robust manner, the results can be compared by the quantiles, though.
The median $\mu_{1/2}$ is chosen to obtain the center of the distribution. It is defined as the central value of distribution, with 50% of the data on each side. I generally show the relative median μ_{cops} to compare results from different absolute label numbers:

$$\mu_{\mathrm{cops}} = \frac{\mu_{1/2} - n_{\mathrm{dedicated}}}{n_{\mathrm{dedicated}}} \tag{3.1}$$

Similarly to the gaussian distribution, a central quantile is chosen to describe the width of the distribution. In this work I define the precision, if not stated differently, as the central 68% of the distribution or the distance between the 16% and 84% quantile, similarly to the σ in the normal distribution. For a convenient comparison of data, I will generally show the relative sigma σ_{cops}:

$$sigma_{\mathrm{cops}} = \frac{\mu_{+\sigma} - \mu_{-\sigma}}{2 \cdot n_{\mathrm{dedicated}}} \tag{3.2}$$

In Figure 3.3 a) the relative median μ_{cops} (see equation (3.1)) is shown for 2 µW, 5 µW, 7 µW and 10 µW laser power against accumulation time t_{ac}. All traces show a steep initial rise. This is the time required to accumulate mDE statistics. They reach their peak between -5% and 0% after 100 ms. The estimations at 2 µW remains at the 2% level during the whole 5 s. In contrast, the curves at higher laser powers decline faster because of photobleaching.
In the axes b) the relative sigma σ_{cops} (see equation (3.2)) is shown. After acquiring the essential mDE statistics after 100 ms the variance stabilizes at less than 20%. For all laser powers the behavior is similar, however, the 2 µW trace requires more time to decline.
From the analysis we can see, that a good estimate on the number is obtained at very

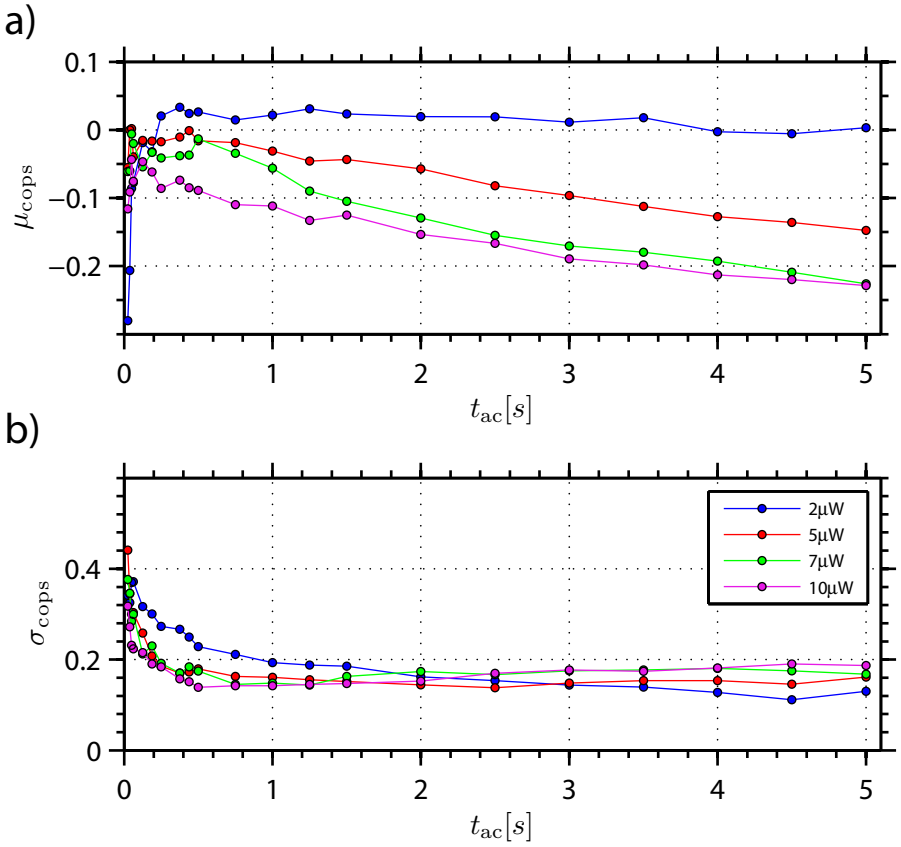

Figure 3.3.: a) Time resolution of NuP4 estimates n_{cops}. The relative median μ_{cops} is plotted against the accumulation time t_{ac} for different molecular brightness. The estimation gives quasi instantaneous results in less than 100 ms. b) The relative sigma over time is plotted against the time t_{ac} for laser powers of 2 µW, 5 µW, 7 µW and 10 µW

short time periods of 100 ms. The precision at 100 ms is about 30% and improving by increasing mDE statistics. However, for laser power larger than 2 µW, the bleaching effect becomes visible and shifts the estimation to lower values. The occurrence of bleaching events prevents an estimation of the unaltered labeling distributions and should therefore be avoided.
To study the photostability of ATTO 647N on a single molecule level, the bleaching events have been analyzed. The bleaching events in each trace from previous measurement of NuP4, have been registered manually. As the bleaching probability at 2 µW is very low, the time until complete photobleaching is very long. Therefore, only the fluorescence transients at 5 µW, 7 µW and 10 µW have been measured until complete photobleaching. The time until photobleaching is shown in the histogram in Figure 3.4.

The bleaching time probabilities are shown as circles and are approximated by a single exponential decay $\mathrm{f}(x) = A\,\mathrm{e}^{(-x/\tau)}$. A is the Amplitude. For laser powers of 5 µW,

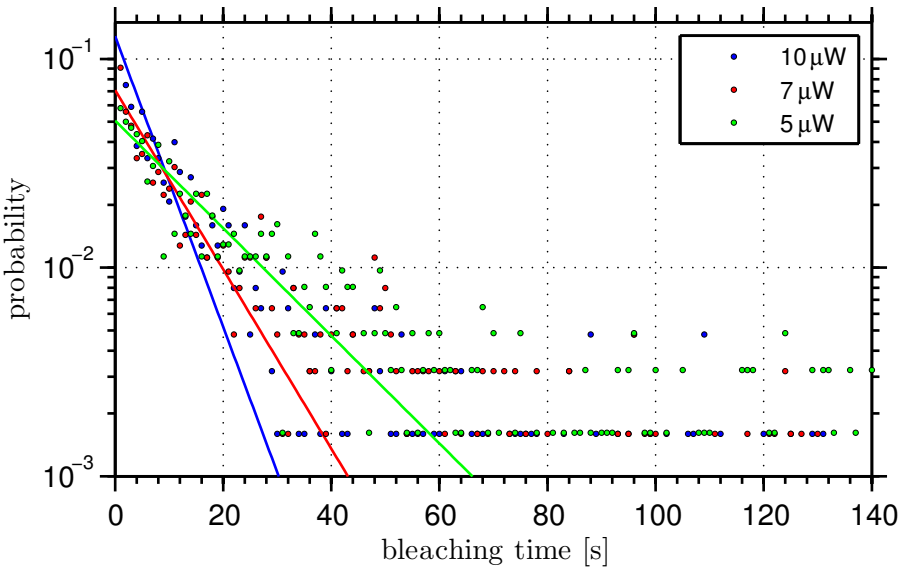

Figure 3.4.: Probability distribution of bleaching times at three different laser powers (blue 10 µW, red 7 µW and green 5 µW). The distributions are approximated by a single exponential decay. For laser powers of 5 µW, 7 µW and 10 µW the half life has been determined to 16.8 s, 10.1 s and 6.2 s. (211, 200 and 233 transients)

7 µW and 10 µW the time constant τ has been determined to 16.8 s, 10.1 s and 6.2 s.
In CoPS a single estimation of numbers can be as fast as 100 ms. Photobleaching has no major effect in this short acquisition time. But by prolonging the analysis interval $t_{ac} > 500$ ms, the bleaching can be observed with CoPS (see Figure 3.3).
On the other hand, we have seen that the molecular brightness is essential for CoPS. The probability of mDE is scaling with powers of p_{exp} [84] and therefore a basic molecular brightness is required for estimating numbers by CoPS.
For example, the low emissive state in Figure 3.2 has a molecular brightness of about $9 \cdot 10^{-4}$ cplcm and the probability that two molecules emit two photons in one laser cycle is $8.1 \cdot 10^{-7}$. In contrast, the bright state possesses a probability of $1.6 \cdot 10^{-5}$ for two photon events in case of two emitters.
Previous experiments showed the feasibility to count fluorescent labels up to 4. In Figure 3.3 the relative median and the relative sigma of the distribution are shown. But the median μ_{cops} and sigma σ_{cops} are calculated in reference to the dedicated number by biochemical preparation. Even when the probe is designed as a standard sample, the attached label number for individual probes is not identical for all probes. It depends on the degree of labeling (DOL) of the nucleotides in probe preparation and some emitters might be not active anymore. To approve the validity of CoPS measurements, the estimates n_{cops} are compared to BS analysis n_{bs}. The number of molecules can be estimated by evaluating the complete intensity transient and counting the intensity drops.

In Figure 3.5, the estimations from BS analysis (blue) and CoPS (red) are plotted in

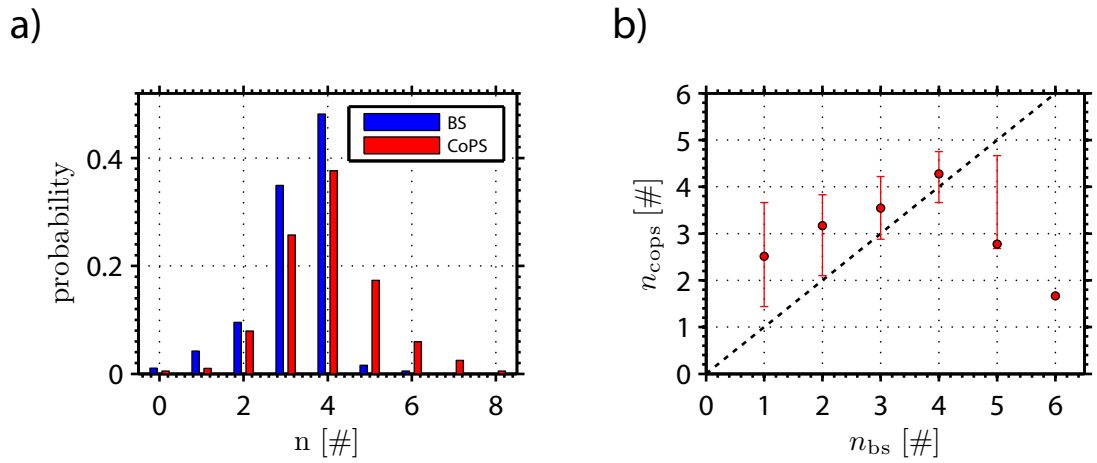

Figure 3.5.: a) Analyzed number distributions of NuP4 by BS analysis (blue) and CoPS (red) (analysis window 125 ms, laser excitation 10 µW, laser repetition 20 MHz) b) Box plot of the corresponding estimations by CoPS to each bar, estimated by BS analysis in a). The box plot shows the median and the central 68% of the data. (233 transients)

histogram a) for 10 µW and an analysis time of $t_{ac} = 125$ ms. Even though the probe was designed as a reference with exactly four labels attached, the number distribution is broader. The most probable numbers of emitters are three and four. Both methods yield similar results, however, the estimates n_{cops} show more results at label numbers larger than four.
Just as in previous observations,[86] up to three probes can bind to the free binding sites of streptavidin [112] and shift the label numbers to larger values. This would be visible in a prominent peak at 6 and 8 emitters, which is not present. The shift to large numbers indicates therefore that CoPS is more likely to estimate large numbers. This is described in more details in section 2.5.2.
To analyze the correlation between estimates by BS analysis and CoPS, I grouped the traces in six categories according to the estimated numbers by BS analysis. The box-plot in Figure 3.5 b) is showing the median and relative sigma of CoPS analysis for each category.
The estimates by CoPS show larger values for BS numbers of 1 to 4. The emitter numbers besides three and four have however no profound statistical basis, since about 67% of the data is accumulated in these two categories (see Figure 3.5 a)). At these values both methods differ only slightly.
By not only looking at the accumulated number distributions but rather at the correlation, the conformity of methods can be explored. BS analysis tends to underestimate the number of labels because frequently bleaching steps occur simultaneously. In contrast, CoPS rather overestimates the number of emitters due to the nonlinear parameter space (see section 2.5.1). However, for label numbers up to 4, both methods estimate the distribution in a consistent manner.

3.1.3. Estimating Number of Labels

In fluorescence spectroscopy and microscopy, labels attached to the probe are the reporters of desired information, for example the location, conformation or stoichiometry.[113, 114] Depending on the labeling procedure the NOL per probe can vary and does not necessarily obey a 1:1 stoichiometry. The most common procedure to engage the DOL is by ensemble spectroscopy (see section 1.1.1). Thereby, the absorption at a characteristic probe wavelength is compared to one of the labels. The outcome is the label-to-probe ratio inside the whole sample batch and it is not given that no free dye remains. The DOL therefore only shows the ensemble average and gives no information about the distribution of labels.
In single molecule experiments we can obtain the NOL distribution by measuring the number of labels attached to single probes. The NOL directly shows the distribution of labeled probes and the center and variance can thus be obtained. Probes with no fluorescent label are not accounted for. And the DOL is calculated by the average of the NOL distribution.
In previous investigations by Ta et.al. [86] a hybridization probe was used (HyP5, see Figure 3.1) as standard sample. But the NOL of this probe can be modified by changing the ratio between long and short DNA base strands during probe hybridization. Smaller concentrations of short DNA lower the probability to obtain a perfectly hybridized probe with 5 attached labels.
Four different samples with different ratios of long base ssDNA and short marker ssDNA have been prepared (ratio 1:4, ratio 1:8, ratio 1:12 and ratio1:16). Each sample was hybridized separately (see section 2.2.2) and immobilized on single-molecule surfaces (see section 2.3). By acquiring 183, 140, 124 and 104 transients from different marker-base-ratios, the attached label number could be assessed by CoPS and BS analysis. For BS analysis each transient was measured until complete photobleaching and the numbers are determined manually. The first 250 ms are selected for analysis by CoPS, due to rapid photobleaching.

In Figure 3.6 a) - d) the estimated NOL distribution by CoPS and BS analysis is shown for different base-marker ratios. By increasing the concentration of the small labeled ssDNA in the hybridization process, the number of labels is rising. Both methods evaluate the NOL distribution with minor differences. But BS estimates are slightly lower than in CoPS. However, the detection of bleaching steps is sometimes misleading, since two or more fluorescent emitters frequently undergo photobleaching simultaneously and appear as single step. In contrast, CoPS tends to overestimate the number of emitters determined previously. Therefore can the NOL distribution only be determined by knowledge of the methods intrinsic estimation variance or by the confidence, that the error is hidden in the label variance.
In Figure 3.6 e) the median and sigma of CoPS (red) and BS analysis (blue) are shown for ratios from a) - d). The integer output of BS analysis prevents the use of quantiles and the points show the calculated median. Error bars indicate the standard deviation. The estimates by BS analysis and CoPS match very well, as seen before. The development of labels per probe by increasing ratio is not linear, which is expected because of the complex probe design and experiments. However, the pronounced increase for

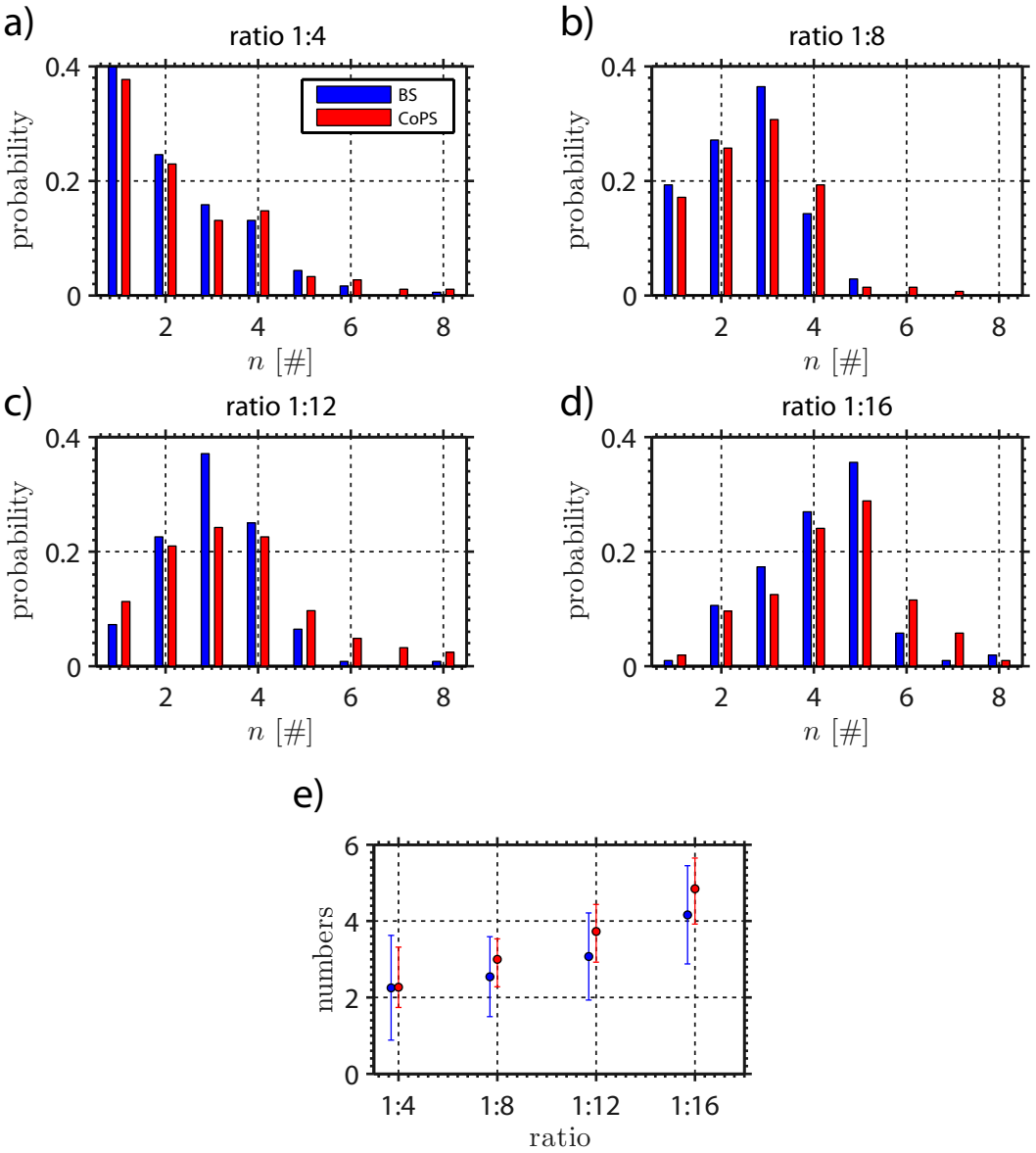

Figure 3.6.: NOL distributions estimated by CoPS (red) and bleaching step analysis (blue) for a set of differently prepared HyP5. The hybridization ratio changes from a) to d) for 1:4, 1:8, 1:12 or 1:16. The estimated distributions by BS analysis and CoPS differ only slightly. From a) to d) the distribution shift to larger numbers. But not only the mean is observable, also the shape of distributions. e) The estimation mean and standard deviation for BS analysis (blue) and a box plot for CoPS (red, median and the σ quantile) indicates the overall shift in numbers by different ratios.

large ratios is unexpected.
In this experiment it is shown that the NOL distribution for HyP5 probes depends on

the probe preparation. Not only the median/mean is shifted to larger values, also the shape of the distribution is skewed. For example, at a ratio of 1:4 the most probable label number per probe is 1 but the average NOL is about 2.25.
In ensemble experiments only the degree of labeling is obtainable, which is the ratio of dye to sample concentration. In single-molecule experiments the NOL per individual probe can be directly determined and the distribution of label numbers measured. This is essential for quantitative analysis on the single molecule level.

In this chapter some basic features of CoPS have been investigated. It has already been shown that counting to numbers up to five is feasible with CoPS and gives similar results to BS analysis. But the applied standard sample has a broad distribution and depends on probe preparation (see Figure 3.6). I investigated a new standard probe NuP4 with a very narrow distribution of numbers. From that we can learn that BS analysis has a small error when counting up to four. The intrinsic estimation variance of CoPS is slightly broader and there is a systematic bias to larger numbers. The bias probably comes from the non-linear parameter space (see section 2.5.1). The mean NOL of NuP4 is therefore larger for CoPS with 4 labels/probe to 3.3 labels/probe in BS analysis. However, the median of CoPS is more robust to outliers and shows 3.8 labels/probe.
An advantage of CoPS is the estimation of numbers and brightness at the same time. In Figure 3.2 we have seen that single-molecule transients can exhibit complex patterns, which are misleading and allow different interpretation. CoPS can differentiate between changes in numbers and changes in molecular brightness.
This is of course only true as long as CoPS can be applied. At low molecular brightness the probability for mDE is small and it takes a long time to accumulate statistics. So far, the application limit was not observed. A major advantage is the time resolution of CoPS, though. Up to 5 molecules can be sized in about 100 ms. The time to measure a fluorescence transient to apply BS analysis is $n \times \tau_{\mathrm{LP}}$ and for four molecules at 10 µW about 25 s.

3.2. Simulations

The lack of a homogeneous stoichiometric standard sample complicates the analysis of quantitative methods, because the bias and precision of the method are disguised by the NOL distribution of the labeling which is difficult to obtain. By comparison of different methods to measure the NOL distribution only the conformity of estimations can be investigated. The bias and precision of each individual method is hidden under the convolution of both methods variances. Full control about number of emitters and molecular brightness is achieved by applying simulations to obtain single molecule data. The simulations can model convenient conditions in a way that bias and variance of CoPS can be evaluated. The simulation parameters and details can be found in section 2.1.6.
In this section I will at first show that simulations deliver similar data as experimental single molecule transients. However, my intention is not to completely simulate all photophysics of organic fluorophores, like bleaching, long triplett times, etc., but rather analyze the bias and the precision of CoPS in the ideal case.
In the later parts I will use simulations of different numbers of molecules to analyze the dependence of estimations on time and investigate the counting limits of CoPS. By evaluating data with varying molecular brightness, I can observe minimal requirements for CoPS and investigate whether the achievable time resolution changes for different laser intensities, i.e. different molecular brightness.

3.2.1. Monte Carlo Simulations

I acquired the single molecule data by MC simulations. The setup-specific parameters were adjusted in order to model the microscope on which I conducted my measurements. The properties of fluorescent emitters are similar to those of the commercially available ATTO 647N dye, which is generally used in this work. The details of the simulation data can be found in section 2.1.6. In short, I modeled the photon emission from a number of n emitters of ATTO 647N. The excitation intensity is also a parameter and is varied during simulations. The properties of ATTO 647N like lifetime, absorption coefficient and quantum yield are available by the supplier.[100] In a second step the detection process was modeled. The limited detection efficiency of the microscope and the detector is part of the simulation. The HBT is also part of the model. Therefore I could apply CoPS to simulated single-molecule transients. To use the modeled data as reference for the estimation limitations of our algorithm, I neglected bleaching events. An important simplification is also the use of the same molecular brightness for all molecules.

In Figure 3.7 a), a single molecule transient acquired in simulation and in experiment is shown. The excitation intensity in the simulation is 8 µW. The experimental data is acquired from a single molecule immobilized on the surface in ROXS buffer (see section 2.4). The excitation intensity is 10 µW and the laser repetition rate 20 MHz. Both molecules show similar intensities at selected excitation powers with 59 kHz and 69 kHz for simulation and experiments, respectively. The red trace observed in experiments

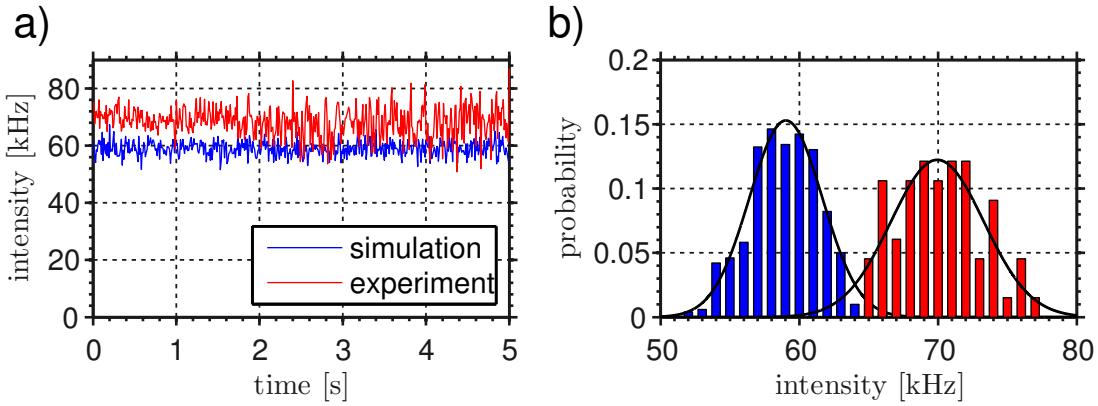

Figure 3.7.: a) Simulated fluorescence transient of one single simulated molecule (blue, 8 µW) and a transient of one single molecule acquired in experiment (red, ATTO 647N, 10 µW). b) Photon intensity histogram of the transients in a). For the experimental data only the first two seconds are accumulated. The black lines indicate a normal fit to the data. The real molecule shows slightly larger intensity and variance. Simulated: ⟨I⟩ =59, FWHM = 6.2 Real Data: ⟨I⟩ =69, FWHM = 7.

shows a constant variance in intensity for the first two seconds, which is similar to the variance of the blue trace obtained in simulation. From second two to five the variance of the intensity increases, probably due to photoinduced processes.
To compare the photon statistics of the simulation and the experiments I plotted the photon count probability of the simulated data and of the first two seconds from the experimental transient in histogram in Figure 3.7 b). The intensity probability distributions shift slightly by 10 kHz and show a typical bell-shaped distribution. The black line shows the Gaussian fit to the data and yields a FWHM of 6.2 kHz and 7.9 kHz for simulation and experiments, respectively.
The MC simulations of single molecules yield similar photon statistics as in the experiment. However, the emission becomes stable over time and shows no random photophysics. This is intended and useful in order to observe the bias and precision in estimations by CoPS.

3.2.2. CoPS with Simulated Data

In Figure 3.8 a) a simulated fluorescence transient of 18 fluorescent emitters is shown in blue (left axes) along with the estimation by CoPS in red (right axes). The transient was simulated at a laser power of 8 µW and shows a steady fluorescence emission. By CoPS estimation, I can obtain n_{cops} from accumulated photon statistics for every 250 ms and throughout the complete transient. The estimates n_{cops} are located mostly around the simulated 18 molecules (solid black line). The erroneous estimations are mostly shifted to larger values and show enlarged error bars deduced from bootstrapping (see Section 2.5.1). However, it seems, that the bootstrapping error do not reflect

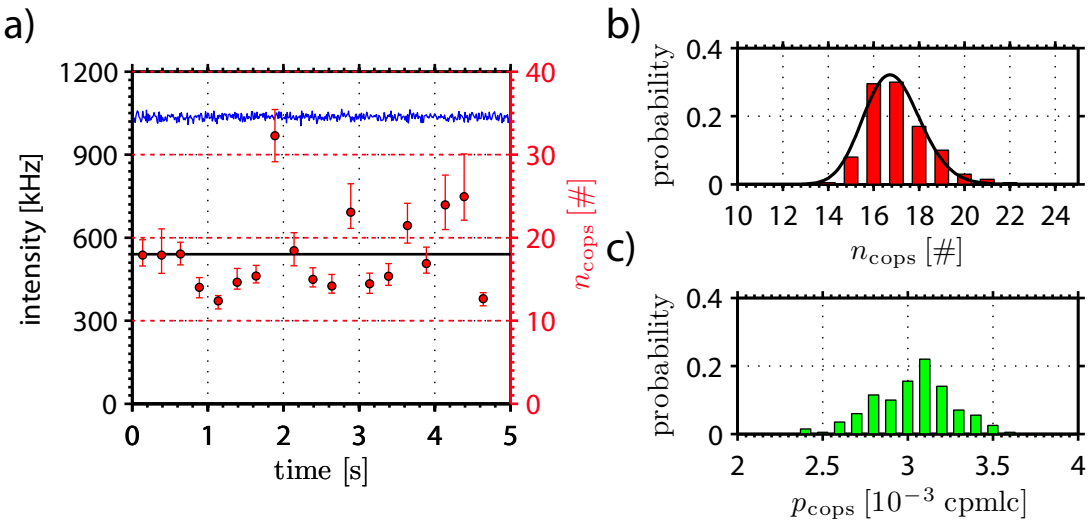

Figure 3.8.: a) Fluorescence transient of 18 simulated emitters (blue, left axes) and estimations by CoPS (red, right axes). The 18 dedicated molecules are indicated by the solid black line. The number (b)) and molecular brightness (c)) estimations from 200 simulated transients are accumulated in the histogram (laser power 8 µW, analysis window 250 ms, 200 estimates).

the measurement error.
To analyze the bias and precision in detail, I have simulated 200 fluorescence transients. In Figure 3.8 b) and c) the accumulated estimates n_{cops} and p_{cops} are shown.
The estimations of n_{cops} are distributed around the value of 17 emitters. The estimates show a non-symmetric distribution, with a tail to high molecule numbers. In contrast the left side of distribution decays fast. The probability distribution of n_{cops} has been investigated in more details in section 2.5.2. However, the distribution of n_{cops} can be fit by a log-normal function (black line). The median μ_{logn} converged to 16.8 and sigma σ_{logn} to 2.5. By calculating the quantiles from the data, the median μ_{cops} is derived to 16.8 and the sigma σ_{cops} is 2.4.
The log-normal distribution resembles the estimated number distribution, because it seems to model the parameter space of CoPS model (see section 2.5.2). But the calculation of quantiles gives similar results for large data sets and avoids the fitting procedure. In all analysis of this work, the quantiles are used to estimate the center μ_{cops} and width of the distribution σ_{cops}.
The median, as the center of the distribution, gives a good estimate on the simulated number with an offset of -6%. The counting precision of 13% is quite narrow.
The molecular brightness p_{cops} is also distributed non-symmetrically, however it is skewed to a large molecular brightness. The median μ_{cops} can be determined to $3.1 \cdot 10^{-3}$ cplcm and the sigma σ_{cops} to $4.4 \cdot 10^{-4}$ cplcm.
The fluorescence transient shows a constant intensity over the whole time and the acquired photons contribute to the mDE statistics required for CoPS. Therefore, the model to estimate the number of emitters is linked to the fluorescence intensity. The

intensity needs to reflect the product of n_{cops} and p_{cops}. This principle is obvious, it is only true in an approximate way, though. The detection of two simultaneous photons is not possible on the same detector, because of the detector dead time. One photon does not attribute to the intensity. But it is accounted for in CoPS. The probability of two photons arriving at the same detector at the same laser cycle is included in the model and both photons are included in estimations of p_{cops}. Nevertheless, when the fitting algorithm converges at largely overestimated numbers (see section 2.5.1), the molecular brightness needs to compensate.

3.2.3. Time Dependency of CoPS Estimates

CoPS analysis is a non-invasive measurement and estimates are obtained quasi-instantaneously. The time resolution is only limited by the required laser cycles in order to accumulate the necessary mDE statistics for the non-linear regression. To obtain the time resolution, estimations of varying acquisition windows t_{ac} are evaluated. For an excitation intensity of 8 µW, 200 fluorescence transients have been simulated for 5 s with 6, 12, 18, 36 or 50 emitters.

In Figure 3.9 a) the estimation median μ_{cops} (see equation (3.1)) is plotted against t_{ac}. For all molecules the median converges already at a t_{ac} of 125 ms. For numbers from 6 to 18 the estimation shows a small offset of about -5%. For molecule numbers of 36 and 50 the underestimation is more pronounced by -17% and -27% respectively. The estimations converge to a constant value over time, because the photobleaching process was not simulated.
A single estimation of n_{cops} requires only about 125 ms and counts numbers up to 18 emitters with a small offset. For larger emitter numbers the evaluation fails. In this case 36 and 50 molecules are estimated as 30 and 37 molecules, respectively.
I am not only interested in the bias, but also in the actual precision of CoPS. Therefore, I plotted σ_{cops} for different molecule numbers in Figure 3.9 b).
The relative sigma σ_{cops} is decreasing rapidly for short times t_{ac} and after approximately 1 s the precision is linearly improving from 10% to 5%. For the molecule numbers of 36 and 50, σ_{cops} is slightly lower than with the lower numbers.
By analyzing the estimation bias and precision of CoPS for different molecule numbers, the feasibility to count up to 18 emitters in few 100 ms is shown. The precision at $t_{\text{ac}} = 1$ s is already at 10%. However, for molecule numbers of 36 and 50, the μ_{cops} underestimated the simulated numbers widely. This is the counting limit of CoPS in this experiment. The model function does not properly fit the simulated mDE statistics anymore. But the statistics are dependent on the molecular brightness (see section 2.5.1). In further simulations with larger molecular brightness, I first investigated the dependency of CoPS on molecular brightness.

3.2.4. Counting Sensitivity to Molecular Brightness

In Figure 3.10 a) I have plotted the μ_{cops} for 18 simulated emitters against t_{ac} at different laser intensities 1 µW, 2 µW, 4 µW, 8 µW, 12 µW and 18 µW. As seen before,

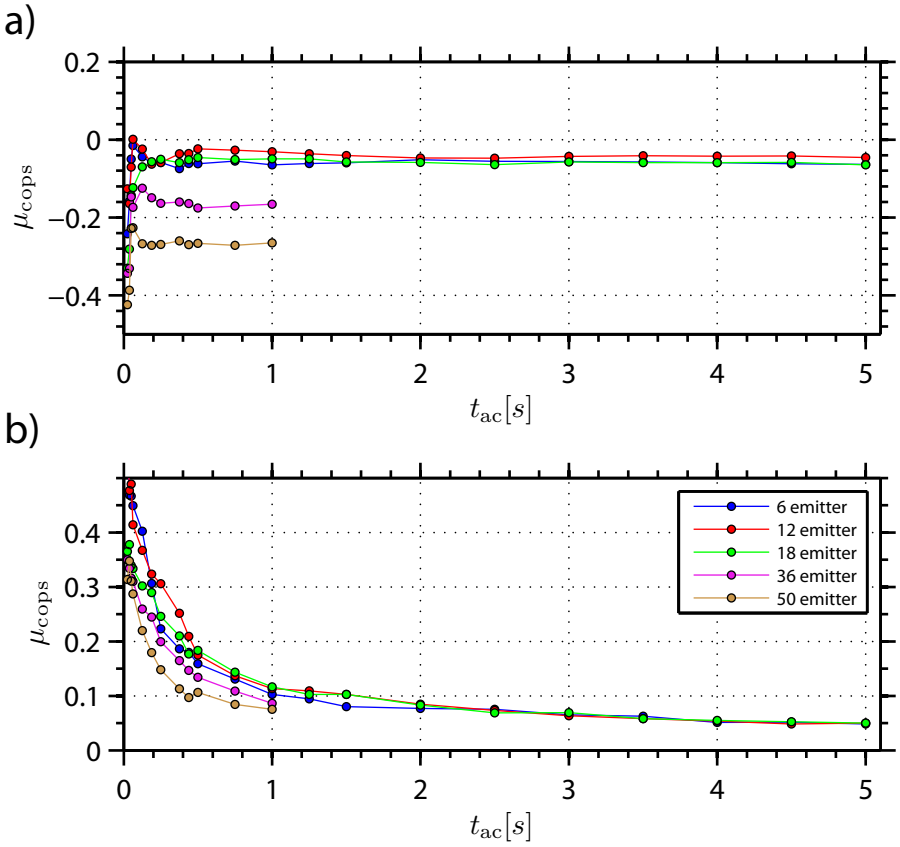

Figure 3.9.: a) Evolution of the median μ_{cops} over the time t_{ac}. b) Evolution of the estimated σ_{cops} by increasing the time t_{ac}. The data was simulated at a laser intensity of 8 µW

the median increases at the beginning of each trace. For laser intensities larger than 2 µW it approaches to slight underestimation of 6% with increasing analysis window time. The offset for laser intensities of 1 µW and 2 µW is larger and approaches -53% and -24% after 3 s.
The relative sigma σ_{cops} is shown in Figure 3.10 b). The fast decay in the beginning can be attributed to the build up of the necessary mDE statistics. After 200 ms, when the statistics has converged, the σ_{cops} for laser powers of 4 µW is highest (with 15%-20%) and between 1% and 10% for other excitation powers.
At laser intensities above 2 µW the relative median μ_{cops} converges quite fast to a constant offset in about 125 ms and σ_{cops} is decreasing with t_{ac}. The precision is increased for higher laser intensities, due to the improved photon statistics by the larger molecular brightness. This is consistent with previous observations.
At excitation intensities of 1 µW and 2 µW μ_{cops} underestimates the simulated number. Nevertheless, the σ_{cops} is still small, although a rather broad distribution is expected from a non-converging fit. In Figure 3.9, the σ_{cops} is very small for 36 and 50 emitter, which could not sized consistently by CoPS. Therefore, it seems that the counting limit

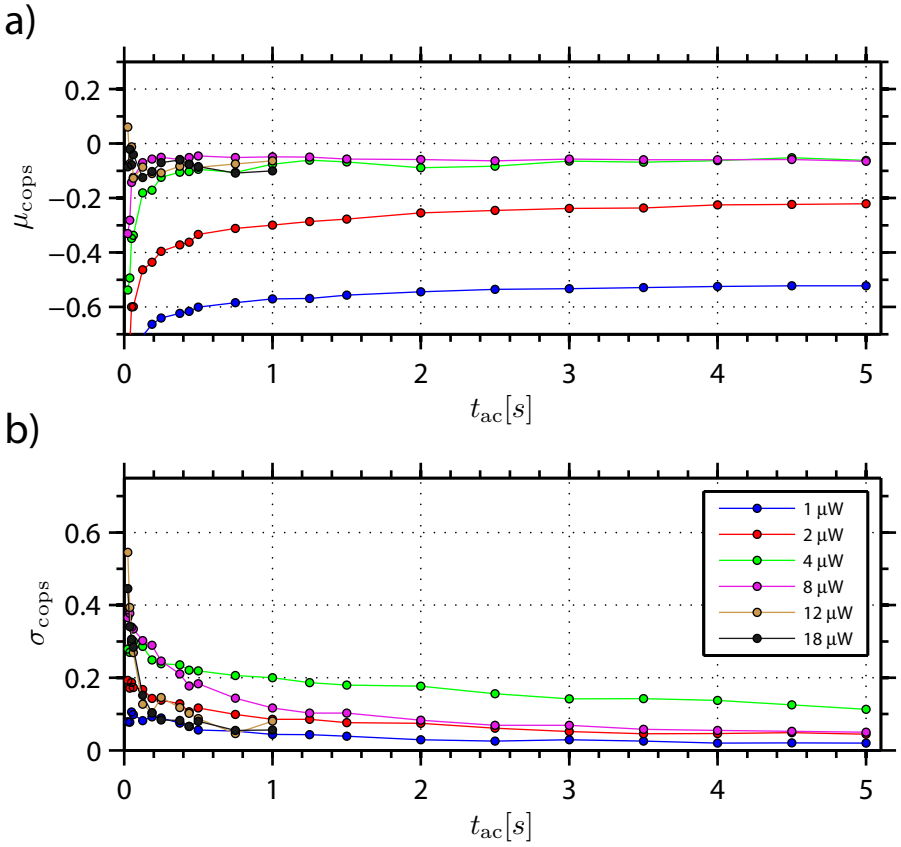

Figure 3.10.: a) The development of the median μ_{cops} over time t_{ac} for 18 simulated emitters at laser powers 1 µW, 2 µW, 4 µW, 8 µW, 12 µW and 18 µW. b) The development of the relative sigma σ_{cops} over time t_{ac} for 18 simulated emitters.

depends on the molecular brightness. And even when the number of emitters is not evaluated correctly, the σ_{cops} is still small.
So far the simulations have shown, that a basic laser power is required for the application of CoPS. If molecular brightness is below a threshold, the μ_{cops} underestimates the observed numbers, but σ_{cops} is still small. This indicates that by further increasing the laser power, the counting limit of CoPS is shifted to larger values.

3.2.5. Basic Molecular Brightness

The excitation intensity is closely linked to molecular brightness (see equation (1.2)) and also the reason for photobleaching of emitters in an experiment (see Figure 3.4). To minimize the influence of bleaching, it is necessary to measure with minimal laser intensities which still allows accurate estimates.

The development of μ_{cops} with increasing laser intensity and therefore molecular bright-

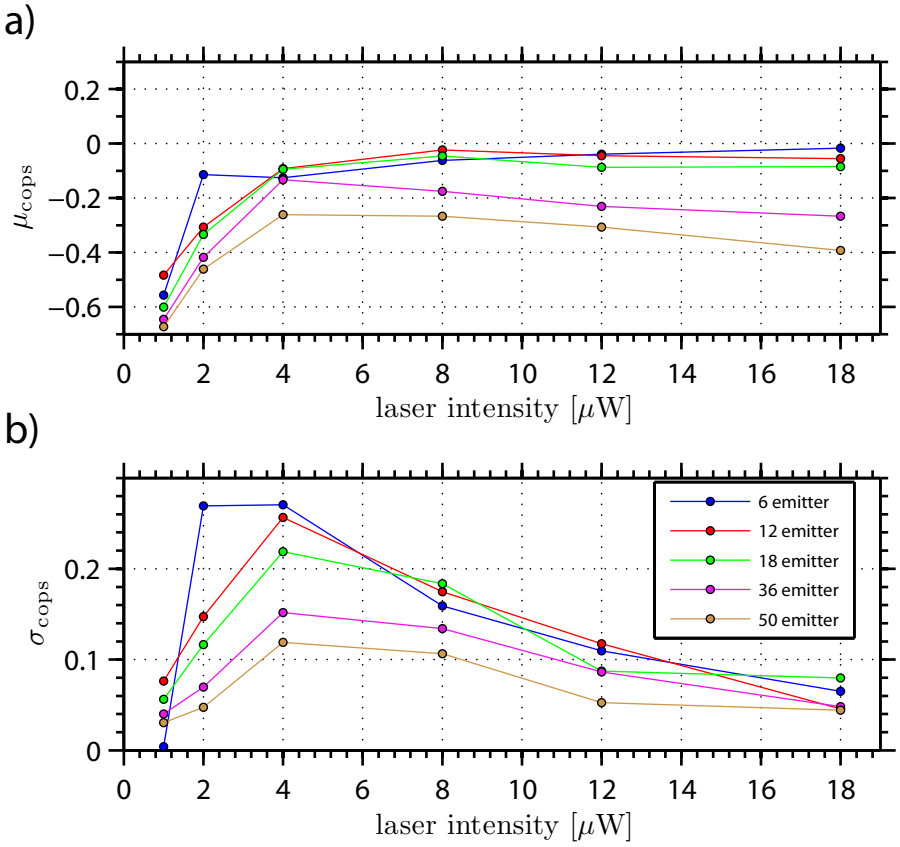

Figure 3.11.: a) The relative median μ_{cops} for $t_{ac} = 500\,ms$ over applied laser intensity. b) Relative sigma σ_{cops} of estimations over laser power.

ness is shown in Figure 3.11. Raising the laser intensity to 4 µW increases to μ_{cops} for all molecules. For molecule numbers from 6 to 18, μ_{cops} approaches -5% for laser intensities larger than 8 µW. For 36 and 50 molecules, in contrast, the μ_{cops} is decreasing to -25% and -40% by increasing the laser intensities.
The dependence on the relative sigma σ_{cops} to the laser intensity shows a strong increase from 1 µW to 4 µW and then decays to 5% for all molecules at large excitation intensities.
The μ_{cops} is underestimating numbers of 36 and 50 emitters even for a molecular brightness of $6.4 \cdot 10^{-3}$ cplcm. Additional simulations at even larger molecular brightness have so far not been conducted, because the computational power to simulate 50 emitter at current molecular brightness is already high. Nevertheless, the acquisition of a signal of 3.2 MHz at 10 MHz for 500 ms is hardly possible with the confocal setup, applied in this work.
However, for the molecule numbers up to 18, CoPS allows sizing of emitters after exceeding a certain threshold level of 8 µW. The estimate is then independent of excitation. By further increasing the laser power, only the precision σ_{cops} is improving to about 5% at 18 µW at $t_{ac} = 500\,ms$.

From these observations, the bias and precision of CoPS is known. However, in experiments we have no a priori information about the NOL of a sample. The first and most important task is to decide if a sample is different from another or if they are same. In the following I will observe the feasibility of differentiating between several close probes.

3.2.6. Counting Resolution

By accumulating statistics about n_{cops}, the probability distribution is sampled and the estimate of μ_{cops} improved. To discern two nearby NOL distributions, they have to be well separated, though.

To study the theoretical limit of discerning two adjacent number of emitters, I simulated 200 transients of 12, 13, 14, 15, 16, 17 and 18 emitters and estimated n_{cops}. In Figure 3.12 a)-g) the probabilities for n_{cops} are shown for the different simulated probes (laser power 8 µW, $t_{\mathrm{ac}} = 250$ ms). In CoPS the probability distribution is described approximately by a log-normal distribution (black line, also discussed in section 2.5.2). The n_{cops} shift to larger numbers when increasing simulated n_{sim}. This is more obvious by looking at the quantiles. The median and the central 68% of the data are plotted as box plot against the simulated numbers in axes h).

All n_{cops} distributions show similar precision and shift to larger numbers. But the distributions are broad and overlap. To investigate the confidence by which they can be discerned I applied a statistical test.

As the probability distribution of CoPS is skewed and not normally distributed I cannot apply tests which are based on the normal distribution. The Kolmogorov-Smirnov test (ks-test) [115, 108] is a two-sided, non parametric test with no assumption of normality.[106] The two sided ks-test analyzes if values of a probability distribution A are significantly larger compared to a second distribution B. The null hypothesis H0 is therefore "the distribution B has equal or larger values than A". The null hypothesis will be rejected if the p_{ks} value drops below a prior confidence level α_{ks}. The p_{ks} value describes the probability to obtain two distributions A and B under the assumption that H0 is true. If the p_{ks} is below α_{ks}, H0 is rejected. The ks-test analyses the maximal distance between cumulative density function (cdf) of both distributions and estimates the p_{ks}.

In the array (3.3) the ks-test is applied for each combination of distributions and the rejected null hypothesis is marked by a ↯. When the p_{ks} is above α_{ks} cannot be rejected and marked with a -. The p_{ks} values are shown in the array (3.4) in percent. The array of a perfect counting resolution would show rejections in the lower left triangle and high p_{ks} in the upper right triangle.

$$\begin{pmatrix} \mathrm{ks}_{12>12} & \cdots & \mathrm{ks}_{18>12} \\ \vdots & \ddots & \vdots \\ \mathrm{ks}_{12>18} & \cdots & \mathrm{ks}_{18>18} \end{pmatrix} = \begin{pmatrix} - & - & - & - & - & - & - \\ \lightning & - & - & - & - & - & - \\ \lightning & - & - & - & - & - & - \\ \lightning & \lightning & \lightning & - & - & - & - \\ \lightning & \lightning & \lightning & \lightning & - & - & - \\ \lightning & \lightning & \lightning & \lightning & \lightning & - & - \\ \lightning & \lightning & \lightning & \lightning & \lightning & \lightning & - \end{pmatrix} \tag{3.3}$$

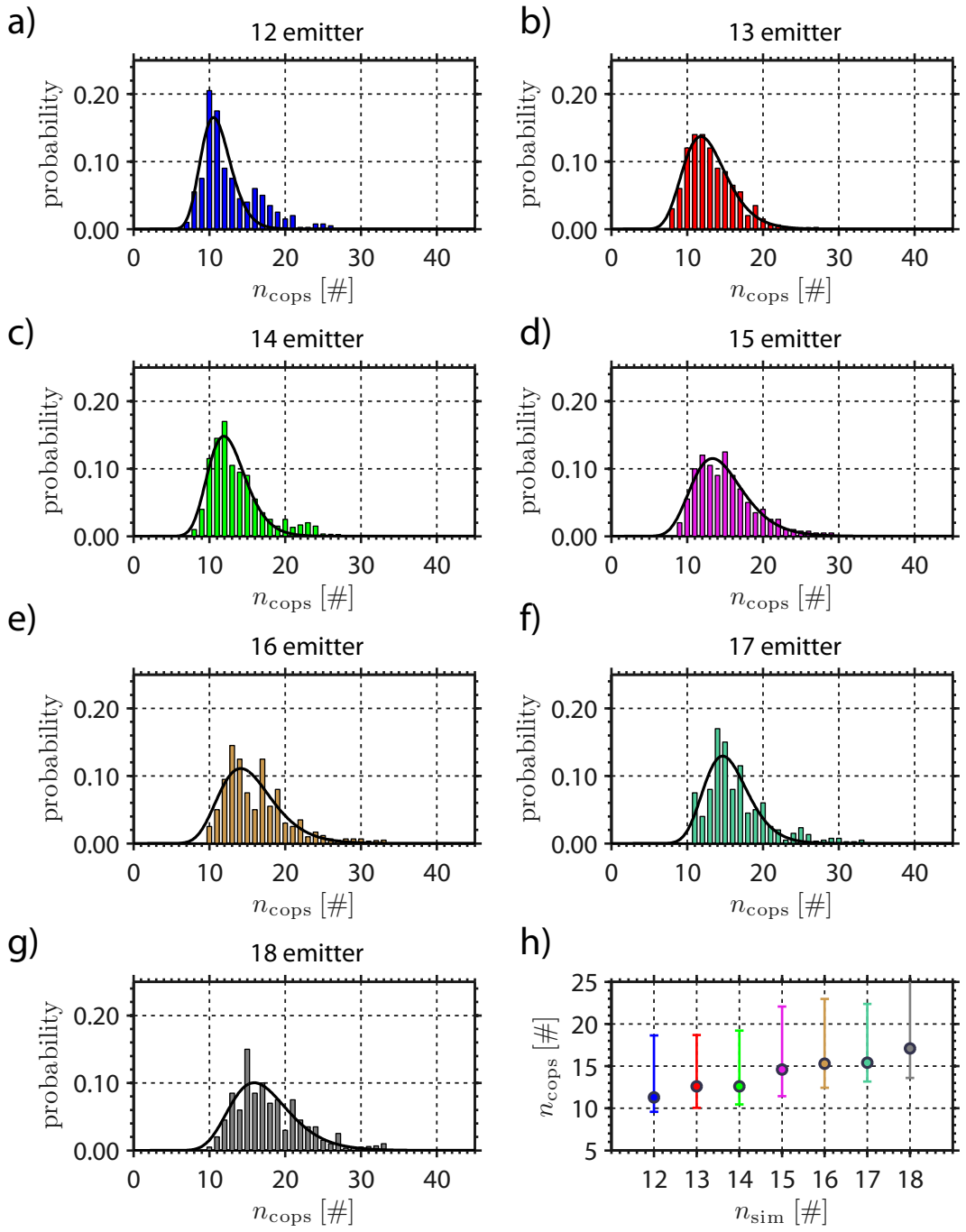

Figure 3.12.: Probability distribution of n_{cops} of simulated probes with 12, 13, 14, 15, 16, 17 and 18 emitters at 8 µW in a) to g) ($t_{\mathrm{ac}} = 250\,\mathrm{ms}$). The black line indicates a log-normal fit. In axes h) the absolute median and the central 68% of the data are shown for all samples.

In the array (3.4) the p_{ks} in % for each individual comparison is depicted as before.

$$\begin{pmatrix} p_{\mathrm{ks}(12>12)} & \cdots & p_{\mathrm{ks}(18>12)} \\ \vdots & \ddots & \vdots \\ p_{\mathrm{ks}(12>18)} & \cdots & p_{\mathrm{ks}(18>18)} \end{pmatrix} = \begin{pmatrix} 100 & 66 & 98 & 100 & 100 & 100 & 100 \\ 0 & 100 & 98 & 100 & 100 & 100 & 100 \\ 0 & 42 & 100 & 92 & 100 & 100 & 100 \\ 0 & 0 & 0 & 100 & 100 & 72 & 98 \\ 0 & 0 & 0 & 1.3 & 100 & 72 & 98 \\ 0 & 0 & 0 & 0 & 3 & 100 & 99 \\ 0 & 0 & 0 & 0 & 0 & 0 & 100 \end{pmatrix} \tag{3.4}$$

From the two sided ks-test it can be seen that the p_{ks} values in the upper right half are all above the α_{ks} value of 0.05 and therefore the hypothesis is not rejected. In the lower left half, the hypothesis is dismissed, except a value near the diagonal. In entry a_{32} the p_{ks} value is 40% and therefore the hypothesis is not dismissed. Generally, it can be stated that in data which is as good as in this simulations, by CoPS it is possible to differentiate between distributions with a counting resolution of 1.

The simulation of fluorescent transients with controllable molecular brightness and stable and known emitter n_{exp} provided much information about CoPS. The estimates of single traces show a log-normal distribution for n_{cops} and indicate that this is a good approximate to the intrinsic estimation variance of CoPS. The minimal time t_{ac} required for applying CoPS is about 100 ms and valid for n_{exp} up to 18. By counting larger numbers, n_{cops} underestimates the simulated number. This is at least true up to a excitation power of 18 µW or a molecular brightness of $6.4 \cdot 10^{-3}$ cplcm.
On the other hand, analyzing transients at low excitation power has shown that a basic molecular brightness of $1.4 \cdot 10^{-3}$ cplcm is necessary to obtain numbers up to 18. The variance σ_{cops} is however, still large and improves with increasing molecular brightness. The estimate probabilities of adjacent n_{sim} overlap, but the counting resolution of n_{cops} is at $t_{\mathrm{ac}} = 250$ ms and 8 µW for the simulated transients very good. Nevertheless, the simulations have been modeled under some strong assumptions, in order to observe the intrinsic estimation variance of CoPS. For example, the equal molecular brightness for all dyes is not valid in experiments. In the following, I will apply CoPS in experiment to large numbers n_{exp}.

3.3. Counting Large Numbers

In the previous section I have shown the ability of CoPS to estimate the number of emitters up to 18 in simulations and analyzed the dependency on analysis time and molecular brightness. However, simulations cannot model all experimental processes. Complex photophysics in heterogeneous environments are not predictable and single molecule fluorescence transients vary greatly in intensity and shape. To observe the counting performance of CoPS in experiments, samples which are different from those in the previous section 3.1 are required. The probe schemes applied so far are do not allow to obtain emitter numbers above five. Labeled DNA oligomers cannot be synthesized to arbitrary lengths and label numbers and the hybridization of the HyP5 probe have already shown a broad distribution of labels for few emitters.
In this section I will introduce a standard sample by which I can achieve emitter numbers n_{exp} up to 36. This allows investigations on the counting limit which I encountered in the simulations (see section 3.2). As in previous simulations the time resolution of t_{ac}, the counting resolution and the dependency on molecular brightness can be assessed.

3.3.1. Quantitative Analysis of DNA origamis

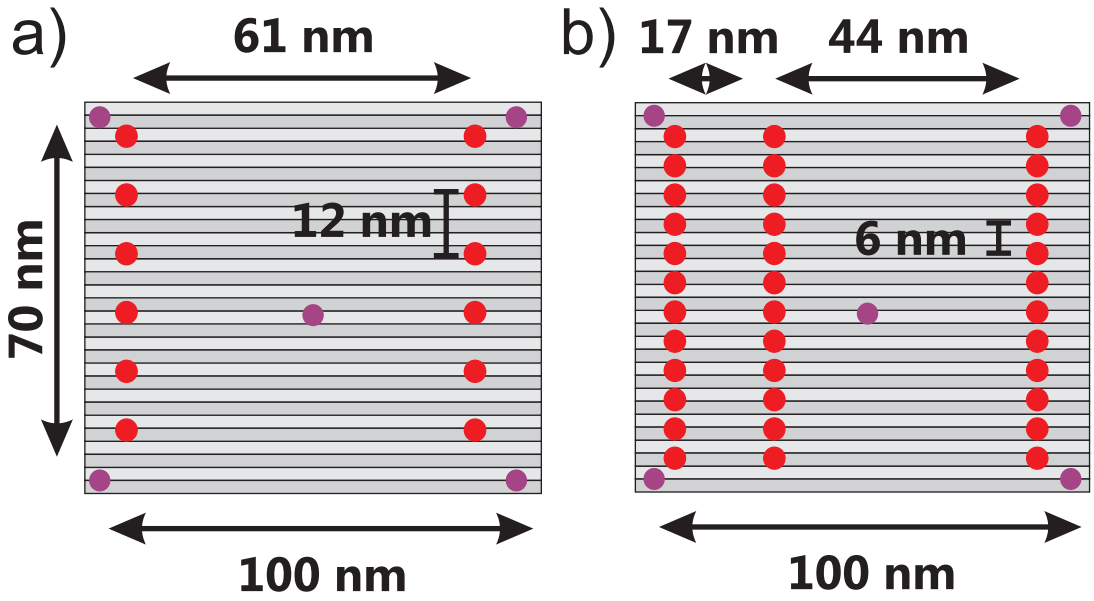

Figure 3.13.: Scheme of two DNA origamis observed in this thesis. a) 12 labels of ATTO 647N (red) are arranged with a spatial distance of at least 12 nm. b) 36 emitters are arranged with a spatial distance of at least 6 nm. The DNA origamis can be immobilized via biotin (violet) to SM surfaces.

A robust and elaborate single molecule probe was introduced in 2006 by Paul Rothemund,[101] namely DNA origamis. Schemes are available in Figure 3.13. They consist

of a long ssDNA which is folded by many smaller synthesized ssDNA to arbitrary patterns upon hybridization.[102] For details see section 2.2.3. In this work, I used DNA origami which have been kindly provided by Jürgen Schmied from the group of Prof. Tinnefeld (TU Braunschweig). The DNA origamis have a rectangular pattern of approximately 100 nm×70 nm side length, therefore smaller than the resolution limit. By labeling a subset of the required smaller staple strands, DNA origamis with arbitrary number of emitters can be produced with high confidence. I studied DNA origamis with attached 6, 12, 18 or 36 dye molecules of ATTO 647N. To avoid photophysical processes between fluorophores, it was ensured neighboring fluorescent dyes were separated by at least 6 nm. I conducted also measurements at 12 nm label distance, but experiments and analysis showed consistent results. In experiments the DNA origamis are immobilized on SM surfaces (see section 2.3) to allow observation of the same probe in the course of time. To enhance photostability and to reduce blinking in experiments, the measurement buffer contained photo-stabilizing reagents acting as a reducing and oxidizing system (ROXS) (see in the Introduction on page 3).

A typical fluorescence transient of DNA origamis labeled with 18 ATTO 647N emitters shows a fast decay in intensity due to rapid photobleaching (see Figure 3.14 a), left axes, blue). By CoPS analysis, (red, right axes) I can estimate n_{cops} with a very high sampling rate (4 Hz) and throughout the complete fluorescence transient. The initial label number n_{exp} is well estimated and the bleaching effect is represented in the decay of estimates n_{cops}. The error bars which describe the width of the bootstrapping distribution (see section 2.5.1) are increased for high number n_{exp} and large for all outliers. The broad bootstrapping distributions arise from varying photon emission during a single analysis bin and indicate that these estimates can be rejected.
The bootstrapping distribution, as the method is implemented, gives no valid estimate of the experimental error of CoPS. The bootstrapping algorithm is used to achieve more robust estimations of n_{cops} and the error bars here indicate the consistency of the mDE inside the analysis bin. The estimation variance of the method is larger which can be seen on the spread of n_{cops} in high numbers and will be discussed in in detail later.
The obtained mDE are shown in Figure 3.14 b). From 18 molecules at 2.1 cplcm 3DE are obtained, but the probability is low. Thus, the estimates are calculated from the detection probability of 1DE and 2DE, for n_{cops} below 10. By increasing the brightness, the probability for mDE rises and therefore the basis of estimation.
Only at longer observation times, single bleaching steps can be identified and show heterogeneous intensity drops (21 kHz, 35 kHz and 30 kHz) for the last three steps at 35 s, 38 s and 50 s. By extrapolating the mean of these intensity drops to the beginning of the transient, the initial number is estimated to 17 labels. By this method it is required to wait until complete photobleaching or to perform calibration with single fluorophores a priori. In contrast, CoPS can determine the label number without calibration within 250 ms.
To assess the time resolution, measurement error and robustness of the method, CoPS has been applied to a complete sample set of fluorescence transients. Data from 520, 1199, 439 and 346 DNA origamis labeled with 6, 12, 18 or 36 ATTO 647N, respectively has been acquired. To avoid false results due to rapid photobleaching only the first

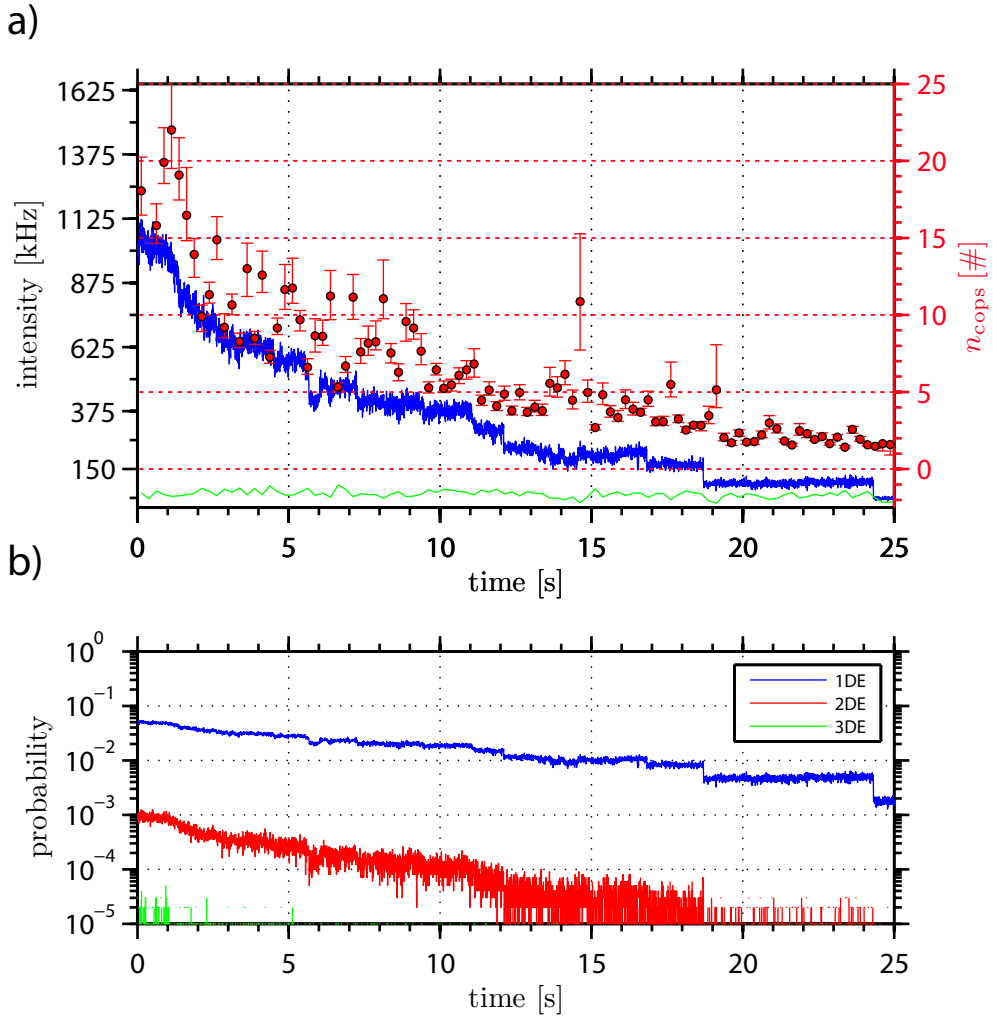

Figure 3.14.: a) Fluorescent transient of a DNA origami with 18 emitters (blue, left axes). By CoPS the number of molecules (red, right axes) and the mean molecular brightness (green, left axes) are estimated. (LP = 10 µW, t_{ac} = 500 ms, n_{cops} are offset for better visualization) b) Probability of 1DE (blue), 2DE (red) and 3DE (green) per single laser cycle.

analysis bin (t_{ac} = 250 ms) was used to estimate the initial number of emitters n_{cops}.

The probability distributions of n_{cops} are shown in the four histograms in Figure 3.15. The peak of distributions shifts with increasing n_{exp} and the width enlarges. The probability distributions show a smooth outline and the data is still described by a log-normal fit (black line, see section section 2.5.1). The characteristic parameters of the distribution and fit can be found in table 3.1

The median value of log-normal fit μ_{logn} shows an overestimation of about 17 % for

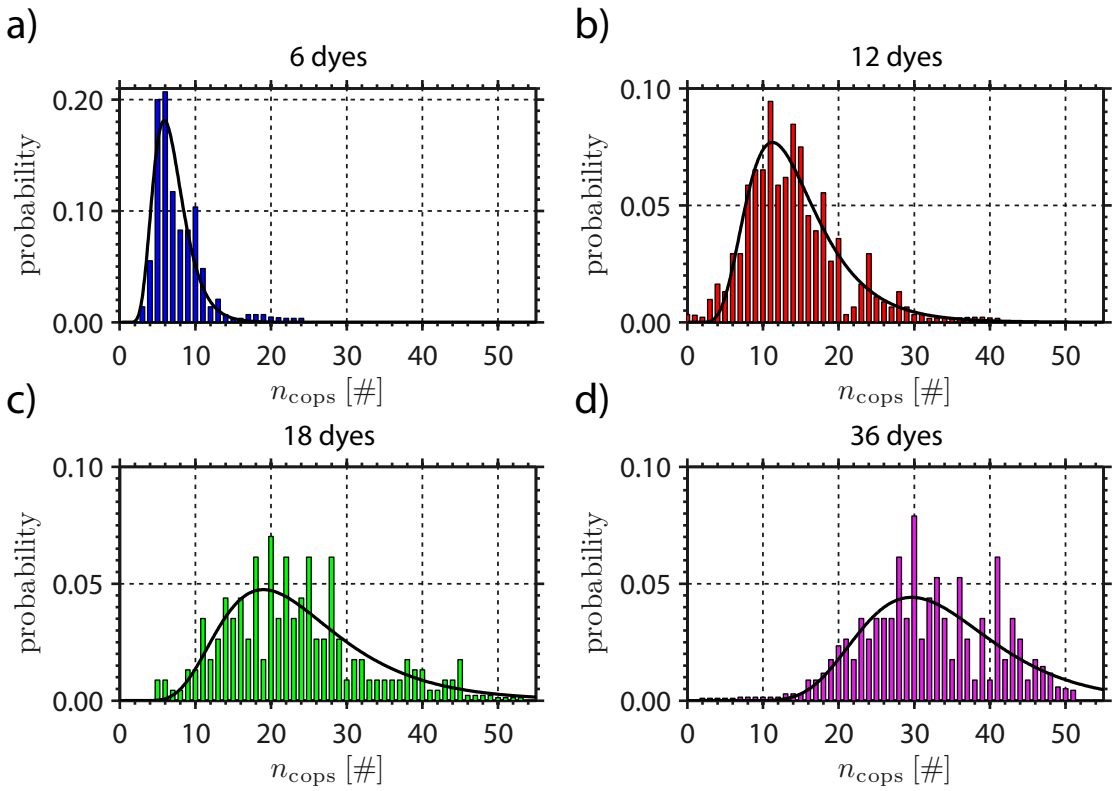

Figure 3.15.: Propability density of n_{cops} from four DNA origami. The distribution are fit by a log-normal fit (black line). The DNA origami were labeled with 6, 12, 18 or 36 dyes and the data is shown in axes a), b), c) or d), respectively. ($t_{\mathrm{ac}} = 250\,\mathrm{ms}$, LP $= 7\,\mu\mathrm{W}$)

Table 3.1.: Mode $\mathrm{m}_{\mathrm{logn}}$, median μ_{logn} and sigma σ_{logn} of the log-normal fits to the estimated numbers in 3.15 and median μ_{cops} and sigma σ_{cops} calculated by quantiles (LP $=7\,\mu\mathrm{W}$, $t_{\mathrm{ac}} = 250\,\mathrm{ms}$)

Molecules [#]	log-normal fit to n_{cops} [#]			quantiles n_{cops} [#]	
	$\mathrm{m}_{\mathrm{logn}}$	μ_{logn}	σ_{logn}	μ_{cops}	σ_{cops}
6	6	7	2	7	3
12	11	13	6	14	6
18	19	22	9	22	9
36	30	30	9	32	9

the DNA origamis with 6, 12 and 18 labels and an underestimation of the sample with 36 labels by about 14 %. The relative sigma σ_{logn} is about 28 % to 50 %. The mode $\mathrm{m}_{\mathrm{logn}}$, which is defined as the most probable estimation value, estimates the dedicated value for DNA origamis with 6, 12 or 18 with a low error of ± 1, however not for the 36 labels. The values in table 3.1, indicate that also for experimental data the description

by quantiles and by log-normal fits is equivalent. But in the following, I will continue to apply the quantiles, as they are more robust.
After validating ability of counting by CoPS up to 18 molecules, the next step is to determine the time resolution for estimations with high confidence. Another point to be investigated, is the possibility to improve counting limits by increasing binning time t_{ac}.

3.3.2. Dependency on Analysis Time

As previously observed CoPS can achieve estimates in less than a second using a pulsed laser source with MHz repetition rate. In the previous chapters the time resolution has been investigated for small molecule numbers (see Figure 3.3) and in simulations (see Figure 3.9). Here, I investigate the influence of t_{ac} on the median μ_{cops} and sigma σ_{cops} in experiments with DNA origami. For different bin sizes t_{ac} in the range of 0.025 s to 2 s, the relative median μ_{cops} and the relative sigma σ_{cops} are calculated.

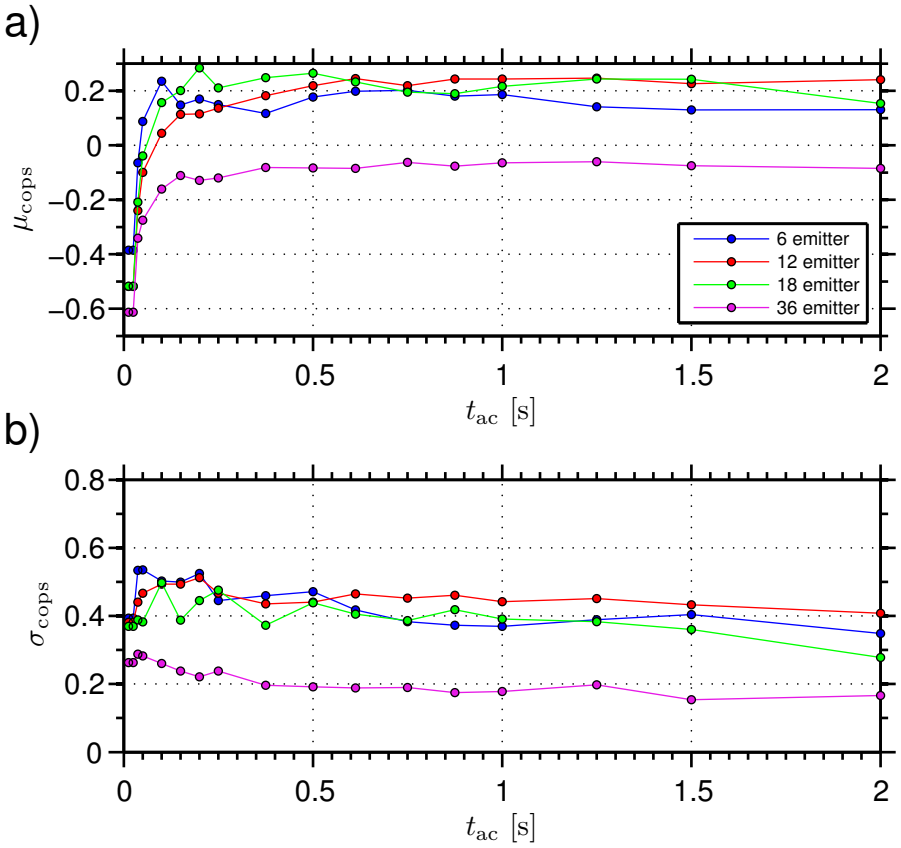

Figure 3.16.: a) The evolution of μ_{cops} of DNA origamis, with 6,12,18 or 36 emitters over analysis time t_{ac}. b) The evolution of the relative sigma σ_{cops} for the same data shown in a) (LP = 7 µW)

In Figure 3.16 a) the relative median μ_{cops} is plotted against t_{ac}. For short times t_{ac},

the estimation is shifted to low numbers for all DNA origamis. This is reasonable, since mDE statistics have not yet converged. With increasing time t_{ac}, the median μ_{cops} rises. When t_{ac} exceeds 250 ms, μ_{cops} levels off at an overestimation of about 15 % to 20 % for 6, 12 and 18 emitters. The curve for 36 labels is shifted to lower μ_{cops} at all analysis times t_{ac}, which is incordance to simulations (see in Figure 3.9).
In Figure 3.16 b) the relative sigma σ_{cops} is shown. At short p_{cops} the variance σ_{cops} is initially rising and then subsequently declining with increasing analysis time p_{cops} for all DNA origamis. The estimation error for $t_{ac} = 250$ ms is about 44 % for 6, 12 and 18 molecules, slightly decreasing to about 30 % to 50 % at 3 s. The relative error for 36 emitters follows the same trend, but is shifted to lower values, which is in accordance with simulations (see Figure 3.9)
The estimation of label numbers n_{cops} reaches a plateau of 20% at about 200 ms. On the one hand the time resolution is in the order of the simulations, on the other hand has the overestimation not been encountered in the simulation. It probably results of a process, which has not been simulated. This will be analyzed in detail in section 4.
Furthermore, the relative sigma σ_{cops} remains constant at 40% for all t_{ac}. In the simulations, σ_{cops} was improving to less than 10% with increasing t_{ac}. The variations σ_{cops} are larger in experimental results and thus, not included in simulations.

3.3.3. Sensitivity on Molecular Brightness

Besides the additional photophysics in real experiments, which can cause the offset and increased variance σ_{cops} of simulations, I have studied the effect of the molecular brightness for CoPS. Samples of DNA origami with 18 emitter have been measured at different laser powers LP of 2 µW, 5 µW, 7 µW and 10 µW. The relative median μ_{cops} and relative sigma σ_{cops} is plotted in Figure 3.17 for each laser intensity.

The relative median μ_{cops} (see in Figure 3.17 a)) shows underestimation of n_{exp} for 2 µW and an overestimation for 5 µW, 7 µW and 10 µW. The median μ_{cops} becomes stable at 15 % to 25 % as observed in the analysis of time resolution. Increasing the molecular brightness up to $2 \cdot 10^{-3}$ cplcm has no effect on the median μ_{cops}. In the slight decay for long t_{ac} the photobleaching effect appears.
The dependency of σ_{cops} (see in Figure3.17 b)) is low. The σ_{cops} declines slightly from 40%±10% to about 30%±10%, consistently for all laser powers. From previous observations it is known that CoPS require a minimal molecular brightness to become stable in its estimation. In this data this is confirmed for a molecule number up to 18.
An advantage of CoPS is large accessible number range. When conducting biological experiments, it is often required to discern two nearby samples, though. Similar to simulations (see section 3.2.6), the counting resolution is investigated here.

3.3.4. Counting Resolution with DNA origami

The possibility to discriminate two distributions which originate from samples with different numbers, is a common application of quantitative methods. The counting

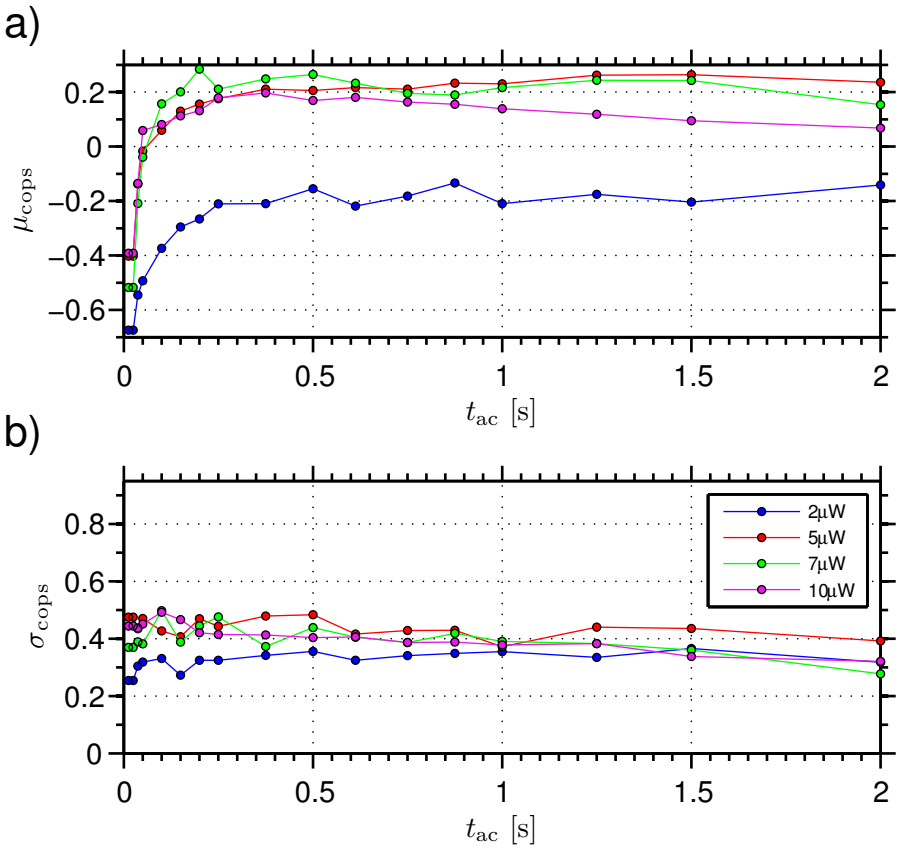

Figure 3.17.: a) Evolution of the relative median μ_{cops} by analyzing DNA origami with 18 labels of ATTO 647N at different laser intensities. b) Evolution of the relative sigma σ_{cops} of data shown in a). ($t_{\mathrm{ac}} = 250\,\mathrm{ms}$)

resolution of CoPS can be investigated in experiments with DNA origamis. Jürgen Schmied from the Tinnefeld group (TU Braunschweig) prepared five blind samples of DNA origami with numbers 13, 14, 15, 16 and 17. The samples have been marked with arbitrary numbers to avoid subjectivity in the analysis.
Before describing this result, I have to state, that this result is preliminary and encountered inconsistencies. The experiments have to be repeated, nevertheless it is an important experiment. The DNA origami showed an intensity which does not at all reflect the designated number of fluorescent emitters, as shown in Figure C.9. Probably the probe preparation failed in these preliminary experiments and results have to be handled with care.

In Figure 3.18 the measured distributions of the DNA origamis with 12 and 18 labels are shown in a) and g). The DNA origamis with numbers 12, 13, 14, 15, 16 and 17 are shown unsorted in the axes b) to f). All the distributions can be fit by a log-normal function, however they show different skewness and broadness. The shift in the estimated values can be best observed in axes h), where I plotted the box plots for the

sorted samples. The center depicts the median of the distribution and the error bars depict the central 68% of the data. The colors correspond to their individual distribution from a) to g).
From the box plot it can be seen that distributions of 12 and 13 emitters are shifted to larger values and surpass all other samples, except the 18 emitters. The samples with 14, 15 and 16 emitters show little variance in their estimations and have a median of about 15. The sample with 17 emitters is between 16 and 18 emitters.
The value difference in distributions can also be observed by a statistical test. Similar to the simulations in section 3.2.6, I applied the two sided ks-test.[107, 108, 106] The non-parametric test uses the null hypothesis that the values of distribution A are significantly larger than those of distribution B. The p_{ks} gives the probability to obtain distributions like the one acquired, if the null hypothesis is true. If the p_{ks} is smaller than the predefined α value, the null hypothesis will be rejected.
In the array (3.5) the ks-test is applied for each combination of distributions and the rejected null hypothesis is marked by a "↯". When the p_{ks} is above α it cannot be rejected and is marked by "-". The array of a perfect counting resolution would show rejections in the lower, left triangle and high p_{ks} in the upper right triangle.

$$\begin{pmatrix} \mathrm{ks}_{12>12} & \cdots & \mathrm{ks}_{18>12} \\ \vdots & \ddots & \vdots \\ \mathrm{ks}_{12>18} & \cdots & \mathrm{ks}_{18>18} \end{pmatrix} = \left(\begin{array}{ccccccc} - & - & \lightning & \lightning & \lightning & - & - \\ \lightning & - & \lightning & \lightning & \lightning & \lightning & - \\ - & - & - & \lightning & - & - & - \\ - & - & - & - & - & - & - \\ - & - & - & - & - & - & - \\ - & - & \lightning & \lightning & \lightning & - & - \\ \lightning & - & \lightning & \lightning & \lightning & \lightning & - \end{array}\right) \tag{3.5}$$

In the array (3.6) the p_{ks} in % for each individual comparison is depicted as before.

$$\begin{pmatrix} p_{\mathrm{ks}(12>12)} & \cdots & p_{\mathrm{ks}(18>12)} \\ \vdots & \ddots & \vdots \\ p_{\mathrm{ks}(12>18)} & \cdots & p_{\mathrm{ks}(18>18)} \end{pmatrix} = \left(\begin{array}{ccccccc} 100 & 100 & 2 & 0 & 0 & 93 & 100 \\ 0 & 100 & 0 & 0 & 0 & 0 & 79 \\ 29 & 91 & 100 & 2 & 8 & 91 & 99 \\ 94 & 100 & 43 & 100 & 13 & 100 & 100 \\ 94 & 100 & 90 & 57 & 100 & 99 & 100 \\ 13 & 81 & 0 & 0 & 0 & 100 & 100 \\ 0 & 6 & 0 & 0 & 0 & 0 & 100 \end{array}\right) \tag{3.6}$$

The trace of the array shows no rejections, as both distributions are the same. This is inherent to ks-test. As the test is applied symmetrically, a rejection of $\mathrm{ks}_{14>13}$ most likely causes the ks-test $\mathrm{ks}_{13>14}$ not to reject. The estimated numbers of the samples with 12 and 13 emitters are large and most of the null hypothesis in row 1 and 2 are rejected (7 of 11). In column 1 and 2, most ks-test do not reject (9 of 11). However, the array of [3:7,3:7] shows a pattern, which would indicate the correct estimates of differences as expected. In the lower left corner of the sub-array, 7 of 10 ks-test reject as expected.
This experiment shows that the counting resolution of CoPS can be as good as few emitters. However, by this experiment it seems, that the data acquisition or probe preparation influenced the estimation of CoPS. By looking at the fluorescence intensities in Figure C.9 the probes with 12 and 13 emitters, show the largest fluorescence

emission. On the other hand, have these experiments been conducted with a relatively low molecular brightness of about 2.1 cplcm. By increasing the molecular brightness, the relative sigma σ_{cops} of each probe would further improve.

In this chapter, the basic properties of CoPS could be observed in experiments, up to a label number of 36. Up to 18 emitters have been consistently determined in about 250 ms. The counting limit of CoPS prevented the correct estimation of 36 emitter, though. In investigations of the molecular brightness p_{exp}, the requirement of a basic p_{exp} was observed. The estimate n_{cops} converges only upon sufficient mDE statistics. So far, I could not investigate if it is possible to determine a even higher number by increasing largely p_{exp}. The possibilities will be discussed in detail in the Discussion. By increasing the laser power and therefore p_{exp} the variance σ_{cops} is reduced. This is necessary when two samples need to be discerned. By testing the counting resolution with DNA origami, I obtained ambiguous results. On the one hand the samples with 12 and 13 emitter showed completely wrong estimates in n_{cops}. On the other side the tests for a subset of the samples performed very well and showed the expected results. The intensity of the samples (see Figure C.9) indicates problems in the sample preparation. Encountering the reason requires further investigation.

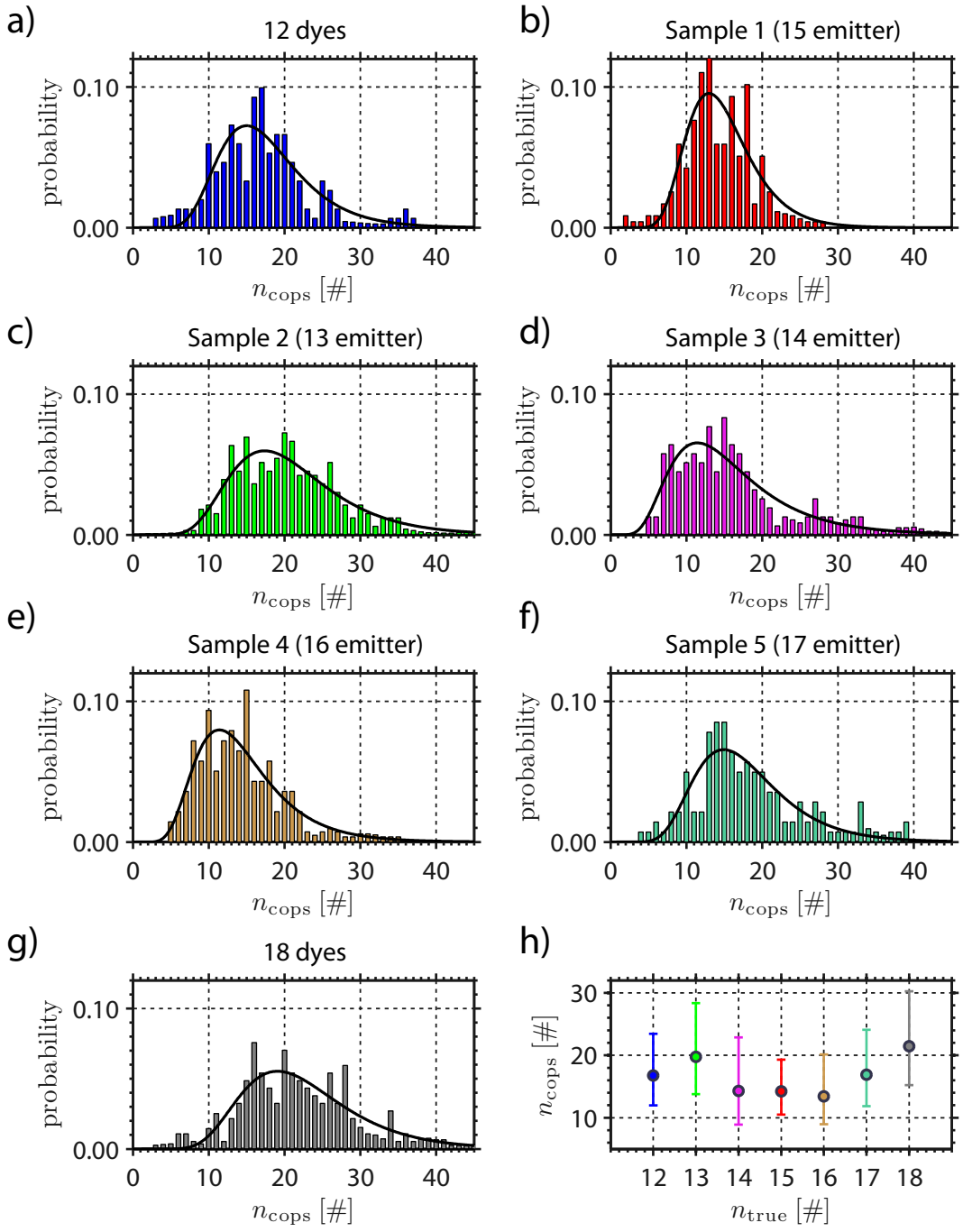

Figure 3.18.: DNA origamis with 12, 13, 14, 15, 16, 17 and 18 emitters. The blind samples show titles with the sample number and the dedicated number n_{exp}. (a) - g)) Each distribution is fitted by a log-normal distribution (black solid line). In axes h) the absolute median and the central 68% of the data are shown for all samples. The colors correspond to the original dstribution in a) to g).

3.4. STED-CoPS

In the previous sections the application of CoPS to different probes was shown with varying label numbers. The measurements have been conducted on a confocal microscope. However, a necessary requirement for CoPS is only the detection in a HBT array of single photon counting detectors with high temporal resolution.
Recently, the diffraction limit (see Figure 1.3) has been circumvented by different methods (see section 1.1.4).[116, 117] STED microscopy confines the possible emission of photons by the superposition of a doughnut shaped depletion profile with the excitation profile. The transition to the S_0 ground state by stimulated emission is very effective for excited molecules in the outer regions of the diffraction limited excitation point spread function (PSF). Thus, the detected fluorescent photons can be attributed to a sub-diffraction volume. A super resolution image is obtained by scanning the excitation spot over the specimen. STED shapes only the illumination profile and can thus be combined with the quantitative CoPS approach.
In section 2.1.3 the principles of STED microscopy are explained with more detail and the microscope setup is described, which has been designed and built in cooperation with Pit Bingen and Thorsten Staudt from the optical nanoscopy group (Prof. Stefan W. Hell, DKFZ, Heidelberg).
In STED microscopy the immobilization of probes at SM surfaces caused problems. Most probably, the standing high-powered STED beam photochemically generated fluorescent compounds. Hence, to immobilize probes poly-L-lysine coated surfaces were used (see section 2.3). According to previous experiments, ROXS buffer is applied to enhance photostability (see section 2.4).
In the first section, the application of STED-CoPS to samples of NuP4 probe (see Figure 2.6) is described. The molecular brightness on the STED-CoPS setup can differ from previous measurements due to the photon detection efficiency and the excitation profile. A minimal molecular brightness is however necessary to achieve sufficient mDE statistics and therefore for CoPS. The counting limit on the setup can be tested by a probe with many labels. As conducted in previous measurements, DNA origami with 36 labels of ATTO 647N (see section 2.2.3) were applied.
For testing the benefit of increased resolution another sample is necessary, in which labels are separated by more than twice the actual applied resolution. In cooperation with Jürgen Schmied (AG Tinnefeld, TU Braunschweig), DNA origamis have been designed with such a spatial pattern.

3.4.1. Molecular Brightness in STED

The molecular brightness is a critical parameter for CoPS because the actual number of emitters can only be estimated with sufficient mDE statistics (see section 3.3.3). The probability for mDE increases with the molecular brightness, which depends on parameters like the detection efficiency of the setup or the Quantum Yield of the fluorescent emitter (see equation (2.3)). For each setup the detection efficiency differs because of the individual optical design. For example, the STED-CoPS setup is a laser-scanning microscope, while the confocal setup utilizes probe scanning. The laser repetition rate

in the STED setup is 18.4 MHz compared to 20 MHz in the confocal.[1] Additionally, the optical elements required for STED cause extra loss of light (see section 2.1.3). The fiber of the detector array, which acts as a detection pinhole, reduces the detection efficiency further.
Another difference, which is inherent to the excitation scheme, is the reduced molecular brightness because of increased STED power. The doughnut shape, which avoids fluorescence emission in the outer rim, closes by increasing the STED power due to saturation.[118] Therefore, some stimulated emission occurs also in the central spot and reduces the observable emission. In the beginning the possibility to size labels on the STED setup was tested and the development of the molecular brightness was analyzed.

In Figure 3.19 fluorescence transients (blue, left axes) of the NuP4 probe at different STED intensities (0 mW, 6 mW, 12 mW and 20 mW in a), b), c), d), respectively) are shown. The excitation power was set to 10 µW. Without STED the fluorescence intensity is initially about 120 kHz and diminishes to about 60 kHz at 20 mW STED intensity. Without STED, the four bleach steps are clearly visible and are about 25 kHz each. With 6 mW of applied STED power, counting by BS is not feasible anymore because the BSs can no longer be identified. At 20 mW STED the fluorescence emission is fragmented and single BS are generally not visible. The emitter number n_{exp} can be estimated by CoPS (n_{cops}, red, right axes) to STED powers up to 20 mW. In a), the initial number of 4 emitters and the decay in n_{exp} is well estimated. The estimates n_{cops} show little variance and each estimate seems robust. In axes b), at 6 mW STED power, the number of labels is still estimated. Estimates by BS analysis are not feasible anymore because only the last intensity drop can be identified unambiguously. The bootstrapping distribution is broad because within a single analysis window t_{ac} the number n_{exp} changes. By further increasing the STED power to 12 mW the variance of n_{cops} and the two molecules which are present between 3 s and 5.8 s are not estimated every time. In d), at 12 mW STED power, the estimates n_{cops} fluctuate in the beginning between 2 and 3 emitters. The estimation n_{cops} then decays with fluorescence intensity to 1 emitter.
The estimations on molecular brightness p_{cops} (green line) show constant lines with little variance without STED and with STED powers up to 12 mW. At 20 mW STED the variations are more pronounced.
By these experiments, the possibility to apply CoPS in combination with STED is demonstrated up to at least 12 mW STED power. The molecular brightness p_{cops} and the number of emitters n_{cops} is estimated in about 250 ms. The obtained numbers n_{cops} could be validated by probe design and BS analysis, when applicable.
It was only possible to measure a few single traces, though. The microscope software of the STED setup did not support automatic PnD. Manual selection and actuation of the laser beam is time intensive and prone to misalignment. This effect becomes more pronounced at high STED powers and increased resolution.
From measurements at different laser powers, the influence of STED intensities on

[1] For better comparison of laser intensities, the given values of the STED setup are corrected, to give the same energy per laser pulse as in the confocal setup. All intensities have been measured in the collimated beam, shortly before the objective.

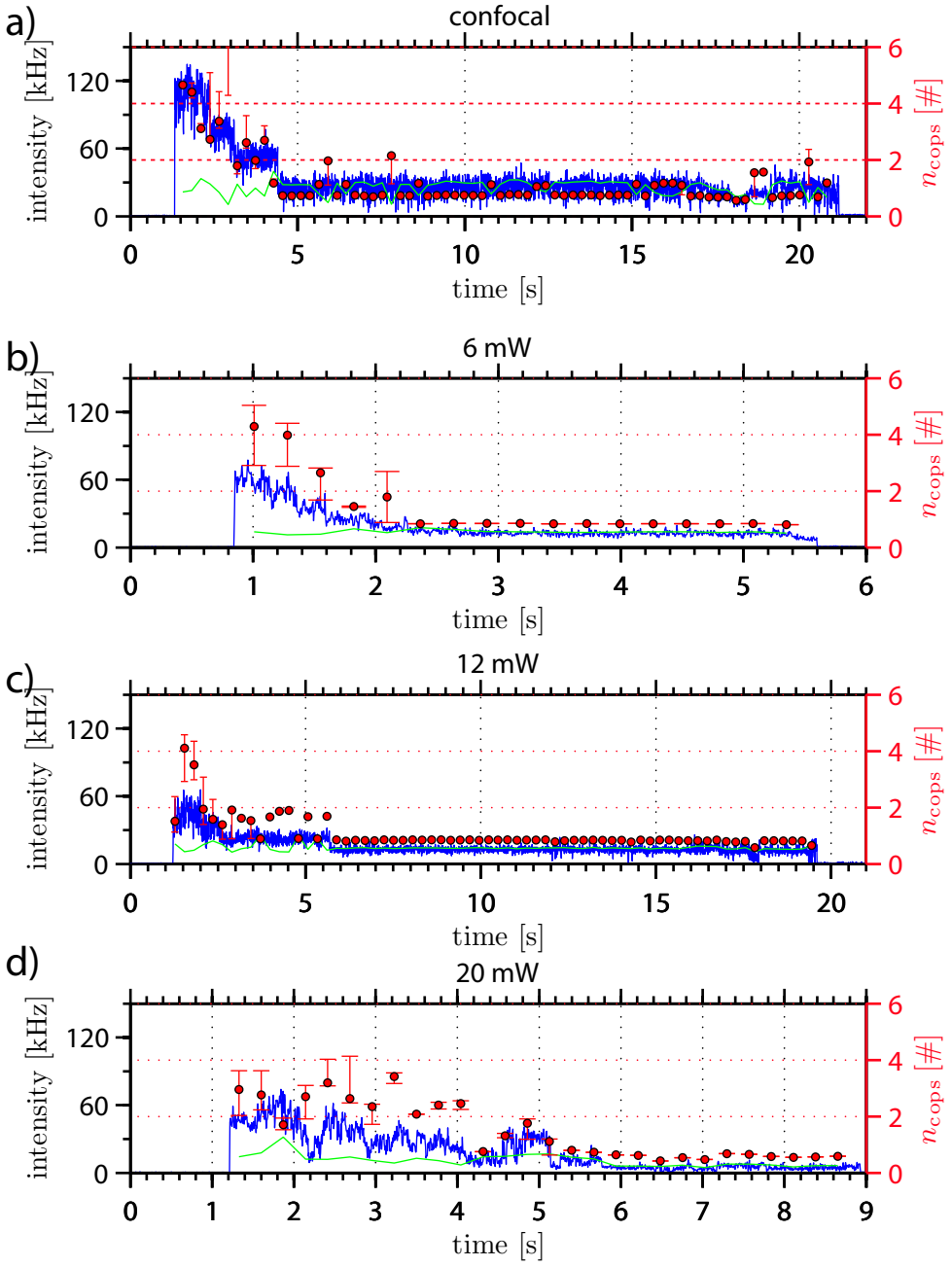

Figure 3.19.: Fluorescence transients of the NuP4 sample acquired at the STED setup (blue, left axes). The estimations of numbers (red, right axes) and molecular brightness (green, left axes) by CoPS is obtained in $t_{ac} = 270\,\text{ms}$. From Figure a) to d) the STED power is set to 0 mW, 6 mW, 12 mW and 20 mW. (LP=10 µW)

the molecular brightness and the resolution can be investigated. The doughnut of the STED beam saturates by increasing power I_{STED} and the resolution increases. The

relation between these parameters has been derived by Hell et.al. [118] and is given by:

$$\Delta x = \frac{\lambda}{2\mathrm{NA}} \frac{1}{\sqrt{\left(1 + \frac{I_{\mathrm{STED}}}{I_{\mathrm{SAT}}}\right)}} \tag{3.7}$$

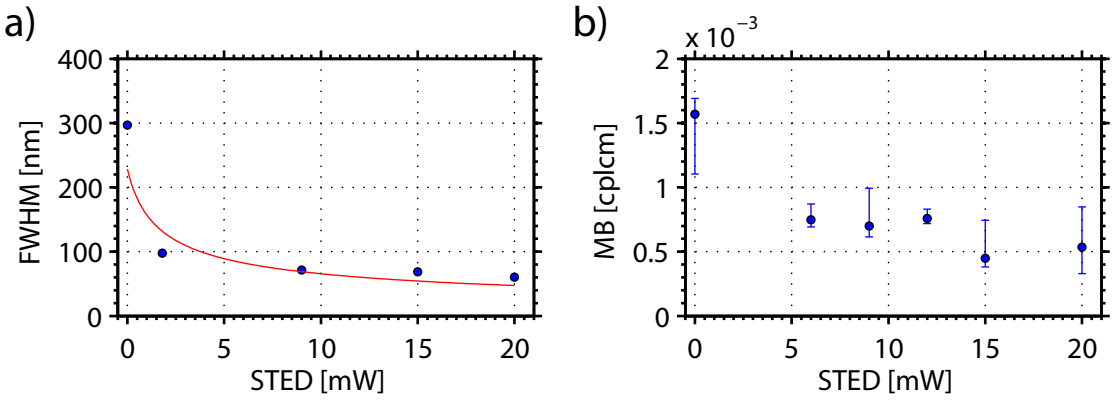

Figure 3.20.: a) The development of the FWHM (blue points) by increasing STED power is shown and the theoretically deduced formula (red line, see parameter and equation (3.7)). b) The development of the molecular brightness (MB) is shown by increasing STED power. The center point indicates the median, the errorbars indicate the 2σ quantile or the central 68% of the data.

The relation between the resolution and the STED power was compared to our experimental data, by fitting the acquired spots with a gaussian distribution and extracting the FWHM thereof. The resolution in Abbe's formula is defined as the minimal distance when two PSF can still be distinguished (see in the Introduction section 1.3). The FWHM is therefore a measure for the actual resolution in microscopy images [119]. In Figure 3.20 a) the development of the resolution is shown at 0 mW, 1.8 mW, 10 mW, 15 mW and 20 mW STED power. The theoretical resolution dependency is plotted for the experimental setup (NA = 1.46, $\lambda_{\mathrm{emission}} = 680\,\mathrm{nm}$, $I_{\mathrm{SAT}} = 1.8\,\mathrm{mW}$) in red. The FWHM is decreasing fast, as excepted and at about 20 mW STED power the resolution is about 70 nm. By looking at the molecular brightness against the STED power in Figure 3.20 b), we obtain about $1.5 \cdot 10^{-3}$ cplcm in the resolution limited image, which is decreasing to about $6 \cdot 10^{-4}$ cplcm for STED powers larger than 5 mW.
In the previous observations, up to 4 fluorescent emitters have been sized up to 12 mW STED power. This corresponds to a resolution of about 80 nm and is about a factor of 3 in improved resolution. At this resolution the molecular brightness p_{cops} is only $6 \cdot 10^{-4}$ cplcm, though. This limits the application of CoPS. However, at low STED powers the resolution is increasing rapidly and at the same time, the molecular brightness of the fluorescent emitters is least influenced.

3.4.2. Counting to Large Numbers

To test the counting limit of STED-CoPS, DNA origami with 36 labels of ATTO 647N have been investigated. To preserve the molecular brightness, a minimal STED power of 1.8 mW was applied, which resulted in a resolution of approximately 100 nm. The labels on the DNA origami are arranged in 3 parallel lines with 17 nm and 44 nm distance (see Figure 2.7) and cannot be resolved at given resolution.

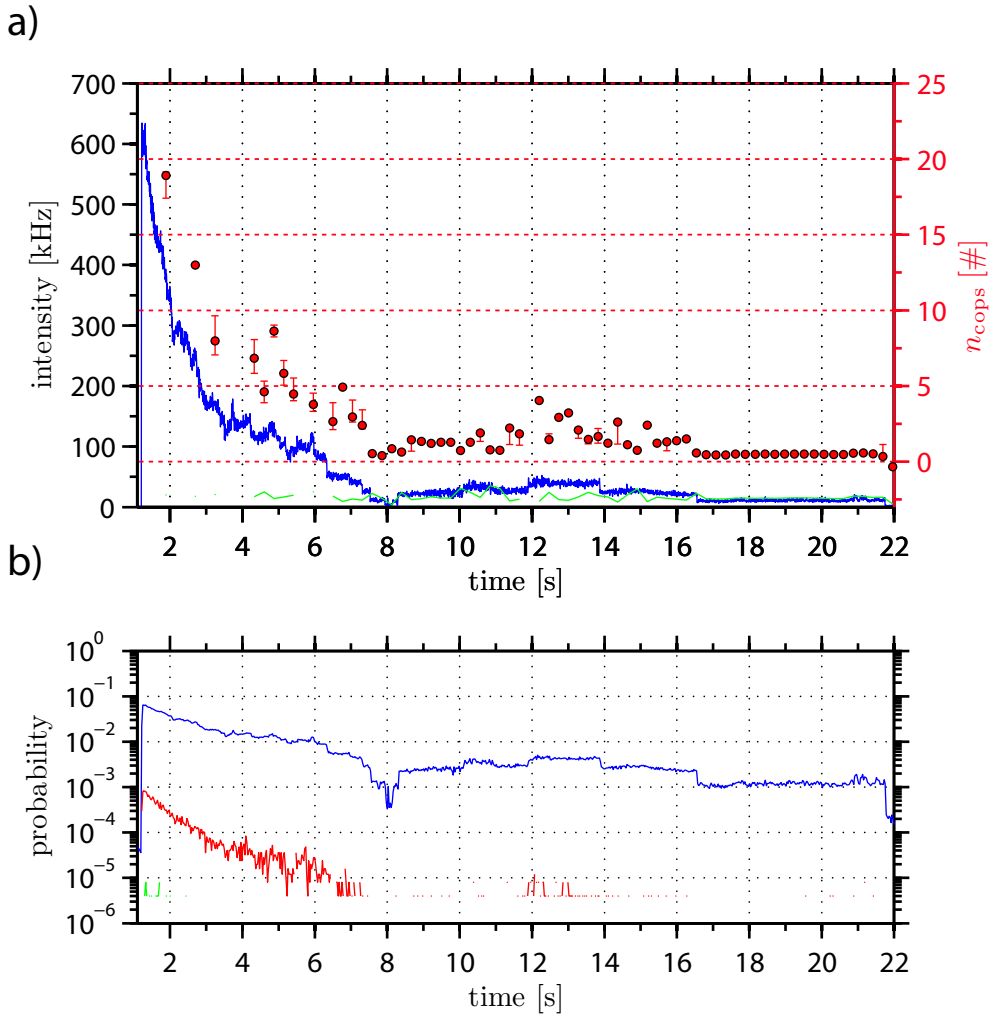

Figure 3.21.: a) Fluorescence transient (blue, left axes) of a DNA origami with 36 labels of ATTO 647N attached at 10 µW excitation and 1.8 mW STED power. The red points (right axes) show the estimates n_{cops}. The molecular brightness p_{cops} is shown in green (left axes). Missing points indicate that the fit did not converge and estimations were omitted. ($t_{ac} = 270$ ms) b) The probability of 1DE (blue), 2DE (green) and 3DE (green) per t_{ac}.

The fluorescence transient (blue, left axes) in Figure 3.21 decays due to photobleaching

in 22 s from about 600 kHz to background level. Individual bleaching steps are only visible after 4 s and even then, they cannot be attributed to a label number. By CoPS (red, right axes) the number of molecules n_{cops} can be estimated with a time resolution of 270 ms. The estimates n_{cops} follow the decay in numbers from 6 emitters to zero emitters. At large intensities, the fit did not converge for most t_{ac} and the points are left blank. The n_{cops} follow the complex transient and the "off"-times of emitters are detected. The estimates of molecular brightness p_{cops} (green, left axes) show approximately a constant line at 15 kHz with a sigma of 4 kHz.
The application of STED-CoPS allows estimation up to $n_{\mathrm{exp}} = 6$. By larger n_{exp} the fit is sometimes not converging and no robust result is obtained. In Figure 3.21 the mDE are shown for the 36 labels. Compared to the previous observation at the confocal setup (see Figure 3.14), the probability of 3DE and 2DE is lower. Furthermore, the STED transient is decaying much faster, because of the increased photobleaching by the powerful STED laser. This affectes the robustness of the fit.
Nevertheless, in the trace at 1.9 s, 2.7 s and 3.2 s an estimate of 19, 13 and 8 fluorescent emitters was obtained. By reference to the molecular brightness $p_{\mathrm{cops}} = 15$ kHz of the complete transient, the actual number n_{exp} can be estimated to 25, 15 and 11 molecules for the individual t_{ac}. It seems the estimation of higher label number is possible. However, the model fit to the data is not robust anymore, probably due to the lower molecular brightness and photobleaching.

3.4.3. Resolving DNA origamis

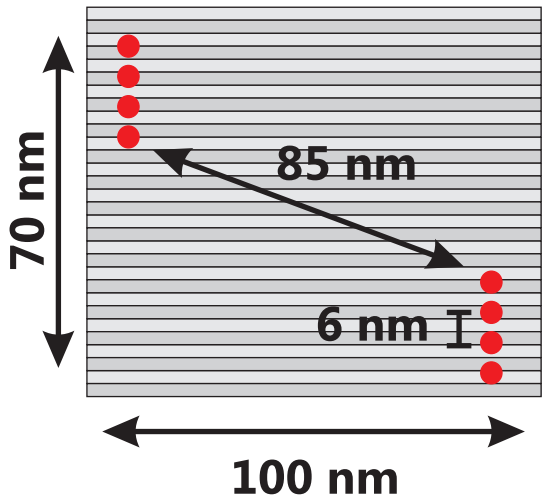

Figure 3.22.: DNA origami with 2x4 labels of ATTO 647N at a distance of 85 nm

In all previous investigations fluorescent probes have been designed as standard sample for confocal microscopy. They were designed with small dye-dye distances to avoid effects of the gaussian excitation profile. And only to the extent that interaction of dyes can be avoided. To profit from the increased resolution by combination of STED measurements, a DNA origami probe with a spatial pattern of 8 fluorescent labels was

designed (see Figure 3.22). In each of the two opposite corners of the DNA origami (STED DNA origami), 4 fluorescent dyes are located and therefore approximately 86 nm apart.

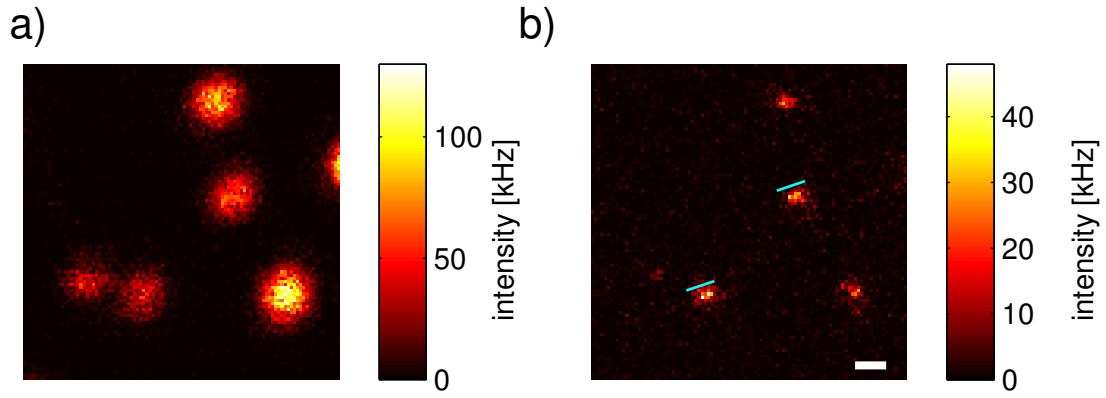

Figure 3.23.: a) STED DNA origami imaged by confocal microscopy (dwell time 500 µs, pixel size 25 nm, excitation intensity 54 µW) b) STED microscope image at 44 mW STED power. The line indicates the orientation of the DNA origami. (dwell time 500 µs, pixel size 25 nm, excitation intensity 54 µW, scale bar 250 nm)

To visualize the spatial structure of the DNA origami, an overview was recorded and a Field of View (FOV) was selected with isolated DNA origamis. In Figure 3.23 a) a typical FOV with 5 DNA origamis is depicted.
To achieve a resolution of about 80 nm, a STED power of at least 20 mW is required (see Figure 3.20). The STED power, dwell time and pixel size was manually optimized to observe good images of the resolved label spots on the DNA origami. The best images have been acquired with a dwell time of 500 µs, a pixel size of 25 nm, an excitation intensity of 54 µW and a STED power of 44 mW. Because of the high STED powers, rapid bleaching of the labels occurs, but it is necessary for resolution. The pixel size should be less than half the resolution according to the Shannon-Nyquist theorem.[120, 121] The small pixel size prolongs the duration of an image and therefore increase bleaching effects.
In Figure 3.23 b) an image of the resolved DNA origami is shown. The two spots are oriented in direction of the line (light blue, it is better visualized in the line profile in Figure 3.24). The FOV shows the same area as the confocal image in a) and was acquired after the confocal image. In the confocal image the upper left DNA origami already shows photobleaching, indicated by the drop in intensity during the scanning process. However, in two of the fluorescent DNA origamis the orientation and two labels spots are visible and a drop in intensity in between.
In Figure 3.24 a) the line profile of a DNA origami in 3.23 is shown. The confocal intensity profile (red) is diffraction limited and has a FWHM of 293 nm. In contrast, the STED profile (blue) shows a dip in between the two peaks.
To analyze the confocal intensity profile, a normal distribution can be approximated to the data. However, the two peaks in the STED profile are just a single pixel apart.

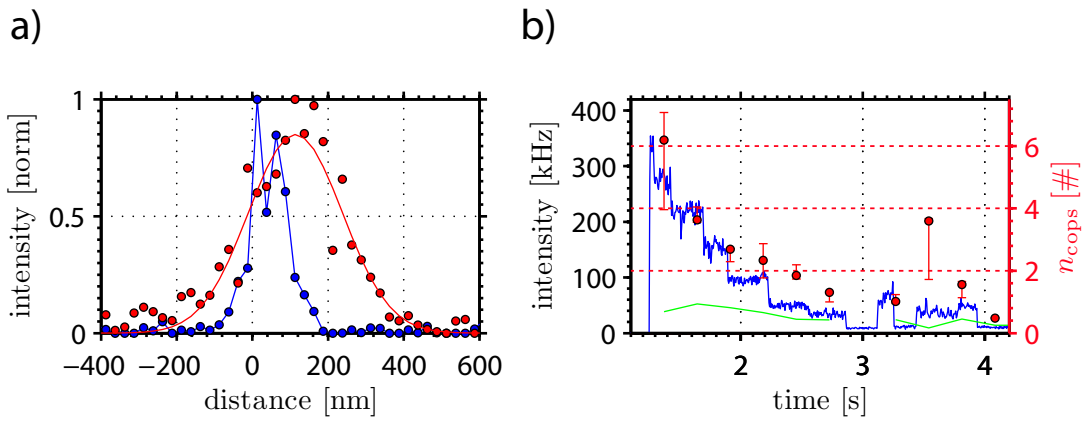

Figure 3.24.: a) The line profile of confocal (red) and STED (blue) image of a single DNA origami with two label spots 85 nm apart. b) Fluorescent transient of a single DNA origami with spatial pattern (blue) acquired without STED. The estimations of molecular brightness (green, left axes) and numbers (red, right axes) by CoPS have been acquired in $t_{ac} = 270$ ms. (LP = 30 µW)

This is why the fitting of two Gaussian functions in order to determine the FWHM and resolution is not reasonable. The fluorescence intensity in the STED image is about a third compared to confocal excitation. The molecular brightness p_{exp} is low. In previous findings (see Figure 3.17 and 3.11), it was shown that a minimal p_{exp} is required to obtain reasonable number estimates from CoPS. Even if the two spots at the DNA origami are resolvable by STED microscopy, counting is only reasonable if it is possible to obtain the mDE statistics from the initial number of the probe.
To resolve the label pattern a high STED power of 44 mW is required. Thus, some of the labels are already bleached by the overview scan and counting is not reasonable anymore. By acquiring a confocal overview, only the resolution limited position and number of fluorescent emitters is obtained. Thus, the PnD approach is not applicable. To obtain information of numbers and locations beyond the resolution limit, the approach to first estimate the number of emitting labels without STED and then observe the location of resolvable spots in a STED image with high resolution is favored. As the number of emitters n_{cops} would be known, the labels can be distributed to the resolved spots in ratio to their fluorescence intensity. Resolving the pattern was shown previously, but the minimal acquisition time is not known.
In Figure 3.24 b) the confocal, fluorescent transient of the 2x4 DNA origami is shown in blue (left axes). The fluorescence intensity drops after about 50 ms from 340 kHz to 280 kHz and then subsequently at 1.3 s, 1.4 s, 1.7 s, 1.9 s, 2.2 s and 2.9 s for 60 kHz, 57 kHz, 69 kHz, 56 kHz, 54 kHz and 22 kHz. The estimations CoPS of molecular brightness (green, left axes) numbers (red, right axes) have been applied in 270 ms.
The estimate $n_{cops} = 6$ is close to the estimate from BS analysis $n_{BS} = 7$, probably because of the fast bleaching step at 1.3 s. To first size the number and then acquire a super-resolution image, a non-invasive method is required, though.

The general idea of first acquiring the number of emitters in about 270 ms and then resolve the underlying structure, seems feasible. However, the powerful STED laser pronounces bleaching and the number which is obtained by CoPS does not necessarily provide the number in the STED image. The approach would be more robust, by an application of more photostable dyes and a better detection efficiency setup. The other approaches need to be concerned again, though.
Nevertheless, the successful application of STED-CoPS was presented in this chapter. By design of a new detection unit, it was possible to combine these two approaches and successfully count standard samples with increased resolution. The molecular brightness is relatively low, due to the detection efficiency of the setup and the large STED power. It is possible only to size generally about 5 to 10 emitters, though. By adjusting the setup for maximum detection efficiency and microscope software, the acquisition of robust and quantitative information would be feasible in super resolution microscopy.

4. Discussion

Currently, there are only few techniques for obtaining quantitative data from fluorescence spectroscopy and each of them is advantageous for certain applications (see Table 1.1). Counting by photon statistics is a non-invasive, i.e. number maintaining approach, by which it is possible to determine the stoichiometry of the same single molecule over time without prior calibration. Furthermore CoPS is relatively easy to implement experimentally. It requires only a sufficient molecular brightness (see equation (1.2)) and a detector array to measure multi detection events (mDE) statistics (see Figure 2.1). The method is independent from the laser intensity, if a minimal molecular brightness is achieved and estimates at the same time the number and molecular brightness.

Method Development

At the beginning of my PhD thesis, CoPS could be applied manually to single fluorescence transients and size numbers of up to 5, which was proven by bleaching step (BS) analysis (see Figure 1.4).[86] Little was known about the minimal acquisition time, the requirements concerning molecular brightness, the counting resolution and the counting number limit. The approach was also sensitive to the initial parameter choices during the fitting procedure.

In order to establish a novel technique for the use in complex environments, like in a living cell, it is necessary to characterize the method sufficiently to generate reliable results, which allow unequivocal interpretation. The characteristic features of the method can be investigated in standardized experiments. The approach can then be transferred to suitable and more complex experiments for which the measured number distribution is a combination of CoPS's intrinsic estimation variance and the number of labels (NOL) distribution of the probe. In experiments only the folding of both distributions is measured. By knowledge of CoPS intrinsic estimation variance, the precision of results can be obtained and the NOL distribution can potentially be unfolded.

Another prerequisite for the unbiased application of a method is a minimal influence of manual operations. Manual data acquisition and analysis is time consuming and error prone. It is then difficult to obtain sufficiently large data sets of equal quality for statistics. CoPS is well suited for automated data acquisition. The acquisition of fluorescent transients by Pick & Destroy (PnD) (see section 2.1.1) can be readily implemented with little efforts in image processing and application of CoPS requires no prior calibration. A important task in my PhD thesis was to establish a robust data analysis. By implementing the bootstrapping approach, the estimations became more

reliable and for each time interval t_{ac} an estimation error can be given (see section 2.5.1). However, the error estimate by bootstrapping is not the overall error of CoPS, it is rather the resampling error inside the analysis bin. The overall error is experimentally investigated in this thesis and will be discussed below.
It was also crucial to implement the software package on the server cluster of Bioquant (University Heidelberg). Its computational power is necessary to apply CoPS to big data sets in reasonable time. To obtain the estimate of a single interval t_{ac}, a regular computer (CPU: Dual-Core 3 GHz, RAM: 4 GB) calculates for roughly 300 s. In contrast, the Bioquant cluster improves the computational time by a factor of about 20. Hence, more robust estimations of numbers on a large scale became feasible.

For the first experimental applications of CoPS, the HyP5 probe (see section 2.2.2) was used as a standard for 5 fluorescent emitters.[86] The evaluation of the NOL n_{cops} in section 3.1.3 indicates, that the NOL per probe n_{exp} has a broad distribution due to sample preparation. The variance in n_{exp} originates from the stochastic hybridization process and by varying the marker/base ratio the NOL mean and variance changes significantly.
To achieve narrower NOL distribution, a probe was designed with four labels covalently linked to nucleotides in a ssDNA strand (see Figure 2.6). The probe still experiences variance in label number n_{exp}, because of photodestruction during the overview scan and the DOL of nucleotides below 1. The NOL distribution is improved as compared to the previous standard sample, though (see Figure 2.6).
For numbers of up to approximately 5, the n_{exp} can also be estimated by counting the consecutive BS (n_{bs}). Both approaches yield similar NOL distributions (see Figure 3.5 and Figure 3.6). The distribution of estimates n_{bs} is narrower than the one obtained by CoPS, which has a tail when approaching large numbers. However, in the experiments only the convolution of NOL distribution with CoPS intrinsic estimation variance is accessible. As long as neither the intrinsic estimation variance of bleaching step analysis or CoPS is known, the real distribution of numbers is hidden. The smaller width of n_{bs} indicates a higher precision of BS analysis for counting up to five, though.

Analysis of the intrinsic estimation variance by BS is difficult, because bleaching steps have to be clearly identified during the whole transient. The application of rigorous criteria for automatic data acquisition is challenging if fluorescent dyes show complex photophysics. The probability for blinking, changes in quantum yield over time and local excitation intensities increases with the number of emitters and may create complex patterns in fluorescence transients for higher numbers. Therefore some bleaching steps might not be identified and the NOL is more likely to be shifted to lower numbers.
The bias and precision of CoPS can be estimated in MC simulations (see section 2.1.6). Suitable simulated fluorescence transients can be obtained by simulation of single fluorescent emitters and the photon detection process. The number n_{exp} and molecular brightness p_{exp} are a priori known and remain constant over time and fluorescence transients by design. The NOL of probes is thereby well defined and the intrinsic estimation variance is solely due to CoPS analysis becomes visible.

The model function behind CoPS (see equation (1.24)) is recursive and piece-wise

defined. The parameter space of the fit follows a complex pattern with many local minima (see section 2.5.1). In the experiments a tendency to overestimate numbers is apparent and the acquired NOL distributions display a tail to large numbers. The observed distributions in simulations and experiments are well described by a log-normal distribution, though. This is investigated by hypothesis testing in section 2.5.2. The intrinsic estimation variance however, could not be derived analytically and is thus estimated by the log-normal distribution.

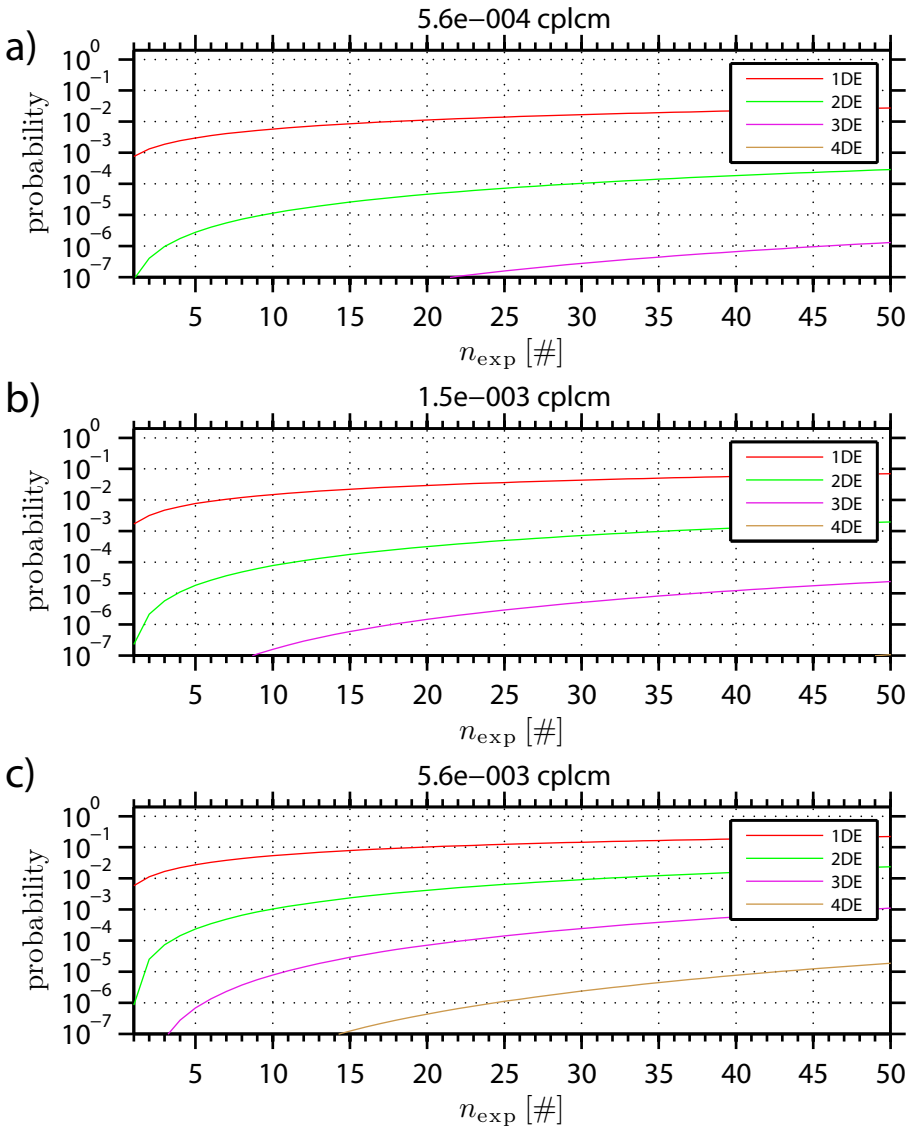

Figure 4.1.: Probabilities for mDE (m = 0, 1, 2, 3, 4) in a HBT setup against n_{exp} for different molecular brightnesses obtained in experiments. (a) $5.6 \cdot 10^{-4}$ cplcm in CoPS-STED measurements (LP=10 µW, STED>6 mW) b) $1.5 \cdot 10^{-3}$ cplcm in DNA origami (confocal, LP=5 µW) measurements c) $5.6 \cdot 10^{-3}$ cplcm in NuP4 (confocal, LP=10 µW) experiments

In Figure 4.1 the probabilities for mDE are plotted against numbers n_{cops} for different molecular brightnesses p_{cops}. The brightness $p_{\text{cops}} = 5.6 \cdot 10^{-4}$ cplcm in a) corresponds to CoPS measurements with LP of 10 µW 6 mW STED power. The laser frequency (LF) in this measurement was 18 MHz, however, the laser power is generally converted to show the same energy per pulse of a LF of 20 MHz (see section 2.1). In b) the brightness $p_{\text{cops}} = 1.5 \cdot 10^{-3}$ cplcm was achieved with DNA origami excited at LP of 5 µW and LF of 20 MHz. In c) highest molecular brightness of $p_{\text{cops}} = 5.6 \cdot 10^{-3}$ cplcm achieved with the NuP4 sample on the the confocal setup at a LP of 5 µW and LF of 20 MHz is shown.
The shape of the curves is similar for all values of molecular brightness. The probability function of mDE show a prominent rise in the beginning and level off for larger numbers. The shift in n_{exp} between the mDE probability functions is larger for small p_{cops} in a) and small for high p_{cops} in c). For example, the probability to obtain 3DE exceeds 10^{-6} in a) at about 45, in b) at about 18 and in c) at about 6 molecules. Therefore, the initial slope is larger for higher brightnesses p_{cops}.
The resolution CoPS can achieve is related to the slope of the probability function of mDE. If the difference in probabilities for mDE is large for adjacent n_{exp}, the difference is more easily measured in experiments. The explanation of these plots is intuitive, but the analytical solution is not, because of the non-linear, piece-wise and recursive equation (1.24). Still Figure 4.1 proved very useful to explain my results and I will refer to this later.

Method Characterisation

The performance of CoPS could be analyzed in simulations and experiments. To investigate the bias and precision of CoPS in experiments, a probe with a defined number of labels is required. I chose DNA origami that can be labeled with up to 220 emitters and the position of each label on the DNA origami can be determined with high precision. The size of the folded DNA origamis is smaller than the resolution limit and all labels experience similar excitation.
Jürgen Schmied from the group of Prof. Tinnefeld (TU Braunschweig) kindly provided me with DNA origamis with different label numbers n_{exp} (see Figure 2.7 and section 2.2.3). Therefore, experiments with high label numbers could be conducted. At a molecular brightness p_{exp} of at least $1.5 \cdot 10^{-3}$ cplcm 18 fluorescent labels of ATTO 647N could be determined (see Figure 3.17).

It turned out in simulation and experiment that the molecular brightness (see equation (2.3)) of the fluorescent emitter is most important. CoPS relies on the detection of simultaneous m photon events in a single laser cycle which occur approximately with p_{MB}^m.[84] The simulation showed that with a molecular brightness above $1.8 \cdot 10^{-3}$ cplcm (see Figure 3.11 and Figure 2.4) the systematic error μ_{cops} level off at about -5% for all numbers up to 18. The preciscion σ_{cops} is directly correlated with the molecular brightness p_{exp}. To obtain a narrow intrinsic estimation variance the brightness p_{exp} should be maximized.

The molecular brightness depends on the detection efficiency of the setup, the applied laser power, absorption coefficient and quantum yield of the dye. In my experimental work, I have improved the detection efficiency of the setup by reducing the number of optical elements (see section2.1.1). The applied laser power should be kept as low as possible to avoid photobleaching,[26] which occurs even in the presence of photostabilization buffers like ROXS. Finally, the choice of dye has a major effect, for its unique absorption cross section and quantum yield. The experiments presented here have been conducted with ATTO 647N, because it is one of the brightest and most photostable fluorescent dyes. The feasibility of CoPS has additionally been tested with other dyes in the blue (ATTO 488) and red spectrum (ATTO 633 [122], Cy5) and was confirmed by BS analysis.

CoPS is non-invasive and can be used to continuously estimate n_{cops} per probe over time, as long as photobleaching is avoided. By analysis within different intervals t_{ac}, the minimal time necessary to acquire sufficient mDE for reasonable estimates n_{cops} was explored. From simulations, a minimal time resolution of about 125 ms for 6 to 18 molecules with a brightness of $3 \cdot 10^{-3}$ cplcm is obtained (see Figure 3.9). For the DNA origami, the time resolution was estimated to about 250 ms for 6 to 18 emitters at $2 \cdot 10^{-3}$ cplcm. And for the NuP4 sample the time resolution was 100 ms above $1.7 \cdot 10^{-3}$ cplcm) (see Figure 3.3).
The minimal required time turned out to be almost identical when assessed with either simulations or experiments. Although, to determine the number from simulated data or from NuP4 data requires less time than for the DNA origami. This might be for the simulated data, due to the modeling without variance in the brightness, or for the NuP4 sample, the low number of molecules in the probe. By looking at Figure 4.1, the initial rise of the probability function for 2DE above $1.5 \cdot 10^{-3}$ cplcm is prominent for low emitter numbers.

Generally, CoPS requires a certain amount of laser cycles to accumulate sufficient mDE statistics. The time resolution is so far defined as the time t_{ac} for which estimates n_{cops} level off (see for example Figure 3.3). The time resolution of 250 ms at a laser repetition frequency of 20 MHz shows that there are $5 \cdot 10^6$ laser cycles necessary to give reasonable results. Increasing the laser repetition rate, would also increase the time resolution proportionally. However, time resolution is nevertheless limited. The time between laser pulses needs to be larger than the fluorescence lifetime of the emitter to assure that the photon detected in the laser cycle is due to absorption from the previous pulse. If not, even single fluorescent emitters would give two simultaneous detection events. As well, the APD detectors experience a dead time of about 100 ns after photon detection and are inactive during this time. By that the mDE statistics becomes biased and therefore the number estimate as well. By increasing laser repetition rate, the average laser power has to be increased to maintain the energy per pulse. Hence, fluorescent emitters are more likely to be in the triplet state, at the subsequent laser pulse. Absorption in the triplet state is known as an initial state for photobleaching.[26] This might be a limiting factor for some experiments. I can state at the moment, that CoPS can estimate the number of emitters n_{cops} continiously with a sampling rate of at least 4 Hz.

As previously shown, has the intrinsic estimation variance of CoPS a tail to large numbers and the number estimates show a systematic error. The bias has been identified to -5% in the simulations, between -2 to +5% in the NuP4 sample and +20% in the DNA origami. In contrast to the simulations, the actual label numbers in the experiments cannot be observed, but photobleaching and the DOL of probes imply a tendency to lower numbers, as previously described.
The overestimation in experiments is actually not yet investigated, but a possible reason is the variance in molecular brightness during experiments. The applied laser intensity obeys a gaussian profile, therefore the position of an emitter in the excitation volume has an effect on its individual molecular brightness. For a DNA origami with an extension of about 100 nm, a molecule placed on the rim of the structure would experience about 75% of the peak laser power at the very center ($\lambda = 635\,\mathrm{nm}$). Additionally, each fluorescent label experiences a slightly different environment, which can change the quantum yield. By CoPS only the mean molecular brightness, averaged over all emitters, is estimated. In these cases the molecular brightness might be underestimated and compensated by overestimated numbers. The effect of the variance in brightness should be investigated in further simulations.

Another property of CoPS encountered during this work is the counting limit between 18 and 36 emitters. In all simulations with different laser powers and experiments with DNA origamis, the number estimation of 36 emitters shows an offset of -20-30% as compared to the estimates of 18 or less emitters. Thereby, the counting limit of CoPS becomes apparent in experiments and simulation.
In Figure 4.1 the dependency of the mDE probabilities on p_{exp} is shown. The brightness $p_{\mathrm{exp}} = 1.5 \cdot 10^{-3}\,\mathrm{cplcm}$ in b) corresponds to DNA origami at 5 µW and 20 MHz. Here, the slope is an indicator for the resolution. At large numbers n_{exp} the probabilities of 1DE, 2DE and 3DE level off and the difference between two nearby p_{exp} diminish, as the number resolution. By increasing the molecular brightness in simulations $p_{\mathrm{exp}} = 5.6 \cdot 10^{-3}\,\mathrm{cplcm}$ in c) the curves become steeper. However, in simulations of 36 molecules their number was not correctly identified, either. Up to now, no simulations with larger molecule numbers have been conducted.
To identify the exact dependency between molecular brightness and the counting limit further studies are necessary. Because the effect appeared in simulation and in experiment, it is intrinsic to the evaluation of mDE statistics in CoPS. A possible reason may be the implementation of the fitting algorithm. So far the algorithm was optimized to estimate low emitter numbers. In this regime mainly the 1DE and 2DE are important. At higher numbers the main difference appears in the 3DE. The fitting algorithm contains so far no weights so the approximation might not be as sensitive to changes in 3DE. Additionally, the counting limit could be observed in more details by further simulations to narrow down the dependency between molecular brightness and counting limit.

The resolution to differentiate between two samples with similar n_{exp} is the main task of a quantitative approach. Therefore, the counting resolution was investigated in simulations and in first experiments. In the simulations, a counting resolution of 2 or better

could be obtained at a molecular brightness p_{exp} of 1.8 cplcm (see Figure 3.12). The MC simulations reveal the inherent influence of CoPS analysis without any variations due to the probe. To consider the case of realistic scenario, I conducted the experiments with DNA origami. The experiment showed ambiguous results (see Figure 3.18). The DNA origami with $n_{\text{exp}} = 12, 13$ have been estimated to be larger than $n_{\text{exp}} = 17$. The problem in these measurements may be caused by sample preparation or data acquisition. By looking at the intensities in Figure C.9, the samples $n_{\text{exp}} = 12, 13$ show a much higher intensity than other samples, except $n_{\text{exp}} = 18$. The estimation of differences between samples $n_{\text{exp}} = 14, 15, 16, 17, 18$ worked better and a counting resolution of 3 emitters or better was obtained. To my knowledge, no similar experiments have been conducted so far. To confirm these results, the experiment should be repeated with the since improved detection efficiency of the setup (see section 2.3).

As previously described (see section 1.1.7), there are many different methods which can be used to obtain quantitative data from fluorescence signals and they differ from each other in their requirements, for example photostability, probe immobilization, etc., and results, for example ensemble averaging, resolution, etc. The time resolution of intensity calibration and FRET based approaches, being only a few µs, is the best by far, because they only accumulate statistics to determine the mean photon emission. However, they require calibration or are limited to few emitters or give only relative molecule numbers. Approaches which rely on photophysics, like bleaching or blinking, require relatively long acquisition time to observe the stochastic processes. Quantitative analysis with CoPS can be achieved in a few 100 ms and is therefore also reasonably fast. CoPS requires no calibration, because it estimates the numbers and molecular brightnesses from the same accumulated statistics. It is also possible to directly follow changes in molecular brightness over time and to potentially measure their dynamics. Similar experiments can be conducted only by intensity fluctuation based methods. However, they are essentially limited to diffusion probes and obtain the statistics over many probes.
Up to now, none of the aforementioned methods (see section 1.1.7) has been studied using standardized probes and simulations in the interesting number space of 5 to 50. Additionally, CoPS seems to be the only method whose estimation error has been investigated to this extent.
CoPS can estimate non-invasively up to at least 18 molecules in a few hundred ms. It is independent of the laser intensity, as long as a minimal molecular brightness of about $1.5 \cdot 10^{-3}$ cplcm is exceeded. The simultaneous observations of molecular brightness and numbers allow the differentiation between changes in numbers n_{exp} or photophysics p_{exp}. The method can be applied in different experimental conditions to gather quantitative information in fluorescence spectroscopy.

Method Applications

An application for CoPS is measuring the NOL distribution of fluorescent probes on a single molecule basis. So far, the DOL is for most probes estimated by ensemble spec-

troscopy and is the mean of the NOL distribution. The NOL on the single-molecule level does not only provide the mean dye/label ratio in the sample, but the distribution of the NOL attached to single probes. This is vital information for all kind of quantitative experiments that are conducted using that probe. Similar experiments have already been conducted by bleaching step analysis.[123]
I could obtain different NOL distributions of the HyP5 probe (see Figure 3.12) by applying different concentrations of marker and base DNA during probe hybridization. A change in ratio resulted in different number distributions and an increase in the small marker strand followed a shift to larger molecule numbers.
Together with Michael Schwering and Kristin Grußmayer (AG Herten), I began to acquire the NOL distribution of several labeled proteins and antibodies used for labeling of structures in standard cell experiments. The standard labeling procedure normally utilizes a primary antibody, which targets the specific structure in the cell and is then subsequently labeled with the secondary antibody. However, a single primary antibody can bind several secondary antibodies, which can bear multiple labels. The number of labels, i.e. targeted protein, is therefore unknown and the results of quantitative experiments should be interpreted with care. By knowledge of the NOL distribution we can at least estimate the variance of a possible counting outcome for protein numbers or even allow analysis of distributions.

Meanwhile several approaches exist, by which the resolution limit can be circumvented. The PALM approach can inherently used as a quantitative approach (see section 1.4). In contrast, the STED approach observes a confined, in which several molecules may be located.
By knowledge of the minimal requirements for CoPS, I was able to successfully combine STED microscopy with the quantitative CoPS approach. In cooperation with Pit Bingen (AG Hell), a new and mobile detection setup was designed, which allowed the detection of mDE at a STED setup (see Figure 2.2). First, it had to be confirmed that the detection efficiency of the setup is large enough to apply CoPS, despite different equipment, like laser scanning, additional optical elements and fiber coupling. We also observed the evolution of the molecular brightness by increasing STED power and therefore resolution.
The achieved resolution-limited molecular brightness, at the STED setup, is similar to the one obtained with the confocal setup used in previous sections (see Figure 2.4) and excess the minimal molecular brightness of $1.8 \cdot 10^{-3}$ cplcm. The decrease in brightness p_{cops} to about $5 \cdot 10^{-4}$ cplcm, at STED powers larger than 5 mW, is strong and affects CoPS's estimation variance and time resolution t_{ac} to estimate numbers (see Simulations 3.2). However, estimates of numbers of up to $n_{\mathrm{cops}} = 4$ in 250 ms could be accomplished by BS analysis. The setup, since it was not specifically designed for the CoPS purpose, achieves only a limited detection efficiency and only low number of molecules n_{cops} could be counted correctly (see Figure 3.21).
In cooperation with Jürgen Schmied (AG Tinnenfeld) a DNA origami with a resolvable spatial pattern of the 8 fluorescent labels was designed (see Figure 3.22). The distance between the labels was calculated to be approx. 86 nm. By a STED power of 44 mW the two spots could be resolved, however it was not possible to apply CoPS and STED at the same time. Even embedded in ROXS, the fluorescent labels bleached already in

the first overview scan and therefore prevented counting of unaltered numbers. Thus, an approach was investigated to first estimate the number of emitters by CoPS, which is only possible because of the non-invasive nature of CoPS, and resolve the number of spots in the focal volume. The estimated number can then be attributed to the actual spots in accordance to their intensities.
In summary, I have shown the successful combination of the quantitative CoPS approach with STED microscopy. The implementation of the STED-CoPS approach, as described here, is just a proof of concept, but can be improved with little effort. The STED setup, initially designed for multifocus STED,[97] can still be optimized for best achievable molecular brightness. Automatic PnD was not implemented in microscope software and localizing the position of probes manually was time consuming and laborious. Generally, it has to be considered, if a PnD approach is suitable for STED-CoPS, because an overview scan with STED changes the observed numbers, however the exact location of probes is necessary for PnD.

Outlook

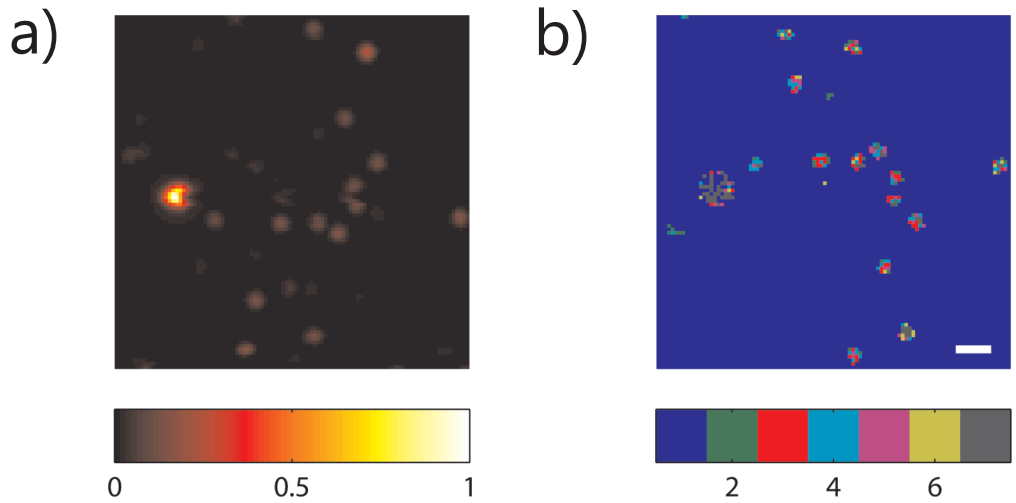

Figure 4.2.: a) Intensity image of the NuP4 sample immobilized on a SM surface b) 2D CoPS image of the same FOV. The estimated numbers n_{cops} from 1 to 7 are shown. ($t_{\mathrm{ac}} = 200\,\mathrm{ms}$, pixel size 100 nm, scale bar 1 µm, LP 5 µW, LF 20 MHz)

A possible alternative, already shown in coincidence analysis [82] or in N&B [45] is the combination of numbers with spatial information in a 2D-imaging approach. Thereby, in addition to a fluorescence intensity image, a map of numbers and molecular brightness is obtained. By that the selective PnD approach would be avoided, which measures only a limited number of fluorescence transients per image. Rather a map would be obtained, *e.g.* of a cell. And the signal would not be the fluorescence intensity, rather the number and brightness, *e.g.* from multimers of membrane proteins.

The acquisition of mDE statistics by a scanning microscope is time consuming, though. A typical image with 100×100 pixels for a reasonable FOV and sampling requires about 33 min for a time interval t_{ac} of 200 ms.

By use of ROXS buffer and the photostable ATTO 647N dye, it is possible to acquire images with sufficient long dwelltime $t_{ac} = 200$ ms to estimate the number n_{cops} and brightness p_{cops} in each pixel. In Figure 4.2 a) the intensity image is shown and in b) the number map. Background pixel are not analyzed (indicated as blue pixel). In the estimates, predominately three labels are obtained from the NuP4 probe. This might be affected by photobleaching during the long pixel dwell times.
By application of ROXS, the bleaching effect can be minimized during long observation times. However, a much faster approach is desirable to apply CoPS analysis in experiments. An alternative can be the application of recently developed complementary metal oxide semiconductor (CMOS) APD detector arrays.[124, 125] These detectors consist of an array of about 100×100 single photon detectors with TCSPC possibilities.[126] Four pixels could be synchronized as a HBT detection array. Therefore mDE statistics could be acquired in parallel for a complete image. The acquisition time would therefore shrink to $t_{ac} = 200$ ms for a small FOV. However, these detectors are currently under development and have to improve. The detection efficiency is about 30% at $\lambda = 600nm$, the dark count rate is high and the electronics recquired to drive a single pixel is relatively large. The active area to the complete detector area (filling factor) is about 30%.[124]

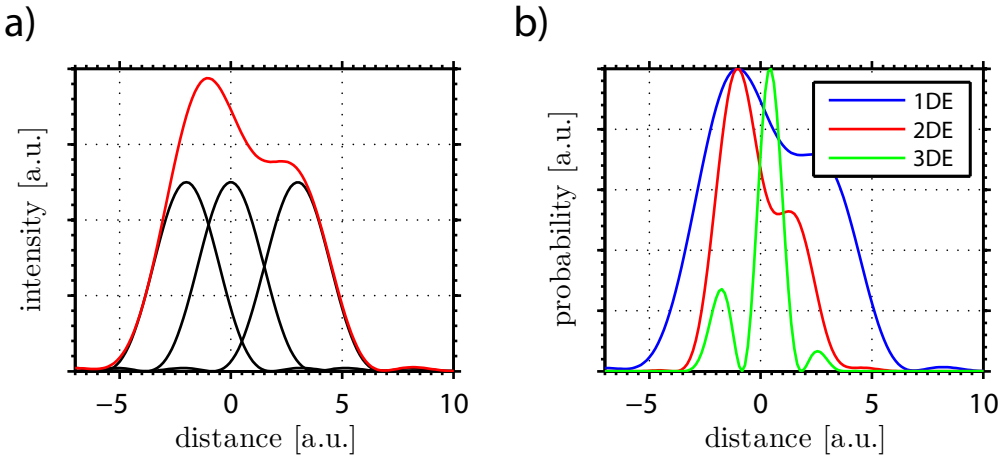

Figure 4.3.: a) The summed intensity of three emitters located at -2,0 and 3. b) The normalized probabilities for mDE of the three emitters. 100nm/pix scale bar 1 µm

In this thesis, the quantitative CoPS approach has been described extensively and also the combination with the super-resolution method STED. The combination was successfully applied and I could identify the important prerequisites. A future direction would however be to use the photon statistics to improve the resolution. Simulations

have shown that in correlation microscopy the resolution can be enhanced, by use of photon antibunching.[127]
In an intensity image, the detected signal is the summed fluorescence intensity of all molecules. Looking at the probabilities for mDE draws a little different picture. Here, the signal is the measured probabilities for mDE which scales with the product of p_{cops}. In Figure 4.3 a) the summed intensity signal (red line) of three emitters (black line) is shown, which cannot be resolved due to the diffraction limit (see equation (1.4)). In b) the normalized probabilities for 1DE, 2DE and 3DE are shown. The probability of 1DE corresponds to the intensity, whereas the probability functions of mDE show a different pattern. The 2DE probability function is skewed to the left side and the 3DE probability function has a narrow peak, right of the 1DE maximum.
Hence, the mDE probabilities show a pattern which differs from the intensity signal and can be obtained experimentally. The locations of emitter could be estimated from the appearance of mDE, in addition to the intensity. Nevertheless, the probability of mDE scales with p_{exp}^{m} and is therefore low. To observe the 3DE in a reasonable amount of time, the molecular brightness has to increase largely. With a perfect optical system, the detection efficiency of a confocal setup is about 24% (see section 2.1.5). Thus, in saturation, the probability to obtain a 3DE in a laser cycle from 3 emitters located at the same spot scales would be 1.4%. Are the spots separated slightly, the mDE signal decay with the amplitude of the PSF to the power of m. The signal of mDE probabilities is therefore low, but also highly sensitive to distance.

A. Abbreviations

CoPS counting by photon statistics
STED stimulated emission depletion
HBT Harnbury-Brown Twiss
mDE multi detection events
1DE 1 photon detection events
2DE 2 photon detection events
3DE 3 photon detection events
4DE 4 photon detection events
cplcm photon counts per laser cycle and molecule
cplc photon counts per laser cycle
ssDNA single stranded DNA
HyP5 hybridization probe with 5 labels
NuP4 nucleotide labeled probe with 4 labels
NOL number of labels
DOL degree of labeling
BS bleaching step
PnD Pick & Destroy
FWHM full width at half maximum
ROXS reducing and oxidizing system
MC Monte Carlo
ks-test Kolmogorov-Smirnov test
cdf cumulative density function
RESOLFT reversible saturable (flurorescence) transitions
PSF point spread function
FOV Field of View
CMOS complementary metal oxide semiconductor
SM single-molecule
TCSPC time correlated single photon counting
APD avalanche photodiode

B. Publications

Irsch, K., Ramey, N. a, Kurz, A., Guyton, D. L., & Ying, H. S. (2009). Video-based head movement compensation for novel haploscopic eye-tracking apparatus. Investigative ophthalmology & visual science, 50(3), 1152-7. doi:10.1167/iovs.08-2739

Schwering, M., Kiel, A., Kurz, A., Lymperopoulos, K., Sprödefeld, A., Krämer, R., & Herten, D. (2011). Far-field nanoscopy with reversible chemical reactions. Angewandte Chemie (International ed. in English), 50(13), 2940-5. doi:10.1002/anie.201006013

Kurz, A., Schwering, M., & Herten, D.-P. (2012). Quantification of fluorescent samples by photon-antibunching. Proc. SPIE, 8228, 82280K-82280K-8. doi:10.1117/12.909099

C. Appendix

DNA Origami

Figures C.1, C.2, C.3, C.4, C.5 show sketches of the DNA origamis. The white and colored ellipses correspond to one oligonucleotide each. The oligonucleotides which were 3'-modified with ATTO 647N are colored in red. Biotin modified oligonucleotides are colored orange.

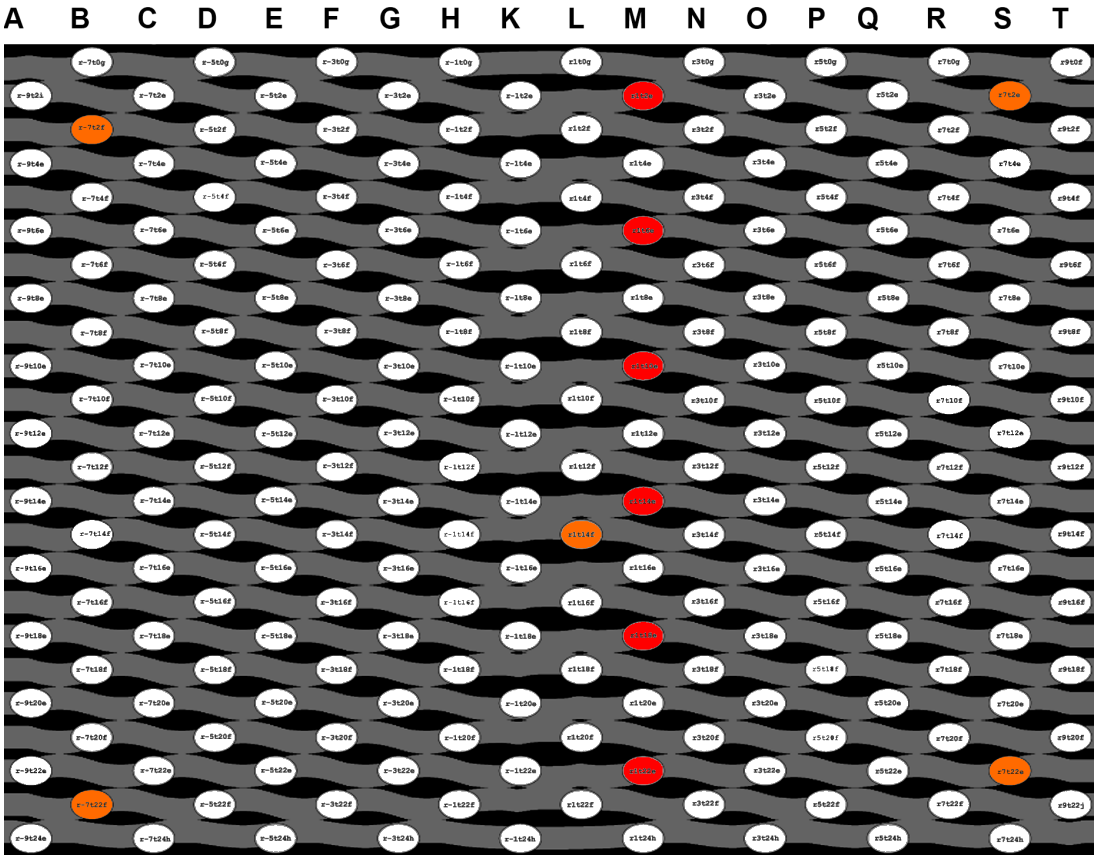

Figure C.1.: Scheme of DNA origamis with 6 ATTO 647N (red) and 5 biotins (orange). The dye-dye distance is in this case 12 nm within the same column.

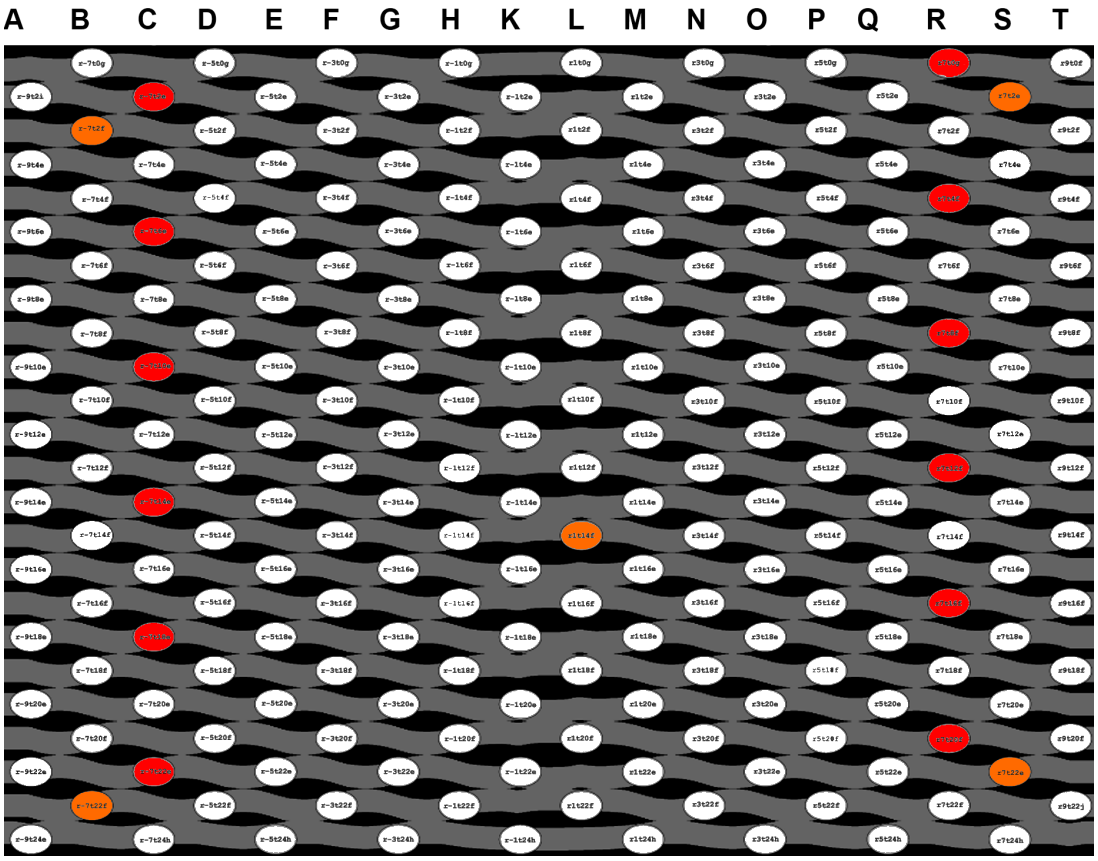

Figure C.2.: Scheme of DNA origamis with 12 ATTO 647N (red) and 5 biotins (orange). The dye-dye distance is in this case 12 nm within the same column.

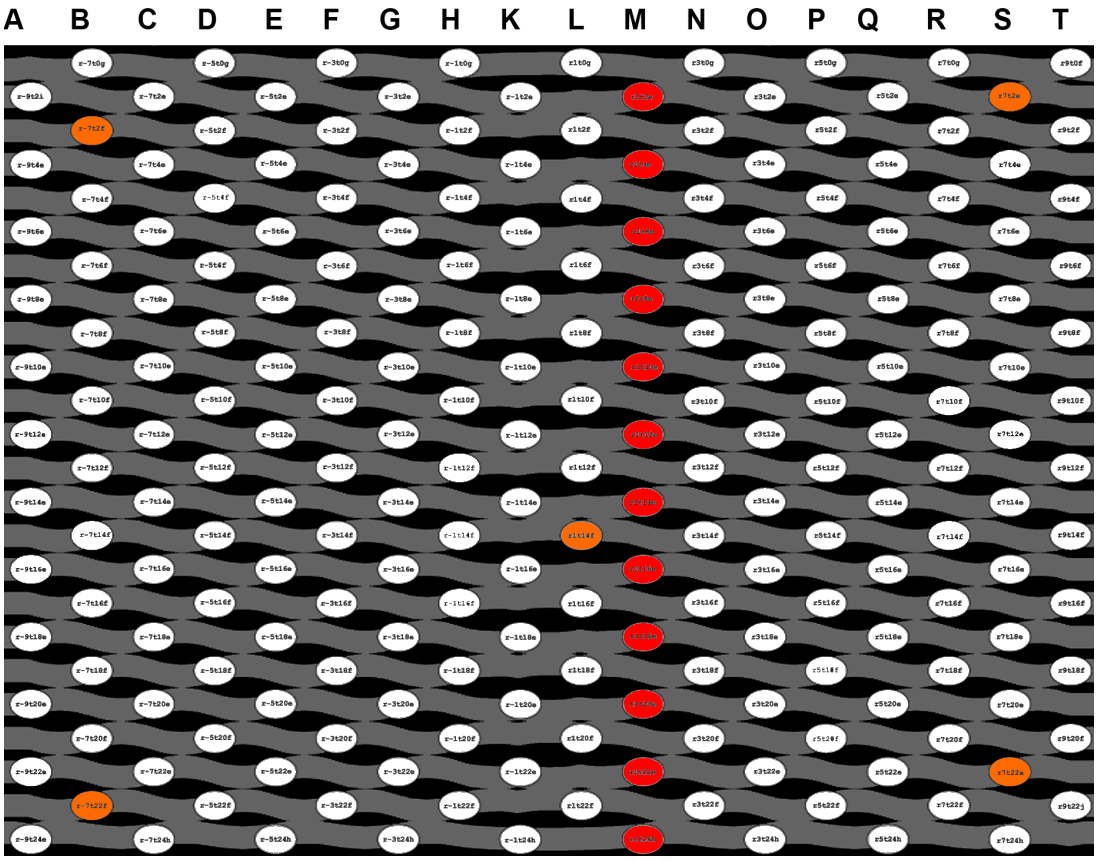

Figure C.3.: Scheme of DNA origamis with 12 ATTO 647N (red) and 5 biotins (orange). The dye-dye distance is in this case 6 nm.

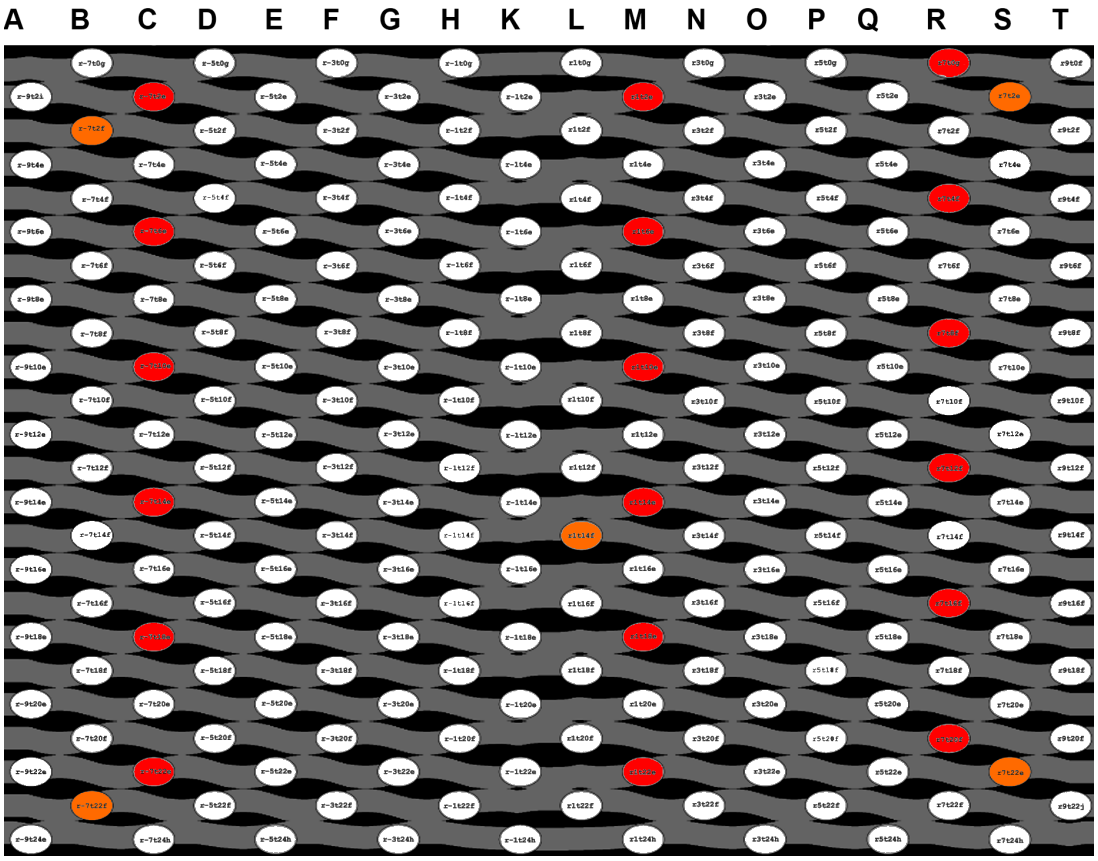

Figure C.4.: Scheme of DNA origamis with 18 ATTO 647N (red) and 5 biotins (orange). The dye-dye distance is in this case 12 nm within the same column.

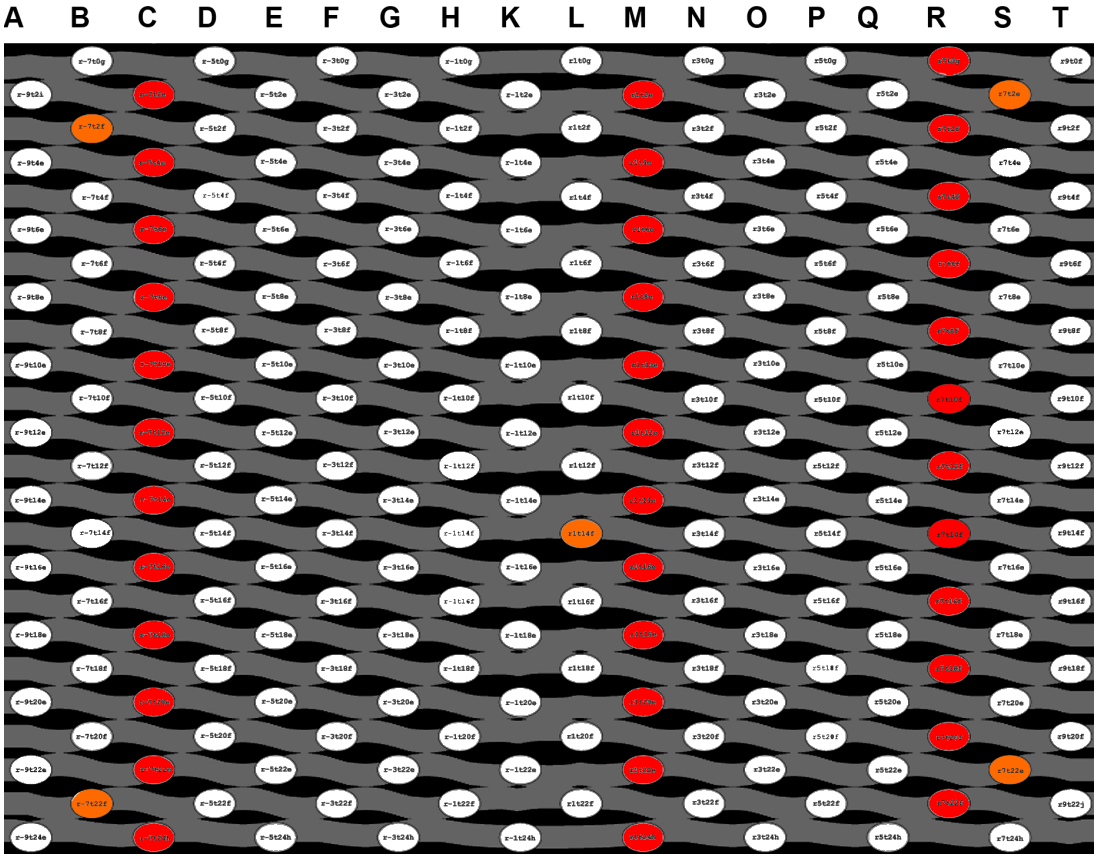

Figure C.5.: Scheme of DNA origamis with 36 ATTO 647N (red) and 5 biotins (orange). The dye-dye distance is in this case 6 nm within the same column.

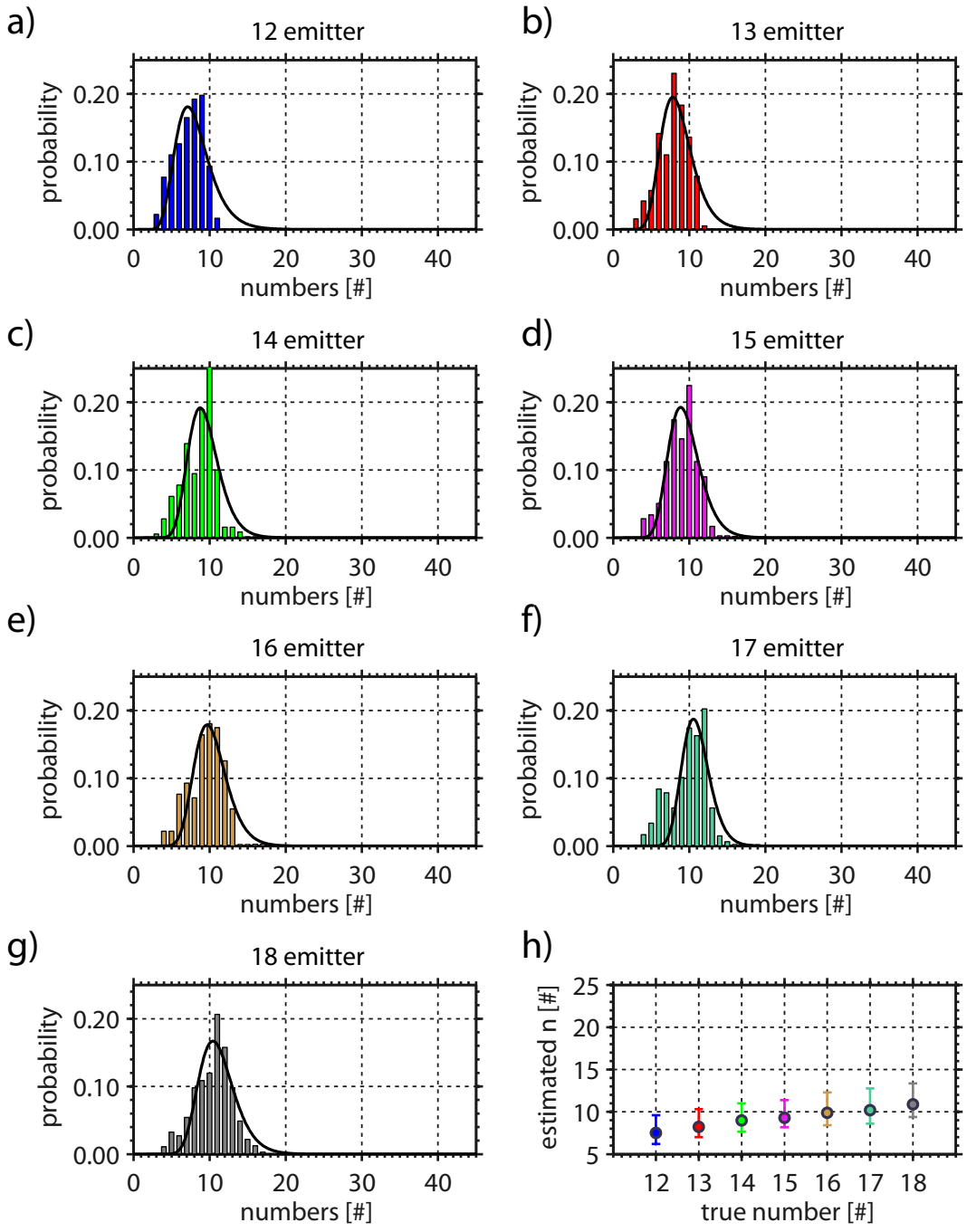

Figure C.6.: Simulated DNA Quest described in section 3.2.6 at 2 µW

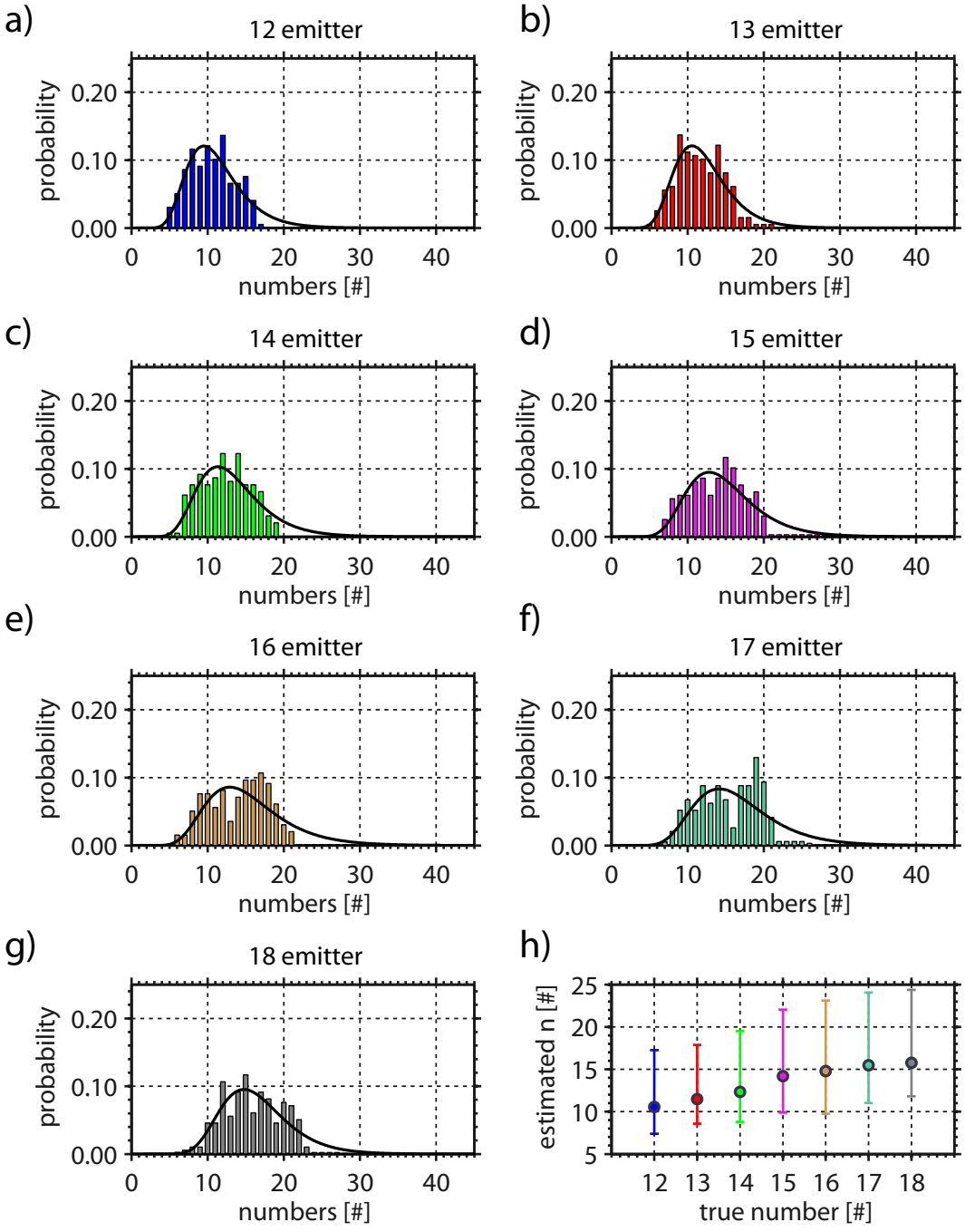

Figure C.7.: Simulated DNA Quest described in section 3.2.6 at 4 µW

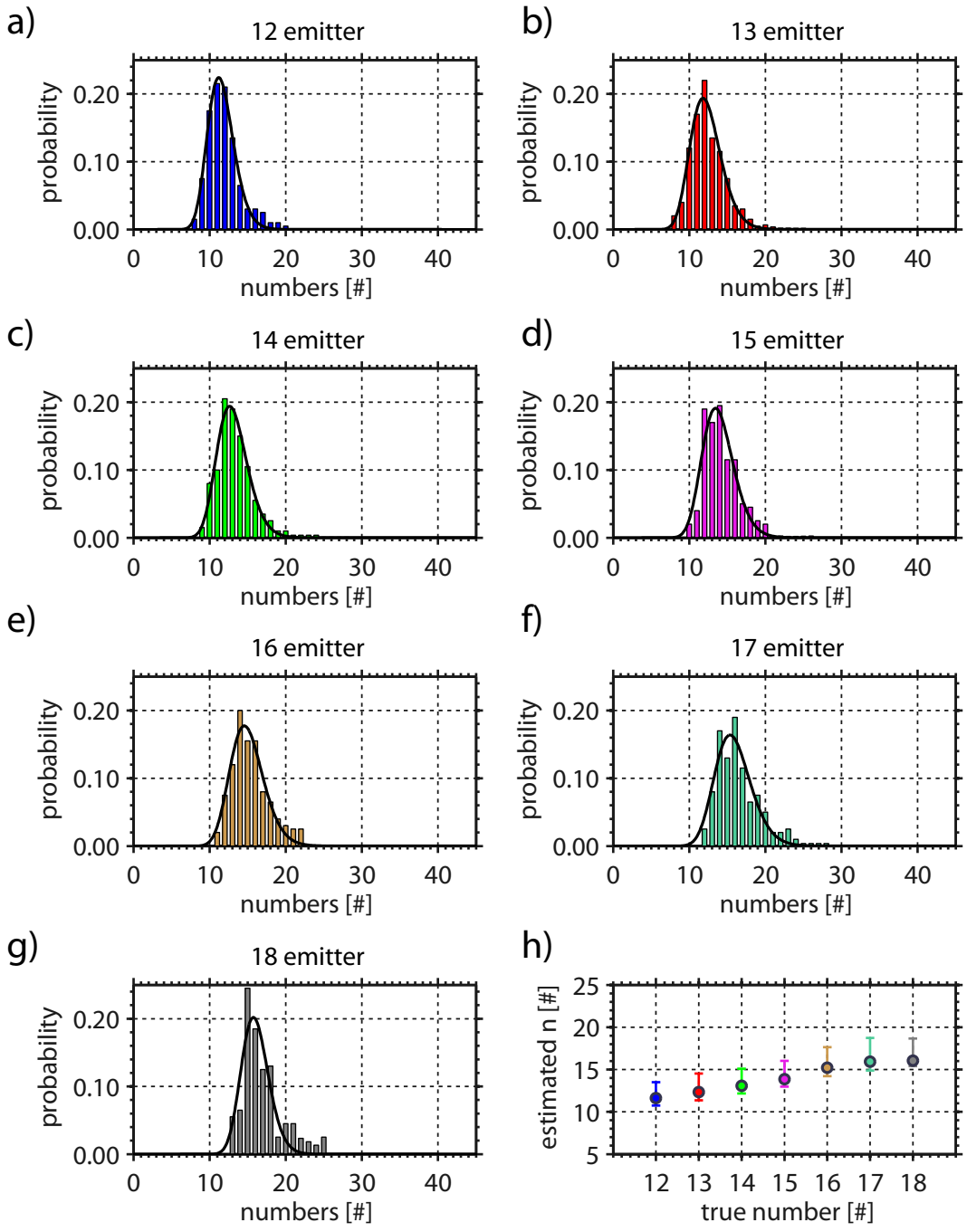

Figure C.8.: Simulated DNA Quest described in section 3.2.6 at 12 µW

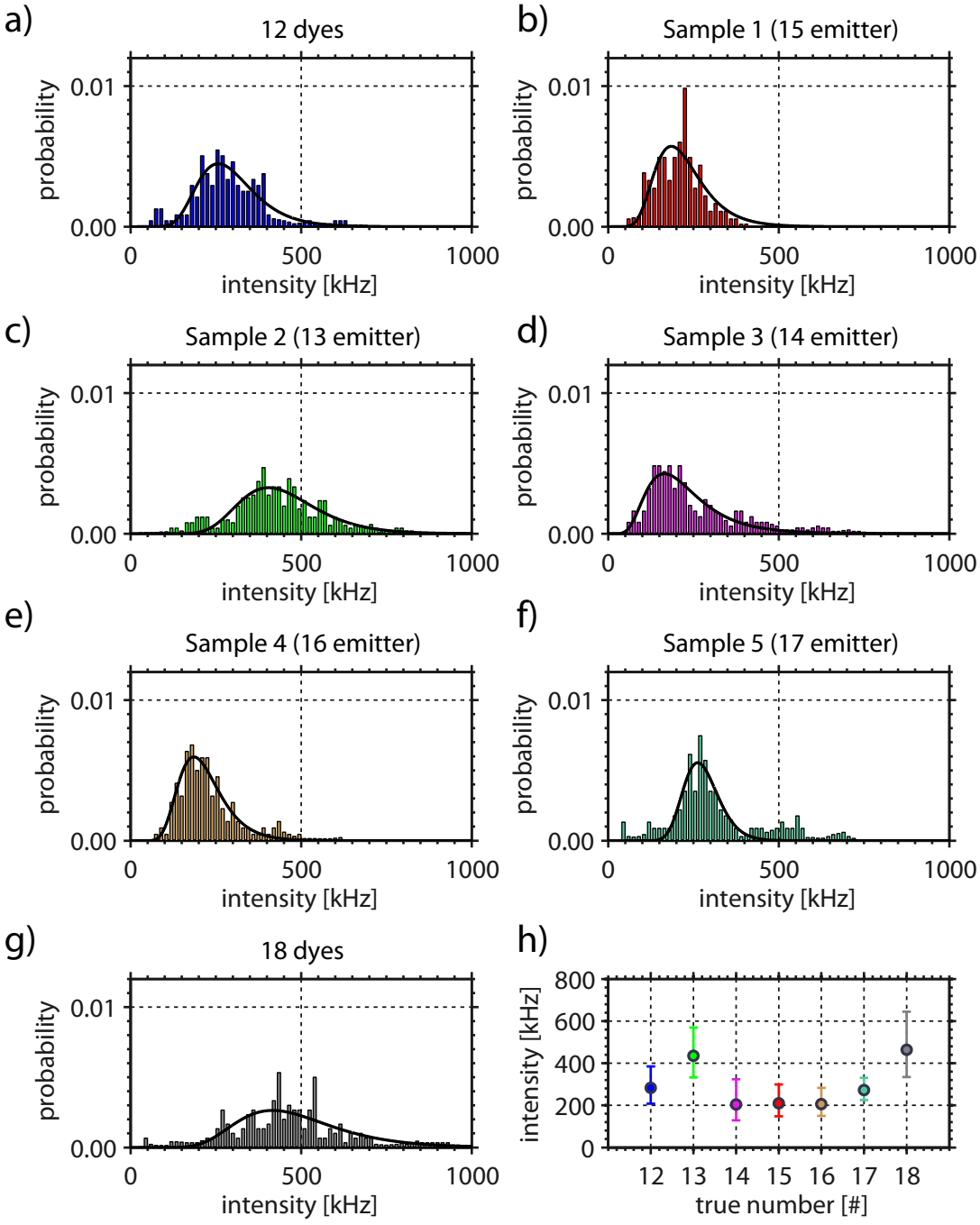

Figure C.9.: Intensiteis of DNA Quest described in section 3.2.6 at 10 µW

Bibliography

[1] R. S. Kasai, K. G. N. Suzuki, E. R. Prossnitz, I. Koyama-Honda, C. Nakada, T. K. Fujiwara, and A. Kusumi, "Full characterization of GPCR monomer-dimer dynamic equilibrium by single molecule imaging.," *The Journal of cell biology*, vol. 192, pp. 463–80, Feb. 2011.

[2] X. Michalet, S. Weiss, and M. Jäger, "Single-molecule fluorescence studies of protein folding and conformational dynamics.," *Chemical reviews*, vol. 106, pp. 1785–813, May 2006.

[3] M. T. Drake, S. K. Shenoy, and R. J. Lefkowitz, "Trafficking of G protein-coupled receptors.," *Circulation research*, vol. 99, pp. 570–82, Sept. 2006.

[4] Nobelprize.org, ""The Nobel Prize in Chemistry 2012"."

[5] M. Gómez-soler, S. Ahern, V. Fernández-due nas, and F. Ciruela, "On the Role of G Protein-Coupled Receptors Oligomerization," pp. 47–53, 2011.

[6] S. R. George, B. F. O'Dowd, and S. P. Lee, "G-protein-coupled receptor oligomerization and its potential for drug discovery.," *Nature reviews. Drug discovery*, vol. 1, pp. 808–20, Oct. 2002.

[7] *Handbook of biological confocal microscopy.* New York, NY: Springer, 2006.

[8] T. Saleh, *Fundamentals of photonics.* Hoboken, N.J: Wiley-Interscience, 2007.

[9] *Molecular biology of the cell.* New York: Garland Science, 2008.

[10] J. Lakowicz, *Principles of fluorescence spectroscopy.* New York: Springer, 2006.

[11] G. G. Guilbaul, *Practical fluorescence.* New York: M. Dekker, 1990.

[12] L. Beer, "Bestimmung der Absorption des rothen Lichts in farbigen Flüssigkeiten," *Annalen der Physik und Chemie*, vol. 162, no. 5, pp. 78–88, 1852.

[13] T. Owen, *Fundamentals of modern UV-visiblespectroscopy.* 2000.

[14] W. Moerner and L. Kador, "Optical detection and spectroscopy of single molecules in a solid," *Physical Review Letters*, vol. 62, pp. 2535–2538, May 1989.

[15] P. Kukura, M. Celebrano, A. Renn, and V. Sandoghdar, "Single-Molecule Sensitivity in Optical Absorption at Room Temperature," *The Journal of Physical Chemistry Letters*, vol. 1, pp. 3323–3327, Dec. 2010.

[16] a. Gaiduk, M. Yorulmaz, P. V. Ruijgrok, and M. Orrit, "Room-temperature detection of a single molecule's absorption by photothermal contrast.," *Science (New York, N.Y.)*, vol. 330, pp. 353–6, Oct. 2010.

[17] S. Chong, W. Min, and X. S. Xie, "Ground-State Depletion Microscopy: Detection Sensitivity of Single-Molecule Optical Absorption at Room Temperature," *The Journal of Physical Chemistry Letters*, vol. 1, pp. 3316–3322, Dec. 2010.

[18] W. Demtro¨der, *Laser spectroscopy.* Berlin: Springer, 2008.

[19] M. Orrit and J. Bernard, "Single pentacene molecules detected by fluorescence excitation in a p-terphenyl crystal.," *Physical review letters*, vol. 65, pp. 2716–2719, Nov. 1990.

[20] T. Ha and P. Tinnefeld, "Photophysics of Fluorescent Probes for Single-Molecule Biophysics and Super-Resolution Imaging.," *Annual review of physical chemistry*, pp. 1–23, Jan. 2012.

[21] D. Koppel, "Statistical accuracy in fluorescence correlation spectroscopy," *Physical Review A*, vol. 10, pp. 1938–1945, Dec. 1974.

[22] J. Widengren, A. Chmyrov, C. Eggeling, P.-A. Löfdahl, and C. A. M. Seidel, "Strategies to improve photostabilities in ultrasensitive fluorescence spectroscopy.," *The journal of physical chemistry. A*, vol. 111, pp. 429–40, Jan. 2007.

[23] J. Vogelsang, R. Kasper, C. Steinhauer, B. Person, M. Heilemann, M. Sauer, and P. Tinnefeld, "A reducing and oxidizing system minimizes photobleaching and blinking of fluorescent dyes.," *Angewandte Chemie (International ed. in English)*, vol. 47, pp. 5465–9, Jan. 2008.

[24] T. Cordes, A. Maiser, C. Steinhauer, L. Schermelleh, and P. Tinnefeld, "Mechanisms and advancement of antifading agents for fluorescence microscopy and single-molecule spectroscopy.," *Physical chemistry chemical physics : PCCP*, vol. 13, pp. 6699–709, Apr. 2011.

[25] T. Cordes, J. Vogelsang, and P. Tinnefeld, "On the mechanism of Trolox as antiblinking and antibleaching reagent.," *Journal of the American Chemical Society*, vol. 131, pp. 5018–9, Apr. 2009.

[26] J. Hoogenboom, E. van Dijk, J. Hernando, N. van Hulst, and M. García-Parajó, "Power-Law-Distributed Dark States are the Main Pathway for Photobleaching of Single Organic Molecules," *Physical Review Letters*, vol. 95, pp. 2–5, Aug. 2005.

[27] T. Vosch, M. Cotlet, J. Hofkens, K. Van Der Biest, M. Lor, K. Weston, P. Tinnefeld, M. Sauer, L. Latterini, K. M\\"ullen, and Others, "Probing Förster type energy pathways in a first generation rigid dendrimer bearing two perylene imide chromophores," *The Journal of Physical Chemistry A*, vol. 107, pp. 6920–6931, Sept. 2003.

[28] E. Abbe, "Beiträge zur Theorie des Mikroskops und der mikroskopischen Wahrnehmung," *Archiv für Mikroskopische Anatomie*, vol. 9, pp. 413–418, Dec. 1873.

[29] *Optik : Wellen- und Teilchenoptik*. Berlin u.a: De Gruyter, 2004.

[30] D. Magde, R. Wong, and P. G. Seybold, "Fluorescence quantum yields and their relation to lifetimes of rhodamine 6G and fluorescein in nine solvents: improved absolute standards for quantum yields.," *Photochemistry and photobiology*, vol. 75, pp. 327–34, Apr. 2002.

[31] U. Resch-Genger, M. Grabolle, S. Cavaliere-Jaricot, R. Nitschke, and T. Nann, "Quantum dots versus organic dyes as fluorescent labels.," *Nature methods*, vol. 5, pp. 763–75, Sept. 2008.

[32] M. Dundr, J. G. McNally, J. Cohen, and T. Misteli, "Quantitation of GFP-fusion proteins in single living cells.," *Journal of structural biology*, vol. 140, no. 1-3, pp. 92–9, 2002.

[33] Y. Sugiyama, I. Kawabata, K. Sobue, and S. Okabe, "Determination of absolute protein numbers in single synapses by a GFP-based calibration technique.," *Nature methods*, vol. 2, pp. 677–84, Sept. 2005.

[34] C. S. Chiu, E. Kartalov, M. Unger, S. Quake, and H. a. Lester, "Single-molecule measurements calibrate green fluorescent protein surface densities on transparent beads for use with 'knock-in' animals and other expression systems.," *Journal of neuroscience methods*, vol. 105, pp. 55–63, Jan. 2001.

[35] J. R. S. Newman, S. Ghaemmaghami, J. Ihmels, D. K. Breslow, M. Noble, J. L. DeRisi, and J. S. Weissman, "Single-cell proteomic analysis of S. cerevisiae reveals the architecture of biological noise.," *Nature*, vol. 441, pp. 840–6, June 2006.

[36] J.-Q. Wu and T. D. Pollard, "Counting cytokinesis proteins globally and locally in fission yeast.," *Science (New York, N.Y.)*, vol. 310, pp. 310–4, Oct. 2005.

[37] C.-S. Chiu, K. Jensen, I. Sokolova, D. Wang, M. Li, P. Deshpande, N. Davidson, I. Mody, M. W. Quick, S. R. Quake, and H. a. Lester, "Number, density, and surface/cytoplasmic distribution of GABA transporters at presynaptic structures of knock-in mice carrying GABA transporter subtype 1-green fluorescent protein fusions.," *The Journal of neuroscience : the official journal of the Society for Neuroscience*, vol. 22, pp. 10251–66, Dec. 2002.

[38] T. Schmidt, G. J. Schütz, W. Baumgartner, H. J. Gruber, and H. Schindler, "Imaging of single molecule diffusion," *Proc. Natl. Acad. Sci. USA*, vol. 93, pp. 2926–2929, 1996.

[39] D. Magde, E. L. Elson, and W. W. Webb, "Thermodynamic Fluctuations in a Reacting System - Measurement by Fluorescence Correlation Spectroscopy," *Physical Review Letters*, vol. 29, no. September, pp. 705–708, 1972.

[40] Y. Chen, J. D. Müller, P. T. So, and E. Gratton, "The photon counting histogram in fluorescence fluctuation spectroscopy.," *Biophysical journal*, vol. 77, pp. 553–67, July 1999.

[41] P. Kask, K. Palo, D. Ullmann, and K. Gall, "Fluorescence-intensity distribution analysis and its application in biomolecular detection technology.," *Proceedings of the National Academy of Sciences of the United States of America*, vol. 96, pp. 13756–61, Nov. 1999.

[42] L. Mandel, "Fluctuations of Photon Beams and their Correlations," *Proceedings of the Physical Society*, vol. 72, pp. 1037–1048, Dec. 1958.

[43] S. a. Mutch, B. S. Fujimoto, C. L. Kuyper, J. S. Kuo, S. M. Bajjalieh, and D. T. Chiu, "Deconvolving single-molecule intensity distributions for quantitative microscopy measurements.," *Biophysical journal*, vol. 92, pp. 2926–43, Apr. 2007.

[44] Y. Chen, L.-n. Wei, and J. D. Müller, "Probing protein oligomerization in living cells with fluorescence fluctuation spectroscopy.," *Proceedings of the National Academy of Sciences of the United States of America*, vol. 100, pp. 15492–7, Dec. 2003.

[45] M. a. Digman, R. Dalal, A. F. Horwitz, and E. Gratton, "Mapping the number of molecules and brightness in the laser scanning microscope.," *Biophysical journal*, vol. 94, pp. 2320–32, Mar. 2008.

[46] M. Höller, *Advanced Fluorescence Fluctuation Spectroscopy with Pulsed Interleaved Excitation Development and Applications.* PhD thesis, Ludwig-Maximilians-Universität München, 2011.

[47] M. a. Digman, P. W. Wiseman, C. Choi, A. R. Horwitz, and E. Gratton, "Stoichiometry of molecular complexes at adhesions in living cells.," *Proceedings of the National Academy of Sciences of the United States of America*, vol. 106, pp. 2170–5, Feb. 2009.

[48] G. Ossato, M. a. Digman, C. Aiken, T. Lukacsovich, J. L. Marsh, and E. Gratton, "A two-step path to inclusion formation of huntingtin peptides revealed by number and brightness analysis.," *Biophysical journal*, vol. 98, pp. 3078–85, June 2010.

[49] M. H. Ulbrich and E. Y. Isacoff, "Subunit counting in membrane-bound proteins.," *Nature methods*, vol. 4, pp. 319–21, Apr. 2007.

[50] M. C. Leake, J. H. Chandler, G. H. Wadhams, F. Bai, R. M. Berry, and J. P. Armitage, "Stoichiometry and turnover in single, functioning membrane protein complexes.," *Nature*, vol. 443, pp. 355–8, Sept. 2006.

[51] M. Heilemann, S. van De Linde, M. Schüttpelz, R. Kasper, B. Seefeldt, A. Mukherjee, P. Tinnefeld, and M. Sauer, "Subdiffraction-resolution fluorescence imaging with conventional fluorescent probes.," *Angewandte Chemie (International ed. in English)*, vol. 47, pp. 6172–6, Jan. 2008.

[52] E. Betzig, G. H. Patterson, R. Sougrat, O. W. Lindwasser, S. Olenych, J. S. Bonifacino, M. W. Davidson, J. Lippincott-Schwartz, and H. F. Hess, "Imaging intracellular fluorescent proteins at nanometer resolution.," *Science (New York, N.Y.)*, vol. 313, pp. 1642–5, Sept. 2006.

[53] M. J. Rust, M. Bates, and X. Zhuang, "Sub-diffraction-limit imaging by stochastic optical reconstruction microscopy (STORM).," *Nature methods*, vol. 3, pp. 793–5, Oct. 2006.

[54] A. Reiner, R. J. Arant, and E. Y. Isacoff, "Assembly Stoichiometry of the GluK2/GluK5 Kainate Receptor Complex.," *Cell reports*, vol. 1, pp. 234–240, Mar. 2012.

[55] R. E. Thompson, D. R. Larson, and W. W. Webb, "Precise nanometer localization analysis for individual fluorescent probes.," *Biophysical journal*, vol. 82, pp. 2775–83, May 2002.

[56] M. Fernández-Suárez and A. Y. Ting, "Fluorescent probes for super-resolution imaging in living cells.," *Nature reviews. Molecular cell biology*, vol. 9, pp. 929–43, Dec. 2008.

[57] B. Seefeldt, R. Kasper, T. Seidel, P. Tinnefeld, K.-J. Dietz, M. Heilemann, and M. Sauer, "Fluorescent proteins for single-molecule fluorescence applications.," *Journal of biophotonics*, vol. 1, pp. 74–82, Mar. 2008.

[58] D. Greenfield, A. L. McEvoy, H. Shroff, G. E. Crooks, N. S. Wingreen, E. Betzig, and J. Liphardt, "Self-organization of the Escherichia coli chemotaxis network imaged with super-resolution light microscopy.," *PLoS biology*, vol. 7, p. e1000137, June 2009.

[59] D. Baddeley, I. D. Jayasinghe, L. Lam, S. Rossberger, M. B. Cannell, and C. Soeller, "Optical single-channel resolution imaging of the ryanodine receptor distribution in rat cardiac myocytes.," *Proceedings of the National Academy of Sciences of the United States of America*, vol. 106, pp. 22275–80, Dec. 2009.

[60] A. N. Kapanidis, T. A. Laurence, N. K. Lee, E. Margeat, X. Kong, and S. Weiss, "Alternating-laser excitation of single molecules.," *Accounts of chemical research*, vol. 38, pp. 523–33, July 2005.

[61] T. Förster, "Zwischenmolekulare Energiewanderung und Fluoreszenz," *Annalen der Physik*, vol. 437, no. 1-2, pp. 55–75, 1948.

[62] W. R. Leifert, K. Bailey, T. H. Cooper, A. L. Aloia, R. V. Glatz, and E. J. McMurchie, "Measurement of heterotrimeric G-protein and regulators of G-protein signaling interactions by time-resolved fluorescence resonance energy transfer.," *Analytical biochemistry*, vol. 355, pp. 201–12, Aug. 2006.

[63] A. N. Kapanidis, N. K. Lee, T. A. Laurence, S. Doose, E. Margeat, and S. Weiss, "Fluorescence-aided molecule sorting: analysis of structure and interactions by alternating-laser excitation of single molecules.," *Proceedings of the National*

Academy of Sciences of the United States of America, vol. 101, pp. 8936–41, June 2004.

[64] B. K. Müller, E. Zaychikov, C. Bräuchle, and D. C. Lamb, "Pulsed interleaved excitation.," *Biophysical journal*, vol. 89, pp. 3508–22, Nov. 2005.

[65] S. Uphoff, S. J. Holden, L. Le Reste, J. Periz, S. van de Linde, M. Heilemann, and A. N. Kapanidis, "Monitoring multiple distances within a single molecule using switchable FRET.," *Nature methods*, vol. 7, Sept. 2010.

[66] F. T. S. Chan, C. F. Kaminski, and G. S. Kaminski Schierle, "HomoFRET Fluorescence Anisotropy Imaging as a Tool to Study Molecular Self-Assembly in Live Cells.," *Chemphyschem : a European journal of chemical physics and physical chemistry*, pp. 1 – 11, Dec. 2010.

[67] A. N. Bader, S. Hoetzl, E. G. Hofman, J. Voortman, P. M. P. van Bergen En Henegouwen, G. van Meer, and H. C. Gerritsen, "Homo-FRET Imaging as a Tool to Quantify Protein and Lipid Clustering.," *Chemphyschem : a European journal of chemical physics and physical chemistry*, pp. 1–10, Dec. 2010.

[68] L. W. Runnels and S. F. Scarlata, "Theory and application of fluorescence homotransfer to melittin oligomerization.," *Biophysical journal*, vol. 69, pp. 1569–83, Oct. 1995.

[69] E. K. L. Yeow and A. H. a. Clayton, "Enumeration of oligomerization states of membrane proteins in living cells by homo-FRET spectroscopy and microscopy: theory and application.," *Biophysical journal*, vol. 92, pp. 3098–104, May 2007.

[70] C. Marquer, C. Fruchart-Gaillard, G. Mourier, O. Grandjean, E. Girard, M. le Maire, S. Brown, and D. Servent, "Influence of MT7 toxin on the oligomerization state of the M1 muscarinic receptor.," *Biology of the cell / under the auspices of the European Cell Biology Organization*, vol. 102, pp. 409–20, July 2010.

[71] L. Szidonya, M. Cserzo, and L. Hunyady, "Dimerization and oligomerization of G-protein-coupled receptors: debated structures with established and emerging functions.," *The Journal of endocrinology*, vol. 196, pp. 435–53, Mar. 2008.

[72] A. N. Bader, E. G. Hofman, P. M. P. van Bergen En Henegouwen, and H. C. Gerritsen, "Imaging of protein cluster sizes by means of confocal time-gated fluorescence anisotropy microscopy.," *Optics express*, vol. 15, pp. 6934–45, May 2007.

[73] M. Fox, *Quantum optics : an introduction*. Oxford New York: Oxford University Press, 2006.

[74] L. Mandel, "Sub-Poissonian photon statistics in resonance fluorescence," *Optics Letters*, vol. 4, p. 205, July 1979.

[75] R. H. Brown and R. Q. Twiss, "Interferometry of the Intensity Fluctuations in Light II. An Experimental Test of the Theory for Partially Coherent Light," *Proceedings of the Royal Society A: Mathematical, Physical and Engineering Sciences*, vol. 243, pp. 291–319, Jan. 1958.

[76] H. Kimble, M. Dagenais, and L. Mandel, "Photon Antibunching in Resonance Fluorescence," *Physical Review Letters*, vol. 39, pp. 691–695, Sept. 1977.

[77] T. Basché, W. Moerner, M. Orrit, and H. Talon, "Photon antibunching in the fluorescence of a single dye molecule trapped in a solid.," *Physical review letters*, vol. 69, pp. 1516–1519, Sept. 1992.

[78] W. Patrick Ambrose, P. M. Goodwin, J. Enderlein, D. J. Semin, J. C. Martin, and R. A. Keller, "Fluorescence photon antibunching from single molecules on a surface," *Chemical Physics Letters*, vol. 269, pp. 365–370, May 1997.

[79] U. Mets, J. Widengren, and R. Rigler, "Application of the antibunching in dye fluorescence: measuringthe excitation rates in solution," *Chemical Physics*, vol. 218, pp. 191–198, May 1997.

[80] P. Tinnefeld, "Time-varying photon probability distribution of individual molecules at room temperature," *Chemical Physics Letters*, vol. 345, pp. 252–258, Sept. 2001.

[81] K. D. Weston, M. Dyck, P. Tinnefeld, C. Müller, D. P. Herten, and M. Sauer, "Measuring the Number of Independent Emitters in Single-Molecule Fluorescence Images and Trajectories Using Coincident Photons," *Analytical Chemistry*, vol. 74, pp. 5342–5349, Oct. 2002.

[82] T. Heinlein, "Counting single molecules in living cells at high resolution by spectrally resolved fluorescence lifetime imaging microscopy (SFLIM) and coincidence analysis," *Proceedings of SPIE*, vol. 5699, no. 0, pp. 141–148, 2005.

[83] J. Sýkora, K. Kaiser, I. Gregor, W. Bönigk, G. Schmalzing, and J. Enderlein, "Exploring fluorescence antibunching in solution to determine the stoichiometry of molecular complexes.," *Analytical chemistry*, vol. 79, pp. 4040–9, June 2007.

[84] H. Ta, *A Novel Method for Quantitative and Structural Determination of Molecular Complexes by Photon Antibunching.* Phd thesis, Ruprecht-Karls-Universität Heidelberg, 2010.

[85] H. Ta, J. Wolfrum, and D.-P. Herten, "An extended scheme for counting fluorescent molecules by photon-antibunching," *Laser Physics*, vol. 20, pp. 119–124, July 2009.

[86] H. Ta, A. Kiel, M. Wahl, and D.-P. Herten, "Experimental approach to extend the range for counting fluorescent molecules based on photon-antibunching.," *Physical chemistry chemical physics : PCCP*, vol. 12, pp. 10295–300, Sept. 2010.

[87] T. Schmidt, G. J. Schütz, H. J. Gruber, and H. Schindler, "Local Stoichiometries Determined by Counting Individual Molecules," *Analytical Chemistry*, vol. 68, pp. 4397–4401, Jan. 1996.

[88] T. Meckel, S. Semrau, M. J. M. Schaaf, and T. Schmidt, "Robust assessment of protein complex formation in vivo via single-molecule intensity distributions of autofluorescent proteins," *Journal of Biomedical Optics*, vol. 16, no. 7, p. 076016, 2011.

[89] K. Herrick-Davis, E. Grinde, T. Lindsley, A. Cowan, and J. E. Mazurkiewicz, "Oligomer size of the serotonin 5-hydroxytryptamine 2C (5-HT2C) receptor revealed by fluorescence correlation spectroscopy with photon counting histogram analysis: evidence for homodimers without monomers or tetramers.," *The Journal of biological chemistry*, vol. 287, pp. 23604–14, July 2012.

[90] N. K. Lee, A. N. Kapanidis, Y. Wang, X. Michalet, J. Mukhopadhyay, R. H. Ebright, and S. Weiss, "Accurate FRET measurements within single diffusing biomolecules using alternating-laser excitation.," *Biophysical journal*, vol. 88, pp. 2939–53, Apr. 2005.

[91] V. V. Gurevich and E. V. Gurevich, "GPCR monomers and oligomers: it takes all kinds.," *Trends in neurosciences*, vol. 31, pp. 74–81, Feb. 2008.

[92] K. Palczewski, "Oligomeric forms of G protein-coupled receptors (GPCRs).," *Trends in biochemical sciences*, vol. 35, pp. 595–600, Nov. 2010.

[93] Y. Hua and R. H. Scheller, "Three SNARE complexes cooperate to mediate membrane fusion.," *Proceedings of the National Academy of Sciences of the United States of America*, vol. 98, pp. 8065–70, July 2001.

[94] W. Wickner, "Membrane fusion: five lipids, four SNAREs, three chaperones, two nucleotides, and a Rab, all dancing in a ring on yeast vacuoles.," *Annual review of cell and developmental biology*, vol. 26, pp. 115–36, Nov. 2010.

[95] M. Minsky, "Memoir on inventing the confocal scanning microscope," *Scanning*, vol. 10, pp. 128–138, Aug. 1988.

[96] M. Reuss, J. Engelhardt, and S. W. Hell, "Birefringent device converts a standard scanning microscope into a STED microscope that also maps molecular orientation.," *Optics express*, vol. 18, pp. 1049–58, Jan. 2010.

[97] P. Bingen, *Parallelised STED nanoscopy*. PhD thesis, Uni Heidelberg, 2012.

[98] R. Eckhardt, "Stan ulam, john von neumann, and the monte carlo method," *Los Alamos Sci*, 1987.

[99] *Monte Carlo methods in statistical physics*. Berlin New York: Springer-Verlag, 1986.

[100] "https://www.atto-tec.com/."

[101] P. W. K. Rothemund, "Folding DNA to create nanoscale shapes and patterns.," *Nature*, vol. 440, pp. 297–302, Mar. 2006.

[102] C. E. Castro, F. Kilchherr, D.-n. Kim, E. L. Shiao, T. Wauer, P. Wortmann, M. Bathe, and H. Dietz, "a primer to scaffolded DNa origami," *Nature Methods*, vol. 8, no. 3, pp. 221–229, 2011.

[103] B. Efron, "Bootstrap Methods: Another Look at the Jackknife," *The Annals of Statistics*, vol. 7, pp. 1–26, Jan. 1979.

[104] G. Gong, "A Leisurely Look at the Bootstrap , the Jackknife , and," vol. 37, no. 1, pp. 36–48, 2012.

[105] S. D. Grimshaw, B. Efron, and R. J. Tibshirani, "An Introduction to the Bootstrap," *Technometrics*, vol. 37, p. 341, Aug. 1995.

[106] *Numerical recipes : the art of scientific computing*. Cambridge, UK New York: Cambridge University Press, 2007.

[107] F. J. Massey, "The Kolmogorov-Smirnov Test for Goodness of Fit," *Journal of the American Statistical Association*, vol. 46, no. 253, pp. 68–78, 1951.

[108] G. Marsaglia, W. Tsang, and J. Wang, "Evaluating Kolmogorov's Distribution," vol. 8, no. 18, pp. 1–4, 2003.

[109] B. J. Aitchison, "The Log-normal Distribution," *Cambridge University Press*, 1957.

[110] E. Limpert, W. a. Stahel, and M. Abbt, "Log-normal Distributions across the Sciences: Keys and Clues," *BioScience*, vol. 51, no. 5, p. 341, 2001.

[111] R. Kasper, "Optimierung von photophysikalischen Eigenschaften organischer Farbstoffe zur Auflösungserhöhung," 2009.

[112] N. M. Green, "Avidin.," *Advances in protein chemistry*, vol. 29, pp. 85–133, Jan. 1975.

[113] A. a. Deniz, S. Mukhopadhyay, and E. a. Lemke, "Single-molecule biophysics: at the interface of biology, physics and chemistry.," *Journal of the Royal Society, Interface / the Royal Society*, vol. 5, pp. 15–45, Jan. 2008.

[114] W. E. Moerner, "New directions in single-molecule imaging and analysis.," *Proceedings of the National Academy of Sciences of the United States of America*, vol. 104, pp. 12596–602, July 2007.

[115] L. Mandel, "Fluctuations of Photon Beams: The Distribution of the Photo-Electrons," *Proceedings of the Physical Society*, vol. 74, pp. 233–243, Sept. 1959.

[116] S. W. Hell and J. Wichmann, "Breaking the diffraction resolution limit by stimulated emission: stimulated-emission-depletion fluorescence microscopy.," *Optics letters*, vol. 19, pp. 780–2, June 1994.

[117] S. T. Hess, T. P. K. Girirajan, and M. D. Mason, "Ultra-high resolution imaging by fluorescence photoactivation localization microscopy.," *Biophysical journal*, vol. 91, pp. 4258–72, Dec. 2006.

[118] V. Westphal and S. Hell, "Nanoscale Resolution in the Focal Plane of an Optical Microscope," *Physical Review Letters*, vol. 94, pp. 1–4, Apr. 2005.

[119] T. a. Klar, S. Jakobs, M. Dyba, A. Egner, and S. W. Hell, "Fluorescence microscopy with diffraction resolution barrier broken by stimulated emission.," *Proceedings of the National Academy of Sciences of the United States of America*, vol. 97, pp. 8206–10, July 2000.

[120] C. Shannon, "Communication In The Presence Of Noise," *Proceedings of the IEEE*, vol. 86, pp. 447–457, Feb. 1998.

[121] R. J. M. Ii, *Introduction to Shannon Sampling and Interpolation Theory*. 1991.

[122] A. Kurz, M. Schwering, and D.-P. Herten, "Quantification of fluorescent samples by photon-antibunching," *Proc. SPIE*, vol. 8228, pp. 82280K–82280K–8, 2012.

[123] J. P. Temirov, A. R. M. Bradbury, and J. H. Werner, "Measuring an antibody affinity distribution molecule by molecule.," *Analytical chemistry*, vol. 80, pp. 8642–8, Nov. 2008.

[124] G.-f. D. Betta, L. Pancheri, D. Stoppa, R. Henderson, J. Richardson, and B. Kessler, "Avalanche Photodiodes in Submicron CMOS Technologies for High-Sensitivity Imaging," 2007.

[125] I. Rech, A. Gulinatti, F. Zappa, M. Ghioni, and S. Cova, "High performance silicon single-photon avalanche diode array," vol. 7320, pp. 73200H–73200H–12, May 2009.

[126] Y. Maruyama and E. Charbon, "An all-digital, time-gated 128X128 spad array for on-chip, filter-less fluorescence detection," in *2011 16th International Solid-State Sensors, Actuators and Microsystems Conference*, pp. 1180–1183, IEEE, June 2011.

[127] O. Schwartz and D. Oron, "Fluorescence antibunching microscopy," *Physical Review*, vol. 18, pp. 1–5, Jan. 2011.

Danksagung

Hier möchte ich meine Worte des Dankes an all die richten, die es mir ermöglicht haben diese Arbeit anzufertigen. Dies wären ins besondere ...

... mein Betreuer, Chef und Mentor, Dirk-Peter Herten. Durch die lockere Art hatte ich viel Raum meine eigenen Ideen umzusetzen. Jedoch konnte ich mich bei Fragen und Problemen stets an dich wenden und die Probleme wurden immer gelöst. Und wenn es zu später Stunde bei einem Glas Wein war.

... meinem Gutachter Wolfgang Petrich. Für die Übernahme der Begutachtung meiner Arbeit und für die konstruktive Kritik beim diskutieren über die Probleme und Zielsetzung der Arbeit. Deine klaren "Anmerkungen" haben mir geholfen die Dinge aus einer anderen Perspektive zu betrachten.

... der Bioquant IT. Ohne den Zugriff auf den Cluster würde mein Rechner heute noch fitten.

... Pit Bingen und Thorsten Staudt aus der nanoscopy group. Die Messtage waren kurzweilig und produktiv. Und das Wetter interessiert im Keller sowieso keinen.

... Jürgen Schmied, Phil Holzmeister und Philip Tinnefeld für die Kooperation mit den DNA origami.

... den Forschis, die ich im Laufe meiner Arbeit betreuen durfte. Ich hoffe Ihr habt so viel von mir gelernt, wie ich von euch.
.... den Lektoren in Person von Flo Kehrle, Michael Schwering, Sabine Vordermayer, Hanna Appelt, Stephan Fagerer, Wolfgang Krätschmer, Arina Rybina und Kristin Grußmayer. Ohne eure großartige Geduld, hätte ich mich wohl in meinen Worten verirrt.

... der Biophotonik Gruppe am KIP, ins besondere Christian "Jodel" Vrancic.

... den Mathematikern, Flo Kehrle und Sebatian Sager, die mir meine Fragen immer umfassend beantwortet haben.

... der Einzelmolekülspektroskopiegruppe am Bioquant. Während einem harten Tag im Dunkellabor, ist die Kaffeepause das Licht am Ende des Tunnels. Insbesondere, Kristin wünsche ich viel Spaß mit CoPS!

.... und allen Freunden die mich auf dem langen Weg begleitet haben. Auf euch ist halt Verlass. Und zum Schluss meiner Familie. Heim kommen ist einfach immer Urlaub.